CHAPTER 1

INTRODUCTION

1.1 THE HELIUM-CADMIUM LASER

Laser systems operating in the blue and U.V. regions of the spectrum are of particular interest because of the large number of applications for intense, coherent, short wavelength radiation. In particular He-Cd lasers, with outputs at 4416 Å and 3250 Å, although of only modest output power, are reliable and relatively inexpensive when compared with the alternative common blue and U.V. laser, the argon ion. The 4416 Å line has application in data recording and display, spectroscopy, photolithography and holographic replication. The 3250 Å transition (of energy 3.8 eV) is one of the shortest wavelength cw lines available and offers advantages over presently used lasers for microfluorescence, biomedical research and photochemical studies.

Helium-cadmium positive column devices are now commercially available but output powers appear to be limited to 50 mW at 4416 Å and 15 mW at 3250 Å.

For this reason other discharge geometries, which also permit oscillation simultaneously on a number of wavelengths, have been investigated. The hollow cathode discharge was found to be a suitable choice of discharge as it proved ideal for excitation of all laser transitions in the cadmium ion. The 4416 Å transition has not been widely investigated in the hollow cathode configuration and the reasons for the output power saturation with increasing current have not been extensively studied. As will be seen in the next section, the exact nature of the excitation mechanism of the $5s^2\ ^2D_{5/2}$ level of Cd II, the

upper level of the 4416 Å transition, is still very much in doubt. Knowledge of the excitation mechanism is required if we are going to establish whether the output power limitation is a fundamental or a discharge limited phenomenon.

Thus, with the ultimate aim of developing a simple, reliable and powerful He-Cd^+ hollow cathode blue laser we have investigated the excitation mechanisms leading to the formation of the $5s^2\ ^2D_{5/2}$ level of Cd II.

1.2 HISTORICAL INTRODUCTION

1.2.1 Fundamental Studies of the Helium-Metal Vapour Systems

Prior to 1968 little study of metal-vapour laser systems was undertaken as such systems that did exist exhibited low performance efficiencies compared to the helium-neon and argon ion laser systems and, also, containment of corrosive and poisonous metal vapours at high temperature posed many problems.

This situation changed after Fowles and Hopkins (1967) and Silfvast (1968, 1969) obtained lasing action on the 4416 Å($5s^2\ ^2D_{5/2}$ - $5p\ \ ^2P_{3/2}$) and 3250 Å ($5s^2\ ^2D_{3/2}$ - $5p\ \ ^2P_{1/2}$) transitions of singly ionized cadmium from the positive column of a capillary discharge seeded with the metal vapour. Based on observations of the parametric variation of laser power with discharge current and helium pressure and the lack of laser action with neon as a buffer gas, Silfvast proposed that Penning collisions between helium atoms in either the singlet (2^1S) or triplet (2^3S) states

with ground state cadmium atoms simultaneously ionize the metal atom and excite the upper laser levels according to the reaction

$$He(2^1S, 2^3S) + Cd(^1S_0) \rightarrow (Cd^+)^* + He(1^1S_0) + e$$

A partial energy level diagram of cadmium, showing the energies associated with the helium 2^1S, 2^3S and He^+ levels, is shown in Figure 1.1.

Browne and Dunn (1973) and Mizeraczyk (1975), from investigation of the parametric behaviour of the product $N(2^3S).N(Cd)$ (the product of the 2^3S metastable density and the cadmium ground state density) and the 4416 Å spontaneous emission also arrived at the conclusion that the Penning collision mechanism is responsible for populating the $5s^2\ ^2D_{5/2}$ level of Cd II in a positive column device.

The role of Penning collisions was first questioned in 1970 by Csillag et al. where studies of a positive column discharge excited by an a.c. current revealed laser power variation that could not simply be explained in terms of Penning ionization. They proposed that a component of the population was in fact due to direct electron impact excitation of the $5s^2\ ^2D_{5/2}$ level, i.e.

$$Cd(1^1S_0) + e \rightarrow Cd^+(5s^2\ ^2D_{5/2}) + e + e$$

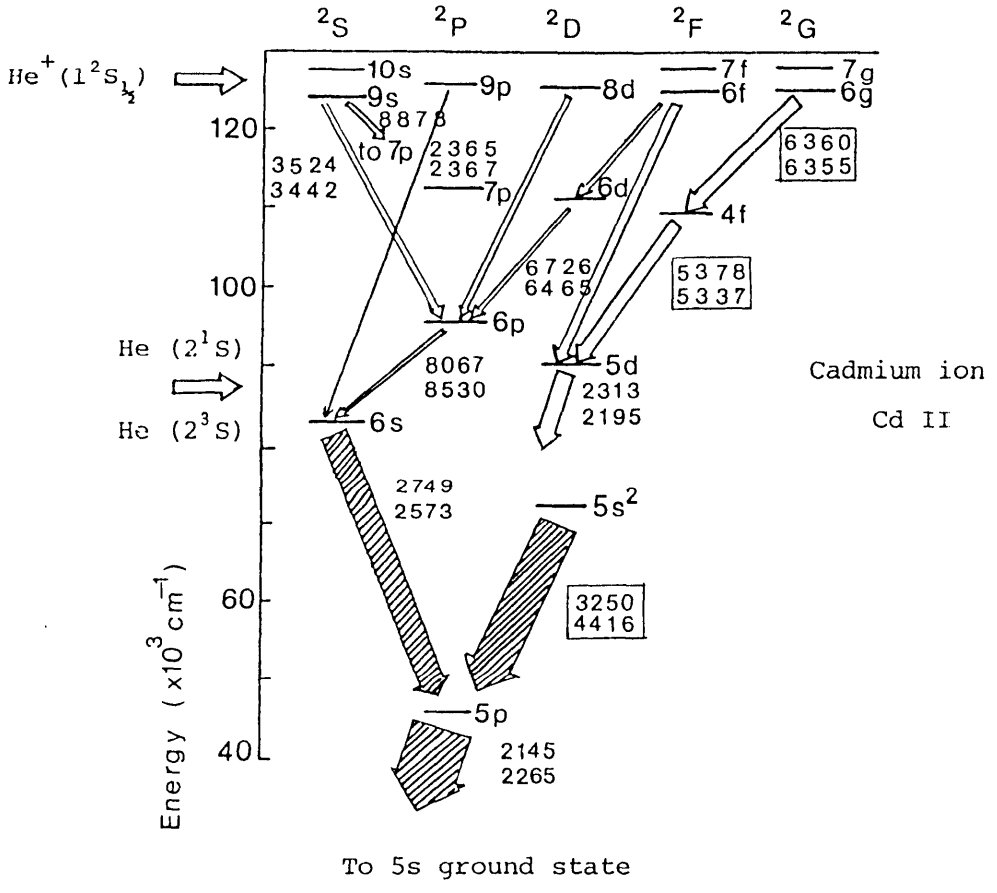

Figure 1.1 Energy level diagram for Cd^+ showing known laser transitions pumped either by Penning ionization collisions with metastable helium atoms (He (2^3S), He (2^1S)) or by charge transfer reactions with helium ground state ions He^+ $(1^2S_{\frac{1}{2}})$. The wavelengths of the laser transitions are enclosed by rectangles (after Webb et al., *1970).*

Janossy et al. (1972) argued that electron collisions with the ground state cadmium ions were important and assumed that the ions were produced by the Penning process.

Further support for the role of electron collision mechanisms in the positive column discharge comes from a series of papers by Mori, Goto and Hattori (1978) and Mori, Murayama, Goto and Hattori (1978). These authors adopted a twofold approach. Firstly, the product $N(2^3S).N(Cd)$ was compared with the 4416 Å spontaneous emission and the differences between the parametric variation of these two terms was taken as evidence to support the role of electron excitation mechanisms. Secondly, they measured the densities of the upper and lower laser levels (the $5s^2\ ^2D_{5/2}$ and $5p\ ^2P_{3/2}$ levels respectively) and, only when electron excitation processes were included in the rate equations for the upper and lower laser levels did the theory fit the experimental results.

On the basis of their studies Mori and his colleagues eliminated the direct electron excitation mechanism because, although the collision cross section for direct electron excitation from the Cd I ground state is unexpectedly large ($\sim 1.5 \times 10^{-16}$ cm^2, Aleinikov and Ushakov, 1970), the low electron density results in the direct electron excitation rate being smaller than the Penning excitation rate and therefore never significant. They argued instead that, in a positive column discharge, two stages of electron impact excitation occur, one from the atomic to ionic ground states and the other from the ion ground state, i.e.

$$Cd(1^1S_0) + e \rightarrow Cd^+(5s^2\ S_{\frac{1}{2}}) + e + e$$

followed by

$$Cd^+(5s^2\ S_{\frac{1}{2}}) + e \rightarrow Cd^+(5s^2\ ^2D_{5/2}) + e$$

The rate of stepwise excitation, they argued, is probably large because the threshold energy of excitation is low and the collision cross section between electrons and ions can be large due to the Coulomb interaction.

Hane et al. (1981) obtained laser oscillation at 4416 Å in a positive column Ne-Cd^+ discharge, in direct contradiction to the experimental results of Silfvast. As the neon metastables possess insufficient energy to excite the cadmium atom directly into the $5s^2\ ^2D_{5/2}$ level, they concluded that the only mechanism capable of sustaining a population inversion was that of the two step electron excitation process proposed by Mori, Murayama, Goto and Hattori (1978).

In order to prove that stepwise excitation can play a dominant role in exciting the $5s^2\ ^2D_{5/2}$ level, Hane et al. (1983a, 1983b) measured the cross section for excitation of the cadmium ion from the ground state to the upper and lower laser levels by electron impact. Using a crossed beam apparatus they found that the excitation cross section was indeed large, having a maximum value of 5×10^{-15} cm^2 at threshold, and was of a similar magnitude to that assumed by Mori, Murayama, Goto and Hattori (1978).

More recently Goto et al. (1983), from a re-examination of the radial profile studies of McKenzie (1975, 1977), have shown that the conclusions of McKenzie are not necessarily correct and the results can only be interpreted when the stepwise excitation mechanism is taken into account. Goto et al. (1983) repeated the studies of McKenzie for a positive column discharge operating under conditions required for laser action.

The helium-metal vapour laser systems have not just been constrained to the one type of gas discharge. In 1970 Schuebel, Sugawara and Tokiwa

constructed hollow cathode helium-cadmium lasers and observed several new cw laser lines of ionized cadmium (5337 Å, 5378 Å, 6355 Å and 6360 Å) in addition to the the well known 4416 Å and 3250 Å transitions. This hollow cathode form of the metal vapour laser utilizes the negative glow region of the discharge as its active medium. Early studies of the negative glow (for example Emeleus and Kennedy, 1934) had established that highly energetic electrons and high ion and electron densities were features of such a discharge.

The excitation mechanism resulting in the new laser lines was attributed to energetically compatible thermal energy charge transfer collisions between the helium ground state ions and metal vapour atoms represented by

$$He^{+} + Cd(1^{1}S_{0}) \rightarrow (Cd^{+})^{*} + He(1^{1}S_{0}) + \Delta E$$

where ΔE is the energy defect between the excited states of the metal ion and the helium ion ground state. (This process is sometimes referred to as Duffendack excitation.)

The positive column He-Cd^{+} gas laser systems have been subject to rigorous investigations aimed at identifying the excitation mechanisms of the $5s^{2}\ ^{2}D_{5/2}$ level of Cd II. However, the hollow cathode devices have not been subject to the same thorough investigation. This is very surprising as there are a number of reasons why the hollow cathode He-Cd^{+} laser is an attractive candidate for further development. Firstly, like the positive column device it offers output at 4416 Å and 3250 Å but, because of differences between these two types of discharge, the output power of the hollow cathode laser at these wavelengths is not necessarily subject to the same limitations as the positive column. Secondly, the

high frequency output noise which is troublesome in conventional 4416 Å Cd^+ lasers is greatly reduced in the hollow cathode configuration because the striation waves which modulate the output are prevented from growing to significant amplitudes by the small anode-cathode spacing (Willgoss and Thomas, 1974; Johnston and Kolb, 1976). Finally, the fact that simultaneous oscillation can be achieved on red, green and blue wavelengths makes this system a possible candidate for development as a white light laser (Fujii et al. 1975; Wong and Grey-Morgan, 1983).

The general excitation processes in these hollow cathode lasers has been studied and the reason for the negative glow region of the discharge being an especially favourable one for the excitation of nearly all cw metal ion laser transitions has been established (Gill and Webb, 1977a and 1977b). However, apart from reports of laser oscillation and of the parametric variation in output power (Piper and Webb, 1973; Fujii, 1973; Fujii et al., 1975; Csillag et al., 1977; Hernqvist, 1978; Grace and McIntosh, 1979) the hollow cathode has not been the subject of detailed examination. Such studies as have been carried out (Grace and McIntosh, 1979; Takasu et al., 1982) have concluded that, although electron processes appear to play an important role in excitation of the $5s^2\ ^2D_{5/2}$ level, the exact nature of the collision mechanism remains in doubt. These conclusions were based on the observation that a significant difference exists between the product $N(2^3S).N(Cd)$ and the 4416 Å spontaneous emission.

It was argued by Grace and McIntosh that, as the hollow cathode has significant numbers of electrons with energies in the range for which the cross section for direct electron excitation is large, this process is likely to be more important in the hollow cathode. This conclusion was

also reached by Gill and Webb (1978) in studies of a hollow cathode He-Zn^+ discharge. They have shown that, for the 5894 Å line, formerly thought to be pumped entirely by Penning collisions (Collins, 1973), up to 70% of the upper level excitation is due to direct electron impact.

On the other hand Takasu et al. maintained that the two step process proposed by Mori and his co-workers and not direct electron excitation was the dominant electron collision process occurring in the hollow cathode discharge.

1.2.2 Afterglow Studies

In an attempt to unambiguously resolve the exact contribution by electronic processes in populating the $5s^2\ ^2D_{5/2}$ level, Goto (1982) made a study of the 4416 Å endlight intensity in a positive column He-Cd afterglow. Results, shown in figure 1.2, were obtained by photographing oscilloscope traces and "clearly showed" the dominance of stepwise excitation in populating the $5s^2\ ^2D_{5/2}$ level in this type of discharge. This conclusion was drawn from the observation that the late afterglow linear decay (Figure 1.2), shown to be associated with Penning collisions, when extrapolated back to the T=0 axis did not pass through the steady state intensity value but at a point considerably lower. Goto then attributed this discrepancy to contributions to the d.c. population by electron impact and calculated the component of the d.c. excitation due to Penning collisions (P) and that due to electron processes (E).

In these studies however, Goto made no attempt to account for the early afterglow "fast" decay which is too long lived to be associated with cessation of the electron impact excitation of this level.

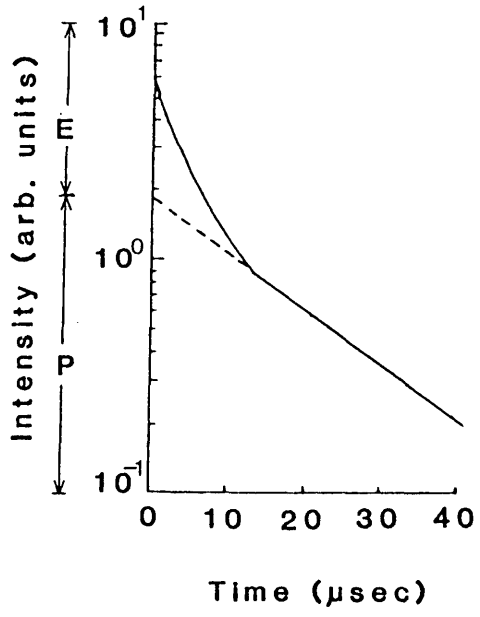

Figure 1.2 Experimental result of Goto showing the decay of the Cd II 4416 Å endlight intensity in a Positive column He-Cd^+ discharge. P and E are the estimates (by Goto, 1982) of the contribution to the d.c. excitation by Penning ionization and electron excitation respectively.

Grey-Morgan and Wong (1983), who obtained data similar to that shown in Figure 1.2 in the afterglow of a hollow cathode He-Cd^+ discharge, arrived at a similar conclusion to that of Goto.

1.3 AN OVERVIEW OF THIS PRESENT STUDY

In the more recent studies of the hollow cathode He-Cd^+ (Grace and McIntosh, 1979; Takasu et al., 1982) and He-Zn^+ (Gill and Webb, 1978)

discharges and positive column discharge (Mizercyzk, 1975) the conclusions concerning the role of electron impact excitation of the $5s^2\ ^2D_{5/2}$ level were arrived at by comparing the parametric variation of the Penning collision rate, given by the product $N(2^3S).N(Cd)$, with the 4416 Å spontaneous emission. Any significant differences between these two parameters was taken as evidence to support the view that electron excitation provides a significant fraction of the $5s^2\ ^2D_{5/2}$ population.

Although this approach is fundamentally sound, the conclusions reached will only be valid provided that all discharge parameters have been included in calculating the collision rate. In previous studies this appears not to have been the case. As will be discussed in Chapter 3, the gas temperature depends on the discharge current, helium pressure and oven temperature and this has implications for the conclusions reached concerning the role of Penning collisions in the hollow cathode $He\text{-}Cd^+$ laser.

In Chapter 4, results of a study of the 4416 Å decay in the He-Cd afterglow will be presented.

Chapters 5, 6 and 7 are devoted to establishing the various collision processes associated with the decay of the 4416 Å transition and a discussion of the implications of the afterglow studies for establishing the collision processes occurring under d.c. discharge conditions.

CHAPTER 2

THEORY OF THE FRACTIONAL ABSORPTION EXPERIMENT

2.1 INTRODUCTION

As indicated in Chapter 1, an investigation of the excitation mechanisms operating in the He-Cd^+ laser requires measurement of the populations of various levels of the atomic and ionic species. The required populations include the atomic and ionic ground states of cadmium and the metastable 2^1S and 2^3S levels of helium.

The only practical way to measure these densities is by absorption spectroscopy. Of the various possible techniques of absorption spectroscopy those of Harrison (1959) and McConkey (1969), in which the same discharge acts as both emitter and absorber, can be applied directl to the measurement of excited state densities in gas discharge devices. The latter technique, in which the light signals emitted from a known volume of discharge are recorded as the length of the volume is varied, is very easily applied to the hollow cathode discharge as switching of individual anodes enables the length of the discharge to be varied in a known manner. Provided that the geometry is such that similar volume elements along the discharge axis contribute similar intensities to the light signal entering the spectrometer, then the degree of absorption ma be determined by comparing the light intensity from a single anode with that from a number of anodes.

In this chapter the optical design criteria, requiring each volume element along the axis of the tube to contribute equal signal levels at

the detector, are established. An expression for the intensity ratio is derived so that the absorption coefficient k_o, for the particular transition being investigated, may be calculated from the intensity ratios resulting from differing lengths of discharge and hence number densities of excited species may be determined. The theory is developed for a single Doppler broadened line and the analysis extended to a line consisting of overlapping fine structure components.

2.2 OPTICAL DESIGN CRITERIA

The paramter $k_o l$, calculated from the absorption experiments, can be determined only if the light intensity received at the detector is independent of distance along the axis of the discharge tube. To achieve this, apertures must be placed in the optical system to ensure that similar volume elements of the plasma along the tube contribute similar intensities to the signal entering the spectrometer. As shown in Figure 2.1, this is achieved by placing two circular apertures between the discharge tube and the spectrometer. The principal stop A is placed near the discharge tube and the smaller stop B is taped to the spectrometer slit. Also, the dimensions and placement of the apertures must be chosen to maximize the light signal received at the detector, and, to ensure that wall reflections do not contribute to the light signal.

Grace (1978), following the analysis of Harrison (1959), has shown that for a discharge segment of length L and diameter 2D, the equations determining the size and placement of the two stops for optimum light collection and, at the same time, ensuring that the signal received from

each volume element in the discharge is independent of the distance from the slits of the spectrometer, are

$$L = Z, \quad R = D/2, \quad r << R$$

where Z is the distance between stop A and the spectrometer stop B and R,r are the radii of stops A and B respectively.

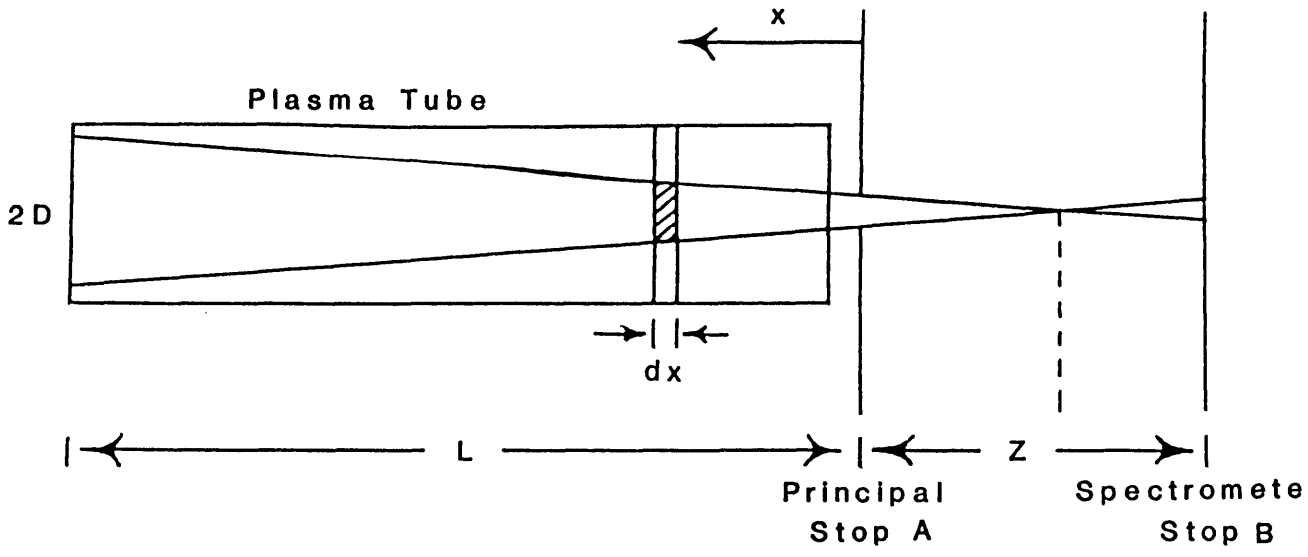

Figure 2.1 Optical arrangement of the absorption experiment

The discharge tube used in the absorption experiments was of 4 mm internal diameter. As it was desired to view only the central 1 mm diameter region of the discharge volume, the following values were used for the experiment.

$$L = Z = 100 \text{ cm}$$

$$R = 0.05 \text{ cm}$$

and

$$r = 50 \ \mu\text{m}.$$

It may be shown (Browne, 1972; Grace, 1978) that diffraction effects at the principal stop are negligible for the chosen aperture size and placement.

2.3 THE SELF-ABSORPTION EXPERIMENT

2.3.1 Analysis of the Self-Absorption Experiment

The fractional absorption of the spectral lines of interest can be measured by comparing the light intensity from a discharge segment associated with a single anode with that from two or more discharge segments provided that the negative glows associated with each of the chosen anodes do not overlap. The theory of the self-absorption technique which enables the absorption coefficient to be determined from the measured intensity ratio will be discussed.

The theory outlined below, which enables the absorption coefficient to be determined from the measured intensity ratio, is based on the treatment of Grace (1978) and assumes that Doppler broadening is the dominant line broadening mechanism. Browne and Dunn (1973) have shown that this assumption is valid for conditions similar to those of the present experiment.

For a single, isolated Doppler broadened spectral line the light intensity emitted per unit length of discharge per unit frequency in the direction of the detector is (Mitchell and Zemansky, Chapter 3)

$$\delta I(\nu) = I_0 \exp(-\omega^2)\, d\nu$$

where I_0 is a constant dependent on the position and nature of the radiating atoms, and

$$\omega = \frac{2(\nu - \nu_0)(\ln 2)^{\frac{1}{2}}}{\Delta\nu_D}$$

where ν_0 is the frequency at line centre and $\Delta\nu_D$ is the Doppler width.

A section of discharge of length dx therefore emits

$$\Delta[\delta I(\nu)] = I_0 \exp(-\omega^2)\, d\nu dx$$

However, self-absorption occurring within the emitting plasma itself attenuates the signal reaching the detector, and the light intensity received is (Mitchell and Zemanksy, p.92)

$$\Delta[\delta I(\nu)] = I_0 \exp(-\omega^2) \exp(-k_\nu x)\, d\nu dx \qquad (2.1)$$

where k_ν is the frequency dependent absorption coefficient of the spectral line.

In the case of a pure Doppler broadened line

$$k_\nu = k_0 e^{-\omega^2}$$

(where k_o is the maximum absorption coefficient), and equation (2.1) can be re-written as

$$\Delta[\delta I(\nu)] = I_0 \exp(-\omega^2) \exp(-k_0 x e^{-\omega^2})\, d\nu dx$$

Thus the light intensity received at the spectrometer per unit frequency ($\delta I(\nu)$) for a plasma segment of length 1 is

$$\delta I(\nu) = I_0 \exp(-\omega^2)\, d\nu \int_0^1 \exp(-k_0 x e^{-\omega^2})\, dx \tag{2.2}$$

$$= \frac{I_0}{k} d\nu [1-\exp(-k_0 l e^{-\omega^2})]$$

Integrating $\delta I(\nu)$ over frequency gives the total intensity collected by the spectrometer for a discharge segment of length 1 as

$$I(\nu) = \frac{I_0}{k_0} \int_{-\infty}^{\infty} [1-\exp(-k_0 l e^{-\omega^2})]\, d\nu \tag{2.3}$$

For a Doppler broadened line

$$d\omega = \frac{2(\ln 2)^{\frac{1}{2}}\, d\nu}{\Delta\nu_D}$$

and equation (2.3) becomes

$$I(\nu) = \frac{I_0}{k_0} \frac{\Delta\nu_D}{2(\ln 2)^{\frac{1}{2}}} \int_{-\infty}^{\infty} [1 - \exp(-k_0 l e^{-\omega^2})]\, d\omega \tag{2.4}$$

Equation (2.4) cannot be evaluated as the value of the constant I_o is not known. However, this constant may be eliminated by calculating the intensity ratio (I_1/I_2) for light intensities I_1 and I_2 emitted from discharges of lengths l_1 and l_2 respectively with

$$\frac{I_1}{I_2} = \frac{\int_{-\infty}^{\infty} [1 - \exp(-k_0 l_1 e^{-\omega^2})]\, d\omega}{\int_{-\infty}^{\infty} [1 - \exp(-k_0 l_2 e^{-\omega^2})]\, d\omega} \tag{2.5}$$

Using equation (2.5) tables of $k_o l$ versus intensity ratio (I_1/I_2) were constructed for particular ratios of l_1 to l_2. The experimentally

obtained intensity ratios could then be used to find the corresponding value of $k_o l$ for the transition under investigation. These $k_o l$ values are related to the number density of the absorbing species (N_1) by the relation (Mitchell and Zemansky, p.125)

$$k_0 l = \frac{2}{\Delta\nu_D}\left[\frac{\ln 2}{\pi}\right]^{\frac{1}{2}} \frac{\lambda_0^2}{8\pi} \frac{g_u}{g_l} N_l \left(1 - \frac{g_l N_u}{g_u N_l}\right) A_{ul} l \qquad (2.6)$$

where A_{ul} is the Einstein coefficient for the transition at a wavelength λ_0 (frequency ν_0) from the upper level u (population density N_u, statistical weight g_u) to lower level 1 (population density N_1, statistical weight g_1).

Provided that the discharge length (l) is known for the experimental conditions, equation (2.6) can be used to evaluate the reduced number density

$$N_l \left(1 - \frac{g_l N_u}{g_u N_l}\right) \qquad (2.7)$$

If, in addition, the condition

$$g_l N_u \ll g_u N_l \qquad (2.8)$$

is satisfied then the experimentally derived $k_o l$ values will yield the absolute number density of the absorbing species (N_1).

2.3.2 The Influence of the Upper Level

According to equation (2.8), the fractional absorption method will only give the absolute density of absorbing species provided that the upper level population (N_u) is much less than that of the lower level (N_1).

The presence of significant upper level populations can be examined using the self absorption technique. Consider the ratio of absorption coefficients for two lines terminating on the same lower level N_1. Denoting one line by 1 and the other by 2, the ratio of the absorption coefficients at line centre for the two lines may be written as

$$\frac{k_1}{k_2} = \frac{\lambda_1^3}{\lambda_2^3} \frac{A_1}{A_2} \frac{g_{u1}}{g_{u2}} \frac{(1 - \frac{g_1 N_{u1}}{g_{u1} N_1})}{(1 - \frac{g_1 N_{u2}}{g_{u2} N_1})} \tag{2.9}$$

If equation (2.8) is satisfied for each transition, i.e. if $g_1 N_{u1} << g_{u1} N_1$ and $g_1 N_{u2} << g_{u2} N_1$, then equation (2.9) reduces to

$$\frac{k_1}{k_2} = \frac{\lambda_1^3}{\lambda_2^3} \frac{A_1}{A_2} \frac{g_{u1}}{g_{u2}} \tag{2.10}$$

and knowledge of λ_1, λ_2, A_1 and A_2 allows the calculation of the ratio of absorption coefficients. If the experimentally determined ratio of absorption coefficients is the same as the value arrived at using equation (2.10), then the effects of the upper level populations can be assumed to be negligible and the number densities derived from experiment will be absolute number densities. If the experimental ratio falls significantly below the expected value then only the reduced number density can be determined.

Values for the ratio of absorption coefficients derived from equation (2.10) for the important excited species in helium are given in Table 2.1.

TABLE 2.1

Absorption Coefficient Ratios for Important HeI Levels from Equation 2.10

LOWER LEVEL	k_0 RATIO	EXPECTED VALUE FROM EQUATION 2.10
2^1S	$\frac{k_0(3^1P - 2^1S)}{k_0(4^1P - 2^1S)}$	3.78
2^1P	$\frac{k_0(4^1D - 2^1P)}{k_0(5^1D - 2^1P)}$	6.26
2^3S	$\frac{k_0(3^3P - 2^3S)}{k_0(4^3P - 2^3S)}$	3.41
2^3P	$\frac{k_0(3^3D - 2^3P)}{k_0(4^3D - 2^3P)}$	6.38

2.3.3. Extension to Complex Doppler Broadened Lines with Overlapping Components

Of the lines investigated at 5016 Å, 4921 Å, 3889 Å and 5875 Å in helium and 3261 Å and 2144 Å in cadmium, only the first two are simple Doppler broadened transitions for which the fractional absorption method can be applied directly. The remaining lines consist of a number of discrete components with overlapping Doppler broadened profiles and the analysis of the previous section must be modified accordingly.

When the components of a line overlap, the absorption can be evaluated only by numerical integration. Values of the intensity ratio can be found once the form of $k_\nu 1$ as a function of frequency ν is known for the transition.

Each component of the line is treated as a simple Doppler broadened line and the $k_o l$ value for each component is calculated. If there are n components to the structure, their relative intensities $I^i (i = 1,2,..,n)$ obey the relationship

$$(k_0 l)^1 : (k_0 l)^2 :.....(k_0 l)^n = I^1 : I^2 :....: I^n$$

The relative intensities are obtained from the theoretical intensity rules for multiplets together with, in the case of the cadmium transitions, the relative abundances of the isotopes.

The one remaining equation necessary to find all the $k_o l$ values is given by a modified form of equation (2.6)

$$\sum_{i=1}^{n} (k_0 l)^n = \frac{2}{\Delta\nu_D} \left[\frac{\ln 2}{\pi}\right]^{\frac{1}{2}} \frac{\lambda_0^2}{8\pi} \frac{g_u}{g_l} N_l \left(1 - \frac{g_l N_u}{g_u N_l}\right) A_{ul} \, l$$

where N_u and N_l are now the total populations over all components of the structure and g_u and g_l are, in this case, the sum of the statistical weights of the individual sublevels of the upper and lower levels respectively.

To calculate the form of $k_\nu l$ for the case of a line with overlapping components the following procedure was adopted. Each component of the line was assumed to have a Doppler broadened profile with the same width $\Delta\nu_D$ and same maximum value of $k_o l$. The separation between the centres of the curves was equated to the measured separation of the components of the line and the individual profiles were weighted according to their relative intensities. The resultant profiles were then added to give a curve of $k_\nu l$ as a function of frequency ν for the line. The replacement of $k_o l e^{-\omega^2 \nu}$ in equation (2.5) by this curve of $k_\nu l$ allows the evaluation of the intensity ratio.

The above integration procedure was performed for each transition studied. Results of these calculations, i.e. graphs of the intensity ratio (I_1/I_2) versus product $k_o l$, are shown in figure 2.2b for the helium triplet metastable density (absorption at λ = 3889 Å) and figure 2.3b for the cadmium ion ground state (absorption at λ = 2144 Å) density.

2.3.4 Structure of the Helium 3889 Å and 5875 Å and Cadmium 3261 Å and 2144 Å Lines

The helium lines at 3889 Å and 5875 Å are closely spaced triplets. This triplet structure arises from the different energies possessed by the J sublevels of the upper and lower states of the transitions due to coupling of the electron spin and the orbital angular momentum. The splitting of the components of the 3889 Å transition is 5-6 GHz (Gibbs and Kruger, 1931) which is less than the Doppler width of 8.4 GHz for each component at 900K. The 5875 Å transition is a closely spaced doublet (separation 2.4 GHz) with a third component at about 35 GHz separation.

The structures of the Cd I intercombination line at 3261 Å ($5^3P_1 - 5^1S_o$) and the Cd II line at 2144 Å ($5p^2P_{3/2} - 5s^2S_{1/2}$) have different origins. Firstly, the isotope shifts of the line must be considered since the cadmium used was of normal isotopic composition with eight stable isotopes. Secondly, the hyperfine splitting of the lines due to the non zero nuclear spin must be considered for the two stable isotopes with odd atomic number. The other isotopes with even atomic numbers have a zero nuclear spin which has no effect on the structure of the line.

The detailed structure of the CdI 3261 Å transition was derived

from the results of Kelly and Tomchuk (1959) and that of the CdII 2144 Å resonant transition was calculated from the data of Contreras and Kelly (1969) and Mori (1978).

For the 3261 Å transition the non zero nuclear spin of the odd atomic number stable isotopes results in the upper level (the 5^3P_1 level) being split into two components having F = 3/2 and F = 1/2 whereas the lower level (the 5^1S_o level) has only one component with F = 1/2 (since S = L = 0). This results in the transition being split into two components as determined by the selection rule $\Delta F = 0, \pm 1$. On the other hand the $^2S_{1/2}$ lower level of the 2144 Å transition is split into two components (F = 1 and F = 0) and between these and the two hyperfine levels (F = 2 and F = 1) of the $^2P_{3/2}$ upper level there are three allowed transitions. In each case the intensity ratios of the hyperfine components can be calculated from the intensity sum rules.

The structure of the 3889 Å helium line and the 2144 Å cadmium line together with the theoretical intensity ratios of the components are shown in figures 2.2a and 2.3a respectively.

2.3.5 Measurement of Gas Temperature and Calculation of Doppler Width

The Doppler width of a spectral line measured at the half power points, resulting from the random thermal velocities of the emitting atoms, is related to the absolute temperature (T_g) of the plasma by

$$\Delta\nu_D = 7.16 \times 10^{-7} \nu_0 \left(\frac{T_g}{M}\right)^{\frac{1}{2}} \qquad (2.11)$$

where ν_0 is the frequency at line centre and M the molecular weight. In order to calculate the Doppler width the gas temperature of the hollow

cathode discharge must be known for the discharge conditions used in the current study.

A convenient method for measuring the gas temperature along the axis of the hollow cathode discharge was to study the rotational structure of a small amount ($<<10^{-3}$Torr) of impurity N_2 present in the system. The 3914 Å N_2^+ line ($B^2\Sigma_u^+ \rightarrow X^2\Sigma_g^+ : v^1 = 0, v^{11} = 0$) was examined. This line has the advantage of being a Σ-Σ transition and is one of the more intense lines emitted by the nitrogen molecule in a hollow cathode discharge in an excess of helium. A full description of the theory, experimental procedure and results is contained in Appendix A2.

The results obtained from experiment, gas temperature variation in the range from 600K - 1200K, agree well with the value of 1200K determined by Gill and Webb (1978) in a discharge tube of similar design to the one used in the present study. Browne and Dunn (1973) on the other hand have measured the gas temperature in a positive column discharge to be 600K. This, however, would be expected since the positive column discharges used in these studies were operated at currents of 200 mA whereas the current range used in the hollow cathode discharge was in the range of 1 - 3 Amps.

The Doppler width, calculated from equation (2.11) and the gas temperature corresponding to the experimental conditions, was used in the evaluation of the intensity ratio (equation 2.5). In fact, the fractional absorption analysis of section 2.3.1 is only very weakly dependent on the gas temperature because the Doppler width enters both the numerator and denominator of equation (2.5) and tends to cancel out. This was checked by calculating a set of intensity ratios versus k_o for Doppler widths covering the whole range of gas temperatures used, at a constant length ratio of 3:1. The variation between the calculated

intensity ratios for the different gas temperatures was less than 1% over the entire range of absorption coefficients used in the present experiments.

2.4 AXIAL EXTENT OF THE NEGATIVE GLOW FROM A SINGLE ANODE

To calculate the number density of absorbing species from the product of $k_o l$ using equation (2.6) the length of plasma (l) associated with a single anode must be known for all possible conditions of helium pressure, current, oven temperature and gas flow rate used in the experiment. Measurements of the axial extent of the negative glow in the hollow cathode discharge tube used in this present study have been made by Grace and McIntosh (1979) for a helium cadmium discharge and by MacKellar (1978) for a pure helium discharge. Their data were used throughout the present investigation.

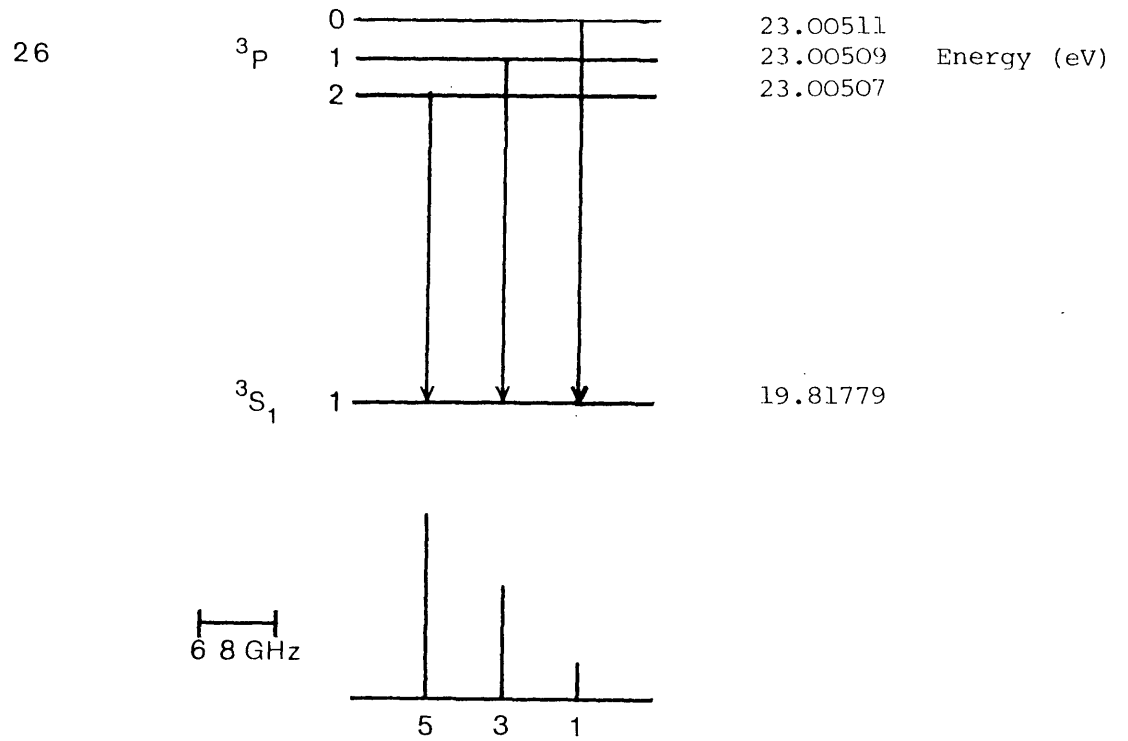

Figure 2.2a Energies and relative intensities of the three components of the 3889 Å helium line

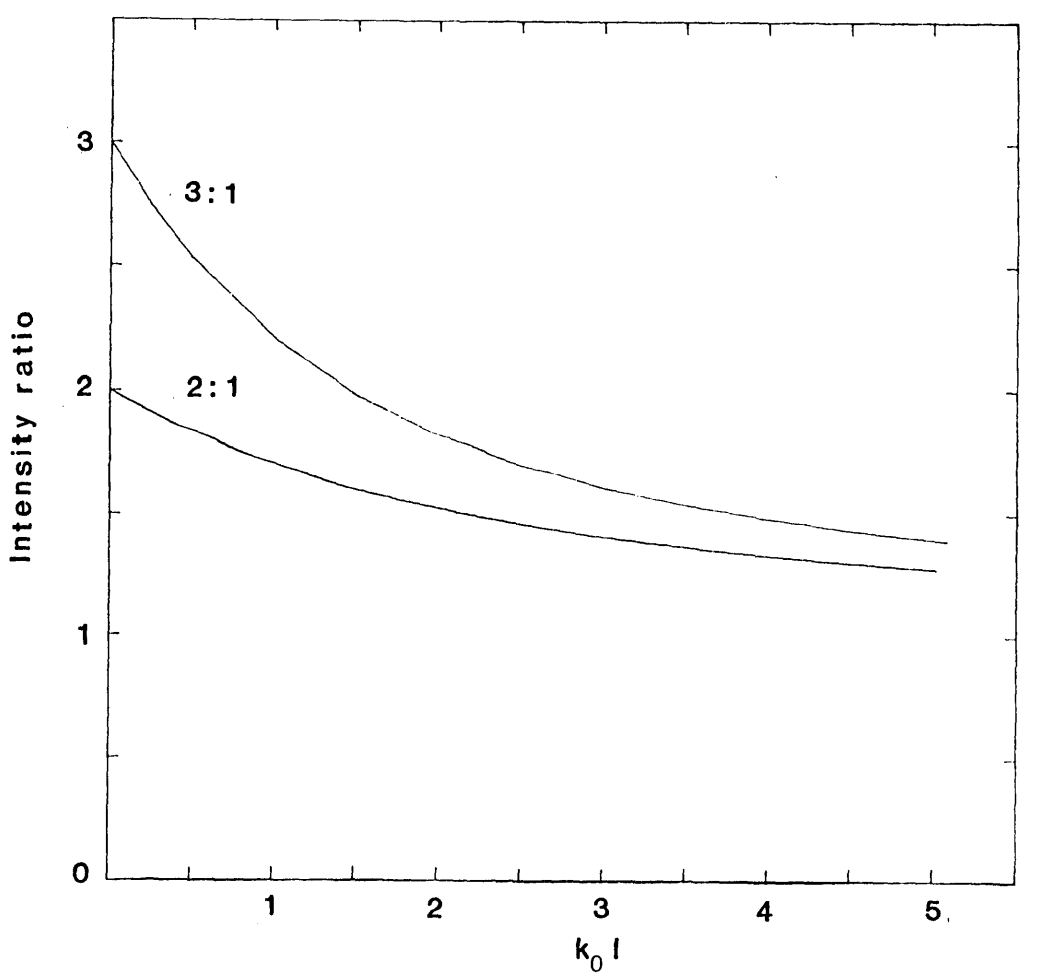

Figure 2.2b 3889 Å intensity ratio versus $k_0 l$ for length ratios of 3:1 and 2:1

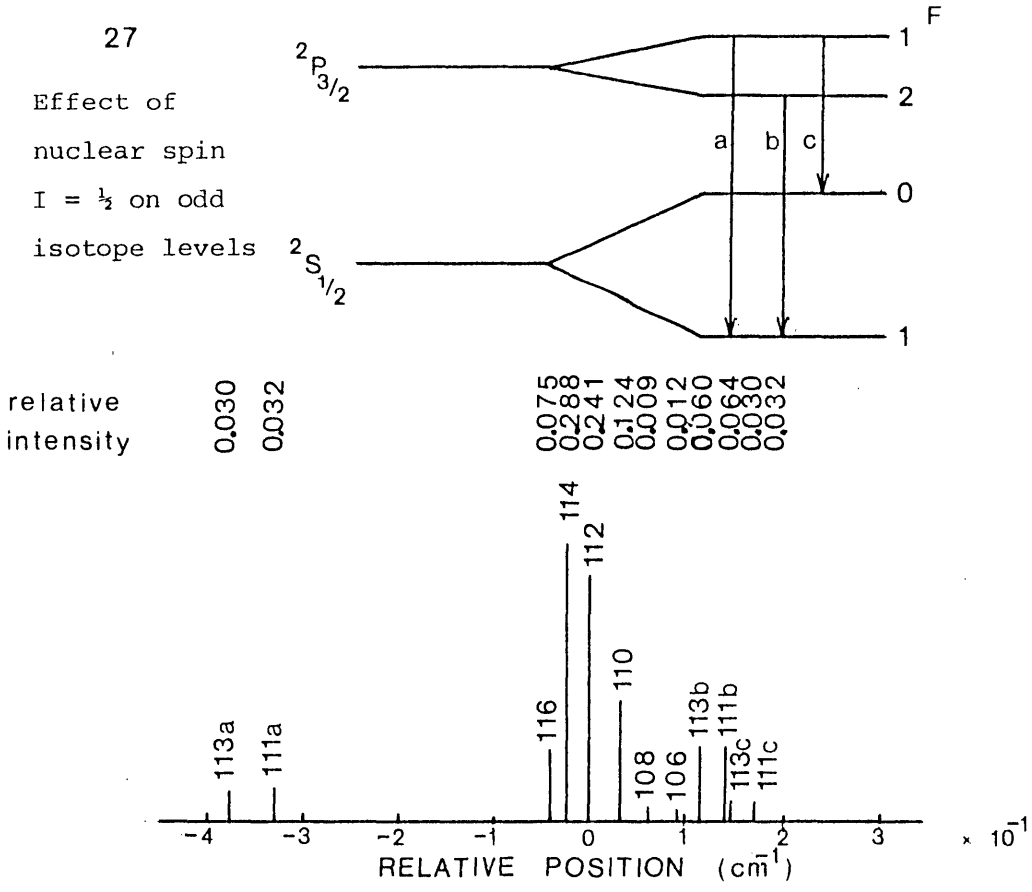

Figure 2.3a Structure of the Cd II line at 2144 Å arising from isotope and nuclear spin effects, together with the intensity ratios of the components

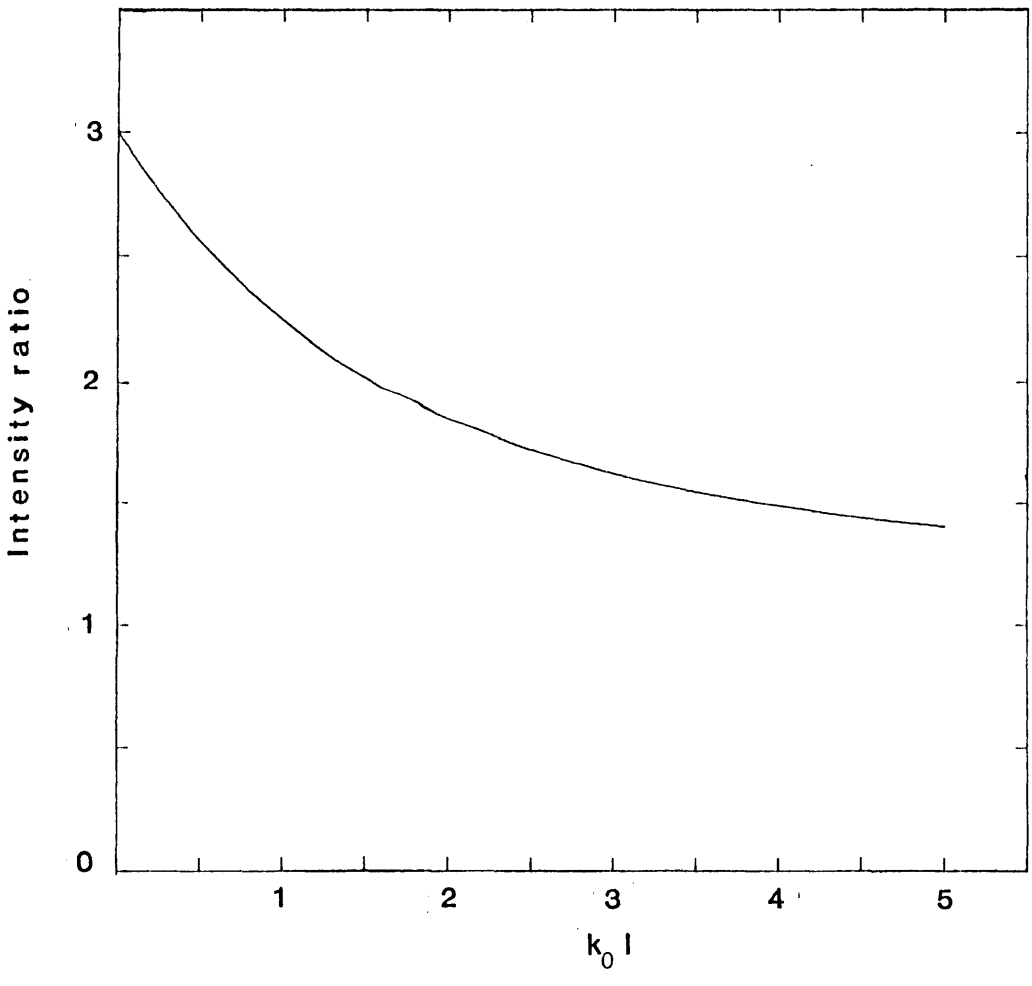

Figure 2.3b 2144 Å intensity ratio versus $k_0 l$ for a length ratio of 3:1

CHAPTER 3

STUDIES OF THE HELIUM-CADMIUM DISCHARGE

3.1 INTRODUCTION

The hollow cathode discharge tube used in this investigation is identical to that developed by Grace (1978) which, in turn, was based on the design of Piper and Webb (1978), and is described in detail in Appendix A1. As discussed in Chapter 2, this particular laser is well suited to application of the fractional absorption technique for number density measurements because switching of individual anodes enables the length of the discharge to be varied in a known manner.

Before proceeding to a discussion of the optical system used in the measurement of excited state densities, the present chapter begins (section 3.2) with a brief discussion of the electron density and electron energy distribution function in a hollow cathode helium-metal vapour discharge. This is done because section 3.2 also includes a description of a spectroscopic technique, based on the assumption of LTE, to measure the electron temperature applicable to the present experiments. The results, showing T_e varying between 0.04 and 0.09 eV, were found to be in reasonable agreement with those of McNeil (1977).

Sections 3.3, 3.4 and 3.5 contain respectively: a description of the optical system used to measure the populations of the helium 2^3S and 2^1S triplet and singlet metastables, together with those of the 2^3P and 2^1P levels (these being the next highest excited levels of neutral helium); the results of those measurements in a helium discharge; and the results

obtained when cadmium was added to the discharge.

The significance of these results lies in the fact that they allow an investigation of the importance of Penning ionization in populating the $5s^2\ ^2D_{5/2}$ upper level of the 4416 Å laser transition. This investigation relies on a comparison of the variation of the Penning collision rate (calculated from the experimentally determined metastable densities) with parameters such as pressure, current and cadmium concentration with the corresponding variation of the 4416 Å spontaneous emission. The measurements of the 4416 Å spontaneous emission and a discussion of its comparison with the Penning collision rate is given in section 3.7.

One important aspect of this comparison has apparently been overlooked by previous investigators who have employed similar methods to reach somewhat different conclusions. These other investigators have neglected to include the effect of gas temperature and its variation with, for example, current. Gas temperature enters the analysis in two ways. Firstly, variations of gas temperature have a marked effect on the values of excited state number densities through the direct effect on spectral line widths; this effect has been taken into account by some, but by no means all, previous workers. Secondly, gas temperature enters directly via its effect on the kinetic gas velocities, in the Penning collision rate. It is shown in section 3.7.1 that the simple assumption that the Penning cross section is independent of energy, would lead to a $T_g^{1/2}$ dependence of the 4416 Å spontaneous emission. Inclusion of this effect of gas temperature in the present work is achieved by means of spectroscopic measurements of the rotational structure of a N_2^+ band (described in Appendix A2 so as not to impede the flow of argument of the present chapter) and it dramatically improves the agreement between the

variation with current of the 4416 Å spontaneous emission and the Penning collision rate.

This important effect appears to have been overlooked by all previous investigators and it is argued in section 3.7.1 that its neglect has caused them to underestimate the role of Penning collisions in populating the upper level of the cadmium ion 4416 Å transition.

These results suggest that the Penning collision mechanism is largely, if not solely, responsible for populating the upper level of the 4416 Å transition. Quantitative verification of this result requires a knowledge of the cadmium ion concentration and, since such a measurement relies on the same optical techniques as that used for the helium densities, the opportunity is taken to present these results in section 3.8.

Some confirmation of the importance of the helium metastable levels in populating the upper levels of the cadmium ion laser transition was sought by replacing the helium with argon whilst keeping the other discharge parameters constant. The results of this investigation, presented in section 3.9, are consistent with the overall conclusion of the chapter, viz, that Penning collisions play the dominant role in populating the $5s^2\ ^2D_{5/2}$ level of Cd^+ in a hollow cathode discharge.

3.2 ELECTRON DENSITY, ELECTRON ENERGY DISTRIBUTION FUNCTION AND ELECTRON TEMPERATURE

As any discussion concerning the role of electrons in the hollow cathode discharge requires a knowledge of both the electron density and

energy distribution function it is convenient to discuss these parameters before proceeding with a description of the spectroscopic studies of the He and He-Cd discharges.

No data for the electron density are available for the specific case of a 4 mm bore hollow cathode discharge but Gill and Webb (1978) and Belal and Dunn (1978) have obtained data in a 3 mm bore He-Zn discharge and a 6 mm bore He discharge respectively.

Figure 3.1 shows the electron densities measured by Belal and Dunn and by Gill and Webb as a function of helium pressure. In view of the fact that these curves have similar magnitudes and shapes for different cathode bore diameters and discharge constituents, it is expected that the electron density of a 4 mm bore He-Cd hollow cathode discharge will show a similar dependence with pressure. The results of Gill and Webb and Belal and Dunn also show that, for a constant helium pressure, the electron density increases linearly with discharge current (see Figure 3.2). Thus it is expected that the electron density in the discharge tube used in this present study will have a similar magnitude and current dependence.

Neither Belal and Dunn nor Gill and Webb have published data showing the variation of electron density with the concentration of metal vapour. However, since charge neutrality must be preserved and He^+ is the dominant ion species in all experimental conditions, the parametric variation of spontaneous emission from a high lying helium ion level should provide a guide to the variation of electron density. The He II spontaneous emission at 4686 Å varies linearly with current, in agreement with the direct measurements of n_e shown in Figure 3.2, but, as is shown in Figure 3.3, does not have a strong dependence on oven temperature. In the absence of more direct measurements we therefore

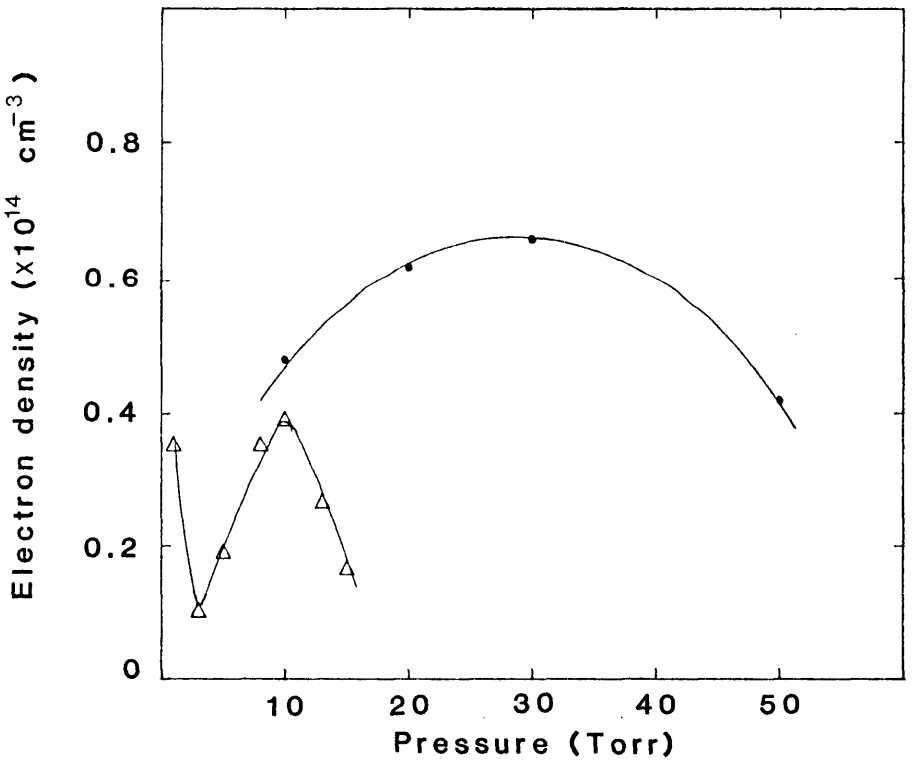

Figure 3.1 Variation of electron density with gas pressure in a pure helium hollow cathode discharge

• — 3 mm bore (Gill and Webb, 1978)

Δ — 6 mm bore (Belal and Dunn, 1978)

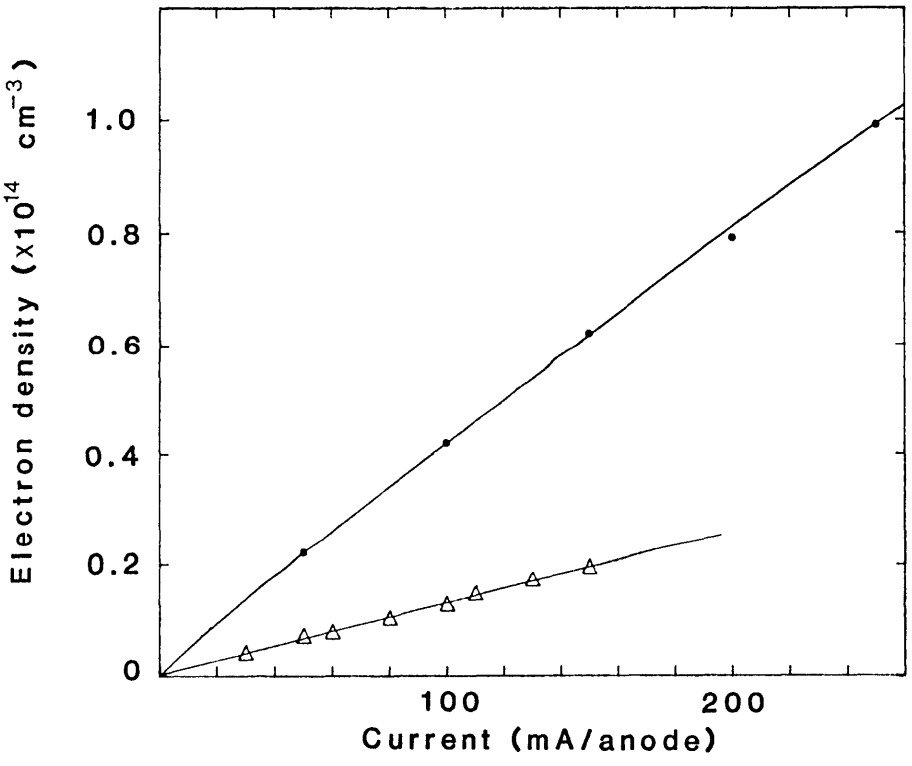

Figure 3.2 Variation of electron density with discharge current at a constant helium pressure of 20 Torr

• — 3 mm bore (Gill and Webb, 1978)

Δ — 6 mm bore (Belal and Dunn, 1978)

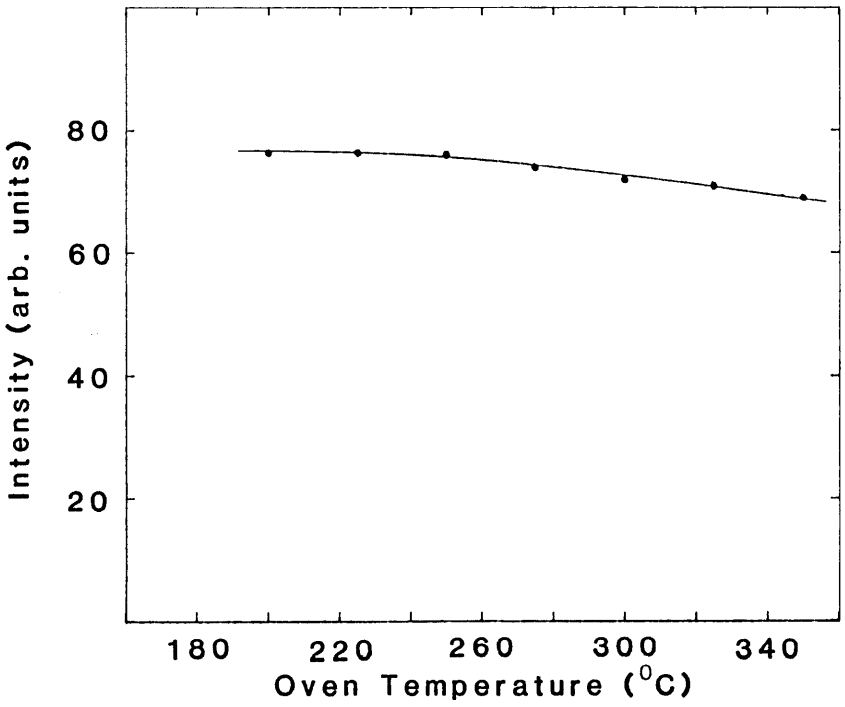

Figure 3.3 He II 4686 Å spontaneous emission as a function of oven temperature. Conditions: 20 Torr helium and 120 mA/anode discharge current

take this as evidence that n_e falls only slightly as the oven temperature is raised.

Along with a need to know the electron density, there is also a need to know the form of the electron energy distribution function for a hollow cathode configuration. Experimental studies by Kagan et al. (1973), Borodin and Kagan (1966), Soldatov (1971) and Gill and Webb (1977) have shown that the electron energy distribution in the hollow cathode differs considerably from that in a positive column discharge.

The hollow cathode discharge operates in the negative glow region and the electron energy distribution function departs strongly from Maxwellian in that it has a greater proportion of high energy electrons.

This arises because of the proximity of the cathode fall to the negative glow. Electrons emitted from the cathode surface are accelerated through the cathode fall and undergo multiplication.

According to Gill and Webb there are three distinct regions to the energy distribution function:

1. An electron beam component at the full cathode energy eV_c resulting from the small number of primary electrons entering the negative glow without undergoing excitation and ionization collisions. The number of electrons in this beam component as a fraction of the total distribution was measured by Webb to be $\sim$0.1 - 0.3.
2. There is a small peak at an energy of eV_t (V_t equals the cathode fall voltage minus 20V) corresponding to those electrons which have undergone one inelastic collision. From eV_t downwards to low energies the distribution shows an appreciable "tail" of high energy electrons. Gill and Webb estimate that the number of high energy electrons between 24.6 eV and eV_t is about 0.3 to 0.45 of the total number.
3. At low energies (<24.6 eV) there is a plasma component which contains most of the electrons in the distribution. This arises because secondary electrons, produced by ionization processes, acquire very little energy from the small electric field present within the hollow cathode.

In order to provide a visual reference and aid in the discussion to follow, a sketch indicating the general features of the distribution function is shown in Figure 3.4.

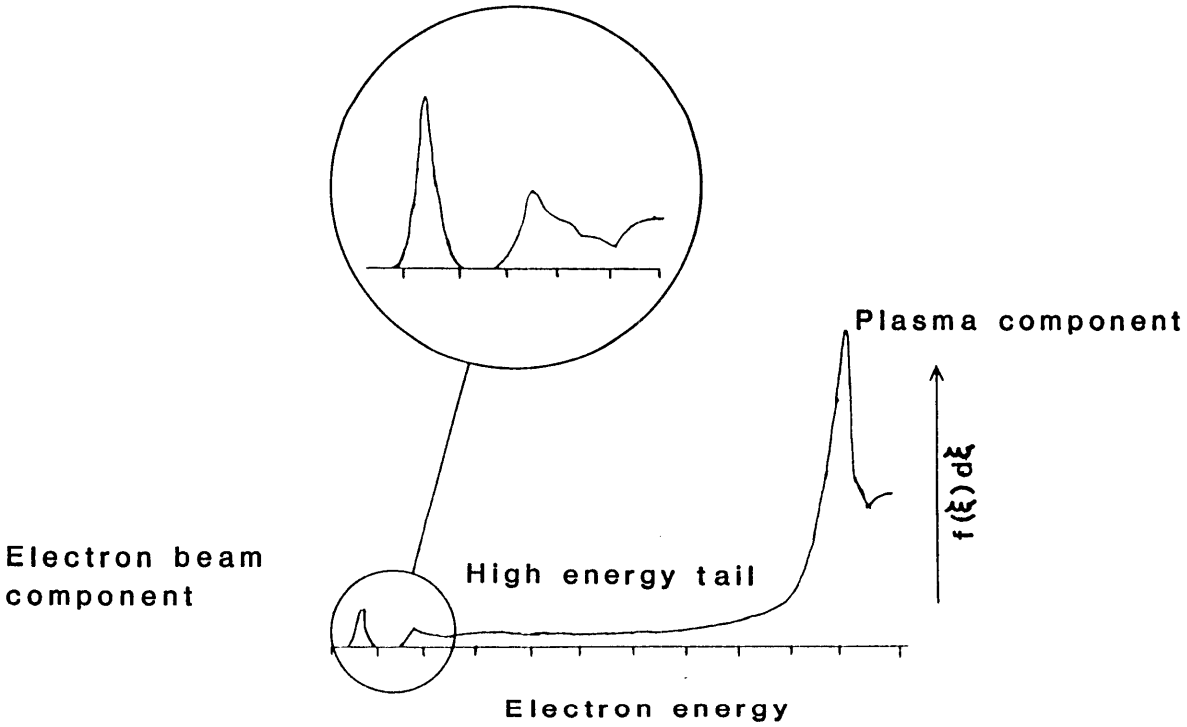

Figure 3.4 A sketch showing the general features of the electron energy distribution function in a hollow cathode discharge

As elastic collisions and inelastic excitation and ionization collisions determine the shape of the distribution function, variation of the discharge parameters of pressure, current and metal vapour concentration should have a marked effect. Indeed studies by Kagan et al. (1973), Soldatov (1971) and Gill and Webb (1977) have shown that:

1. An increase in the helium pressure results in the most probable energy shifting to lower energies and conversely a decrease in the pressure shifts it to higher energies.

2. An increase in the discharge current shifts the most probable energy to higher electron energies and decreases the height of the maximum.

3. An increase in the metal vapour concentration shifts the most probable energy to lower electron energies.

As mentioned previously, the electrons in the hollow cathode are believed to consist primarily of two groups: a small number of high energy electrons and a larger number of secondary (thermal) electrons. Knowledge of the mean electron temperature for the group of secondary electrons and its variation with current and pressure is helpful in calculating the importance of electron collision mechanisms. To determine the electron temperature the following method was used.

The relative intensities of lines in the spectral series np^3P_o - $2s^3S_1$ of He for n = 3 - 13 were measured in a pure helium discharge. Measuring the electron temperature in this manner assumes a thermal velocity distribution for the electrons which, for the situation examined here, is not strictly the case. However, the measurements should reflect an effective temperature for the more numerous slow electrons. This method requires the existence of a local thermal equilibrium (LTE) amongst the bound states of the radiating species being examined, and this can only be expected if collisional processes are more important than radiative decay and recombination. This condition could not be evaluated because of the large uncertainties associated with the electron energy distribution function. Such estimates as could be made, using a Maxwellian velocity distribution and the collision cross section data of Fujimoto (1978), suggest that this condition is never satisfied thus placing doubt on the assumption of LTE that is required for the analysis.

In view of the fact that the existence of LTE is questionable no accurate electron temperature data can be obtained from this experiment but the results should indicate approximately the energy of the more numerous slow electrons.

To determine the electron temperature from the spectroscopic intensity data the following expression relating the intensity ratio to kT_e was used (Griem, 1963);

$$\ln\left[\frac{I_{ji}\,\lambda_{ji}^3\,f_{ik}}{I_{ki}\,\lambda_{ki}^3\,f_{ij}}\right] = \frac{E_k - E_j}{kT_e}$$

where the I's are the total integrated intensities of the transitions at wavelengths λ_{ji} and λ_{ki} respectively, and f's are the corresponding absorption oscillator strengths, E_k and E_j are the energies (eV) of the upper levels (k and j) of the transitions and kT_e is the Boltzman constant k multiplied by the electron temperature. Thus a plot of $E_k - E_j$ as a function of $\ln(I_{ji}\,\lambda_{ji}^3\,f_{ik}/I_{ki}\,\lambda_{ki}^3\,f_{ij})$ will yield a straight line of slope kT_e.

Figure 3.5 shows results of the electron temperature measurement obtained using the $np^3P_o - 2s^3S_1$ series of He I. For these experiments, the detection system, consisting of a spectrometer and photomultiplier, was calibrated using a calibrated tungsten ribbon lamp. Over the range of currents applicable to experimental conditions the np^3P_o levels appeared to be in LTE for $n > 7$ on the basis that a straight line was obtained on the graphs of $E_k - E_j$ versus $\ln(I_{ji}\,\lambda_{ji}^3\,I_{ik}/I_{ki}\,\lambda_{ki}^3\,f_{ij})$ for values of the principal quantum number greater than this. As shown in Figure 3.5 the electron temperature increases linearly from 0.04 eV to 0.09 eV as the current increases from 60 mA/anode to 200 mA/anode. Also shown is the variation of kT_e with helium pressure. The results obtained are in good agreement with those of McNeil (1977) for a He hollow cathode

discharge. The presence of the strong cadmium spectra made it impossible to extend the present measurements to the He-Cd discharge.

The results of the electron temperature measurement would suggest that the most probable energy of the group of thermal electrons is at energies << 1 eV. The results obtained, and those of McNeil should, for the reasons already discussed, be treated with caution. The need for this caution was emphasized by the fact that, for one set of experimental conditions, the observed electron temperatures were lower than the gas temperature results reported in section 2.3.5. This unphysical result

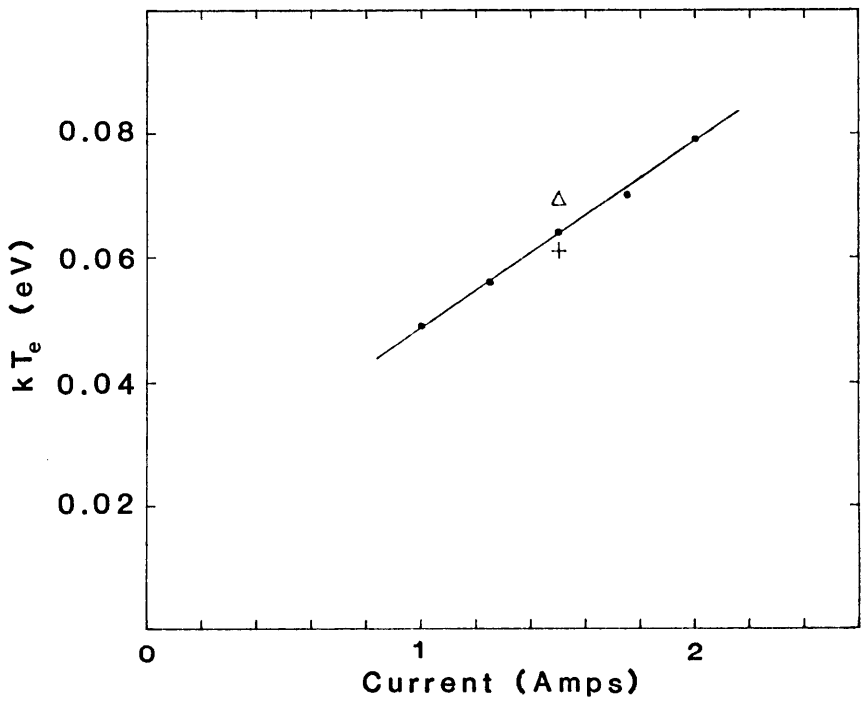

Figure 3.5 Plot of the measured electron temperature (kT_e) versus discharge current in a "pure" helium hollow cathode discharge: • for 20 Torr, + 30 Torr and Δ for 10 Torr

casts doubt on the assumption of LTE, used to determine T_e, and suggests that the He I ($n \geq 7$) and the $N_2^+ B^2\Sigma_u^+$ (used respectively for T_e and T_g measurements) are both equilibrated by the gas rather than the electrons.

3.3 THE OPTICAL SYSTEM

3.3.1 Optical Alignment Procedure

The placement and dimension of the two optical stops which enable metastable densities to be determined along the axial region of the discharge tube were described in section 2.2. Stop B, of radius 50 μm, was mounted with black tape to the entrance slit of the spectrometer. The 1 mm diameter principal stop was mounted in the micropositioning section of an Oriel spatial filter (Model 1522) and placed as close as possible to the end of the discharge tube in accordance with the criteria established in section 2.2.

The optical stops were placed on the axis of the discharge tube by the following procedure: A small collimating telescope, mounted in vertically and horizontally adjustable mounts, was placed on the optical rail and adjusted until it was aligned with the optical axis of the discharge. The principal stop was positioned, back illuminated and adjusted until it was concentric with the centre of the graticule on the collimating telescope. The smaller stop was then placed on the entrance slit of the spectrometer, which itself was mounted on a rigid platform that was adjustable in both the vertical and horizontal directions. The smaller stop was then back illuminated and, by adjustment of the

spectrometer mount, was positioned until it was concentric with the principal stop as viewed through the collimating telescope. Finally, a He-Ne laser was passed through the collimating telescope, discharge tube and the stops A and B to provide easy reference for alignment checks and re-alignment.

Light from that section of the discharge lying within the viewing cone of the stops entered a 0.5 m Ebert scanning spectrometer (Jarrell Ash Model 82-025). The output from the spectrometer was detected by a photomultiplier (EMI 9750 QB) connected to an electrometer (Vibron Model 33B-2) and the signal displayed on a chart recorder (Rikadenki B261).

A discharge length ratio of 3:1 was found to be convenient for the measurement of metastable densities. Discharges with lengths in this ratio were obtained by operating a single anode (associated with discharge length 1) and three anodes with non-overlapping glow regions to obtain a discharge of length 3l. Under these conditions the external wall temperature was less than the oven temperature and auxiliary heating was required to prevent condensation of metal vapour on the tube walls. This auxiliary heating was provided by passing a current of $\sim$10A through a 2.5 m length of tungsten ribbon (2.5 $\Omega\ m^{-1}$ resistance) wrapped along the entire length of the discharge tube and insulated with asbestos tape and aluminium foil.

3.3.2 Check of Alignment

The optical system described in section 2.2 is such that equal light intensities should be obtained from equal lengths of the discharge. This may be checked directly in the present experiment by comparing the

signals obtained when each individual anode is run separately. Typical results for the 3889 Å intensity as a function of anode number are shown in Figure 3.6.

These results show that, with the exception of the two end anodes, the light signal is independent of distance from the spectrometer. The lower signal from the end anodes is due to small ceramic inserts which limit the associated discharge length.

This alignment check could be carried out at any stage of the measurements and regular checking showed that the system remained stable during the course of the experiments.

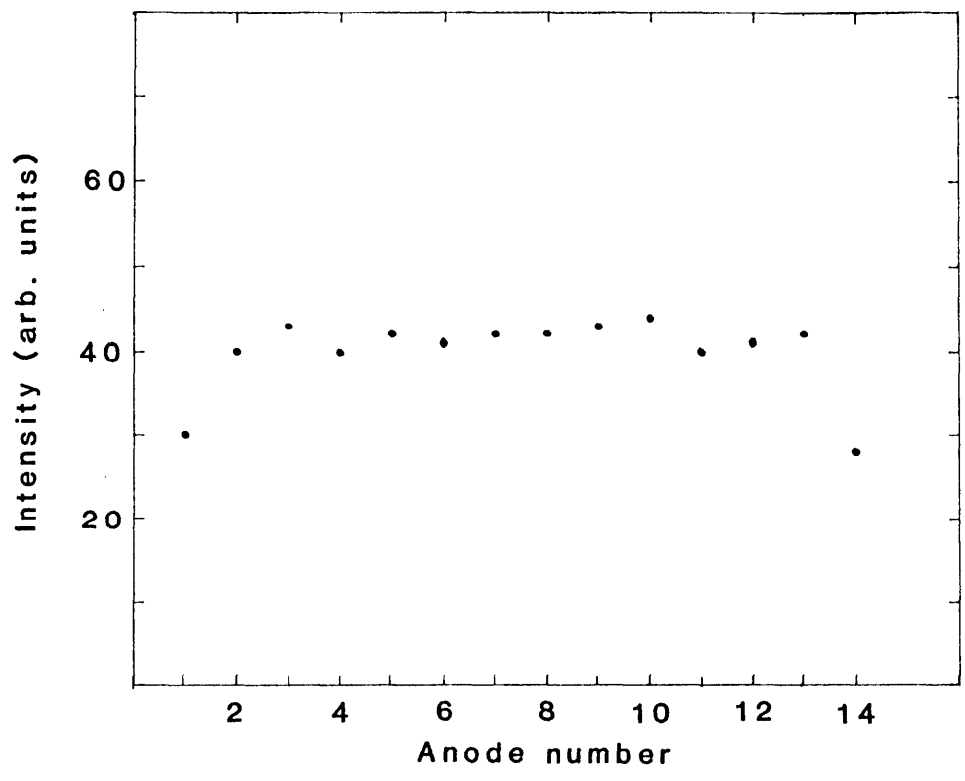

Figure 3.6 Variation of the 3889 Å spontaneous emission with different spectrometer-to-plasma distances. Anode 1 is the anode nearest the spectrometer

3.4 DENSITY MEASUREMENTS IN PURE HELIUM

3.4.1 Upper Level Effects

As stated in section 2.3.2. the reduced number densities will yield the absolute density provided that the population of the upper level of the transition is negligible. With the geometric arrangement of optical stops used in the fractional absorption experiment, insufficient intensity was available to make a study of the upper level effects for the 2^3S level. For the 2^1S population, only at 3965 Å ($4^1P - 2^1S$) was the intensity sufficient to allow an estimate to be made. Using the analysis of section 2.3.2 the absorption coefficient ratio was found to be

$$\frac{k_0\ (3^1P - 2^1S)}{k_0\ (4^1P - 2^1S)} = 3.6 \pm 0.6$$

which is very close to the expected value of 3.78. No systematic variation of this value with current and pressure was observed.

Thus the upper level populations have little or no effect on the reduced number density calculation and the intensity ratio measurements could be converted directly to the absolute density of the 2^1S species. Further support for this, and for extension of the conclusion to the 2^3S species, comes from the fact that the measured populations of the 2^1P, 2^1S and 2^3P levels were 5-10 times smaller than that of the 2^3S level. Since it would be expected that the density of other high lying levels ($>2^1P$, 2^3P) including the 3^3P, 3^1P levels, upper levels of the 3889 Å and 5016 Å transitions respectively, must be smaller still, the intensity ratios were converted to absolute (rather than reduced) number

densities in all cases.

3.4.2 Gas Temperature Effects

As discussed in Appendix A2, the gas temperature in pure helium is a monotonically increasing function of current and, since the Doppler width of a spectral line is proportional to the square root of the gas temperature then the Doppler width itself is increasing. Although it was shown in section 2.3.5 that the intensity ratio was only very weakly dependent upon gas temperature this is not the case when the number density (or reduced number density) is calculated from the absorption coefficient k_0.

From equation (2.6)

$$N_1 \propto \Delta\nu_D \, k_0$$

and thus gas temperature variations will have a direct impact on the calculated number density.

In the light of the gas temperature data this factor, apparently overlooked in previous investigations, will be included in the calculation of the excited state densities from the fractional absorption experiment.

3.4.3 Density Measurements in Pure Helium

Results showing the 2^1S, 2^3S, 2^3P and 2^1P density variations with current and pressure in a pure helium discharge are shown in Figures 3.7

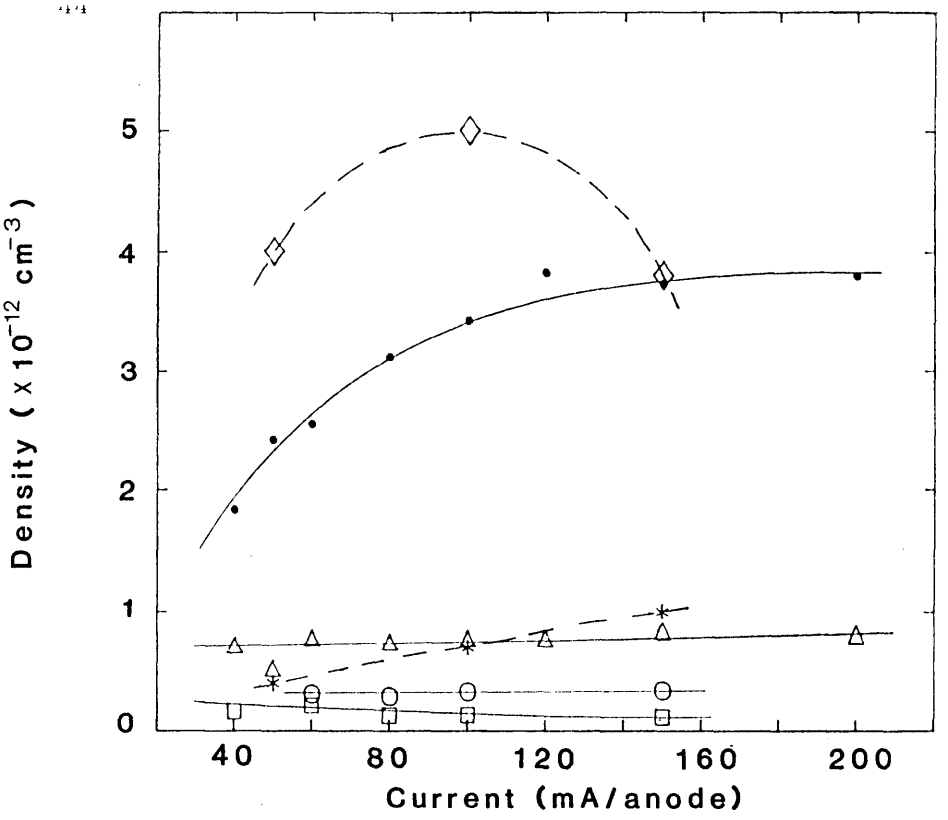

Figure 3.7 Current dependence of the 2^3S (•), 2^1S (Δ), 2^1P (o) and 2^3P (□) densities in a "pure" helium discharge at 20 Torr. Also shown are the results of Browne and Dunn (1973) (◊) in a positive column discharge and McIntosh et al. *(1978) (✳)*

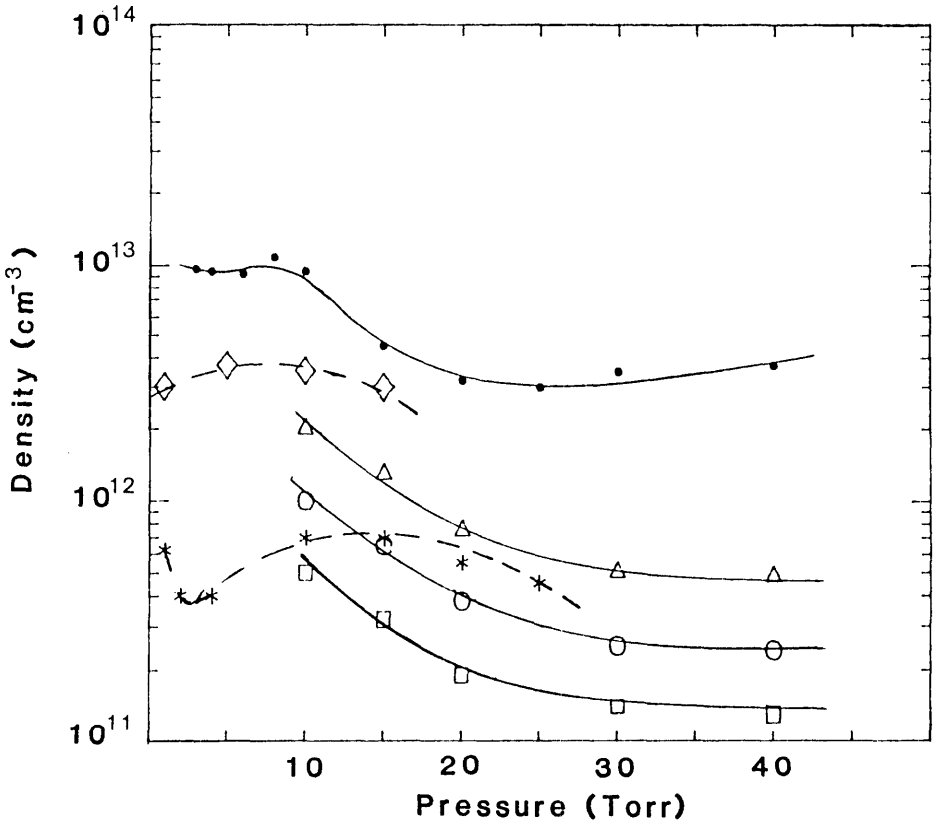

Figure 3.8 Pressure dependence of the 2^3S (•), 2^1S (Δ), 2^1P (o) and 2^3P (□) densities in a "pure" helium discharge at a current of 120 mA/anode. Also shown are the results of Browne and Dunn (1973) (◊) and McIntosh et al. *(1978) (✳)*

and 3.8. These densities were calculated from the fractional absorption at 5016 Å, 3889 Å, 5875 Å and 4921 Å for the 2^1S, 2^3S, 2^3P and 2^1P levels respectively.

The 2^3S density increases linearly with current up to 100 mA/anode after which the metastable density saturates. On the other hand, for the current range studied (40 mA/anode - 200 mA/anode), the 2^1P, 2^1S and 2^3P densities remain very nearly constant.

On the basis of the differing statistical weights, one would expect the population of the 2^1S level to be one third that of the 2^3S, but the results show an order of magnitude difference between these populations. This difference between the experiment and expected value could be due to the reaction

$$He\ (2^1S) + e \rightarrow He\ (2^3S) + e$$

The cross section for this reaction is large at low energies (Marriott, 1966) and hence it provides an efficient means for depleting the 2^1S density when there is a predominance of thermal electrons.

The saturation of the He (2^3S) density with current is expected on the basis of the following argument. The rate equation for the 2^3S species can be written as

$$\frac{dN(2^3S)}{dt} = n_e N_0 k_{0m} - \frac{N(2^3S)}{\tau_D} - n_e N(2^3S)\ k_{mj}$$

where n_e, N_o and $N(2^3S)$ are the electron, ground state helium and 2^3S metastable densities respectively. The production term $(n_e N_o k_{om})$ represents production via electron excitation from the ground state plus cascade from other high lying helium levels. The electron de-excitation term $(n_e N(2^3S)\ k_{mj})$ includes de-excitation to the ground state,

ionization and excitation and $N(2^3S)/\tau_D$ is the loss rate via diffusion. Assuming steady state conditions (i.e. $dN(2^3S)/dt = 0$) then the metastable density can be written as

$$N(2^3S) = \frac{n_e N_0 k_{0m}}{(1/\tau_D) + n_e k_{mj}} \tag{3.1}$$

and for high current densities $n_e k_{mj} >> \tau_D$ so that

$$N(2^3S) \rightarrow \frac{k_{0m}}{k_{mj}} N_0 \tag{3.2}$$

thus predicting saturation with increasing current. Insufficient data are available to permit a quantitative calculation of the $N(2^3S)$ saturation density.

Figure 3.8 shows that the densities of the 2^3S, 2^1S, 2^1P and 2^3P levels decrease for pressures greater than 8 Torr. At the same time it is observed that the relative populations of the levels remain very nearly constant.

An increase in the helium pressure shifts the peak in the electron energy distribution function to lower electron energies and results in an increase in the collisional knockdown rate. Also, the threshold for q_e is 19.8 eV (q_e the excitation collision cross section) while that for q_i is $\backsim$5 eV (q_i the ionization collision cross section) and consequently any shift to lower energies of the plasma component of the energy distribution will cause an increase in $\langle q_i v \rangle$ and a smaller decrease in $\langle q_e v \rangle$ which depends rather more on the tail of the distribution which is less affected by the change in pressure. The net result of these

effects would be a decrease in the metastable density. Increasing the helium pressure also increases the probability of forming molecular metastables He_2^*, but no evidence for the presence of these species was ever found.

The variation with pressure of the population of the 2^3P, 2^1P and 2^1S levels can be explained by similar arguments to those applied to the 2^3S population.

Figure 3.8 shows that, for helium pressures greater than 35 Torr, the He (2^3S) density remains constant. As discussed in section 4.5.3 for increases in helium pressure above 35 Torr the electron density saturates. At the same time it would be expected that the change in the peak of the electron energy distribution would not be very marked, thus resulting in a stabilization of the electron excitation, de-excitation and ionization rates and hence the metastable density.

Figures 3.7 and 3.8 show a comparison between the present results and those of other groups. Although the comparisons are complicated by different discharge types and tube diameters, all the data show similar current and pressure dependence to those observed in the present study.

Since the effect of the change in gas temperature with current and its consequence for the measured level population has apparently been overlooked in previous investigations, Figure 3.9 is included to illustrate the important change this makes to the shape of the curve representing 2^3S density as a function of current.

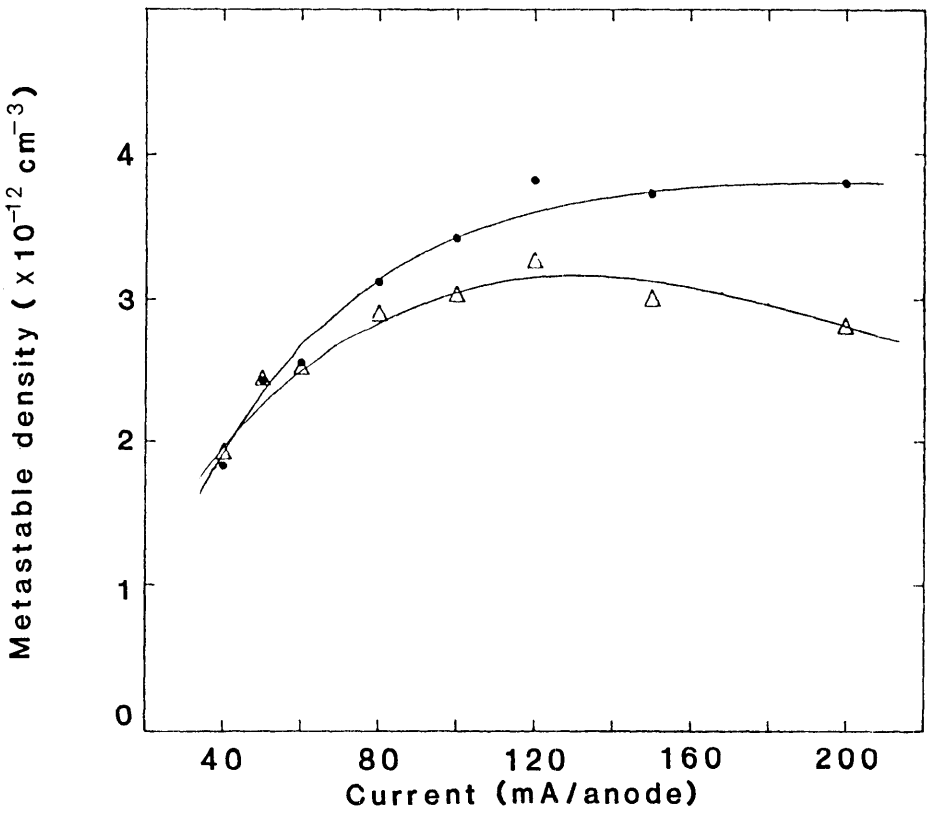

Figure 3.9 *A comparison showing the effect of including the gas temperature dependence of the Doppler width on the calculated 2^3S density.*

Δ - *result assuming constant Doppler width corresponding to* T_g = 620 K

• - *result, accounting for the Doppler width variation with gas temperature*

3.5 EFFECTS OF ADDING CADMIUM VAPOUR TO THE DISCHARGE

3.5.1 Excited State Populations as a Function of Increasing Cadmium Concentration

The effect on the densities of the 2^3S, 2^1S, 2^3P and 2^1P levels of adding cadmium vapour to the discharge is shown in Figure 3.10. With increasing cadmium concentration the density of all levels is reduced. In particular the 2^3S metastable level undergoes the largest variation, decreasing by a factor of 80 over the oven temperature range studied.

This reduction in density is due to a number of effects. In the presence of cadmium, excited helium atoms will be destroyed upon a collision with a cadmium atom so that equation (3.1) governing the 2^3S metastable density must be rewritten as

$$N(2^3S) = \frac{n_e k_{0m}}{(\frac{1}{\tau_D} + k_{mj} n_e + K^P_{TOT} N_{Cd})}$$

where $K^P_{TOT}N_{Cd}$ is the Penning collision rate. Since the Penning rate is a significant fraction of the electron de-excitation and ionization rates and becomes more significant with increasing cadmium concentration, the effect of this collision mechanism would be to reduce the metastable density. Also, as discussed in section 3.2, the addition of cadmium to the discharge shifts the peak in the electron energy distribution to lower energies resulting in an increase in the de-excitation and ionization rates of the triplet level and thus a reduction in the metastable density. Lowering the peak of the electron energy distribution should also decrease the rate of excitation of the 2^3S level, but this is at least partly offset by the increase in the cathode

fall potential and a corresponding increase in the energy of the "beam" electrons. Browne and Dunn (1973) found that the decrease in the rate of excitation of the 2^3S metastable level was the main reason for the decrease in population in a He-Cd positive column device.

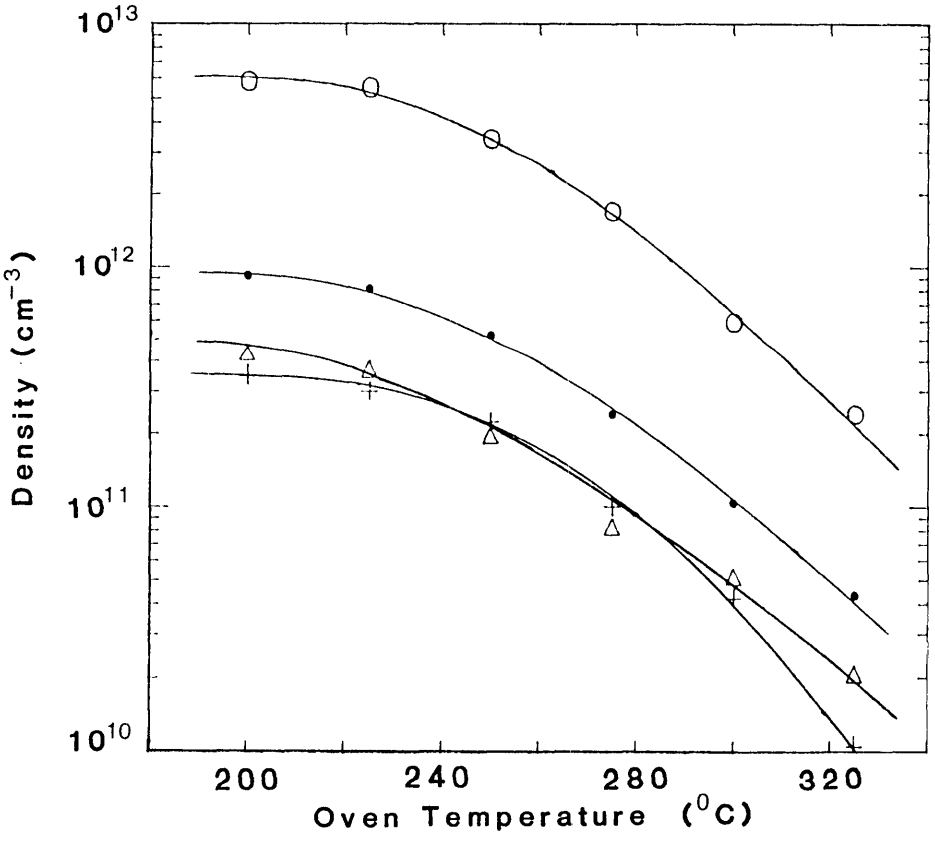

Figure 3.10 Oven temperature dependence of the 2^3S (O), 2^1S (•), 2^1P (Δ) and 2^3P (+) densities for a helium pressure of 20 Torr and a discharge current of 120 mA/anode

The decrease in the 2^1S metastable density can also be explained in terms of increased losses through Penning collisions, electron knockdown and ionization and a slight decrease in the electron excitation rate. The dependence on cadmium concentration is not as marked as for the

triplet metastable density because the 2^1S excitation cross section is a slowly varying function of electron energy and not a rapidly varying function peaking at threshold as for the 2^3S level.

3.5.2 Variation with Discharge Current and Helium Pressure

Variation of the 2^3S, 2^1S, 2^3P and 2^1P densities with increasing current and pressure are shown in Figures 3.11 and 3.12. With increasing current and pressure the behaviour of the helium levels is similar to that in pure helium except that, for the reasons discussed in section 3.5.1, the curves have been shifted to lower density values. The only major difference is that the saturation current for the He (2^3S) metastable density has been shifted to a higher value. This is again expected from the crude model represented by equation (3.1) because, with inclusion of the Penning collision term, the condition for saturation becomes

$$n_e k_{mj} > \frac{1}{\tau_D} + K^P_{TOT} N_{Cd}$$

and a larger electron density (i.e. discharge current) is required to produce saturation.

The results presented in Figures 3.10, 3.11 and 3.12 are in reasonable agreement with those of Grace and McIntosh (1979) for the same tube as used in this present study, Browne and Dunn (1973) for a helium-cadmium positive column discharge and Gill and Webb (1978) in a hollow cathode He-Zn discharge. As discussed in section 3.4, comparison of

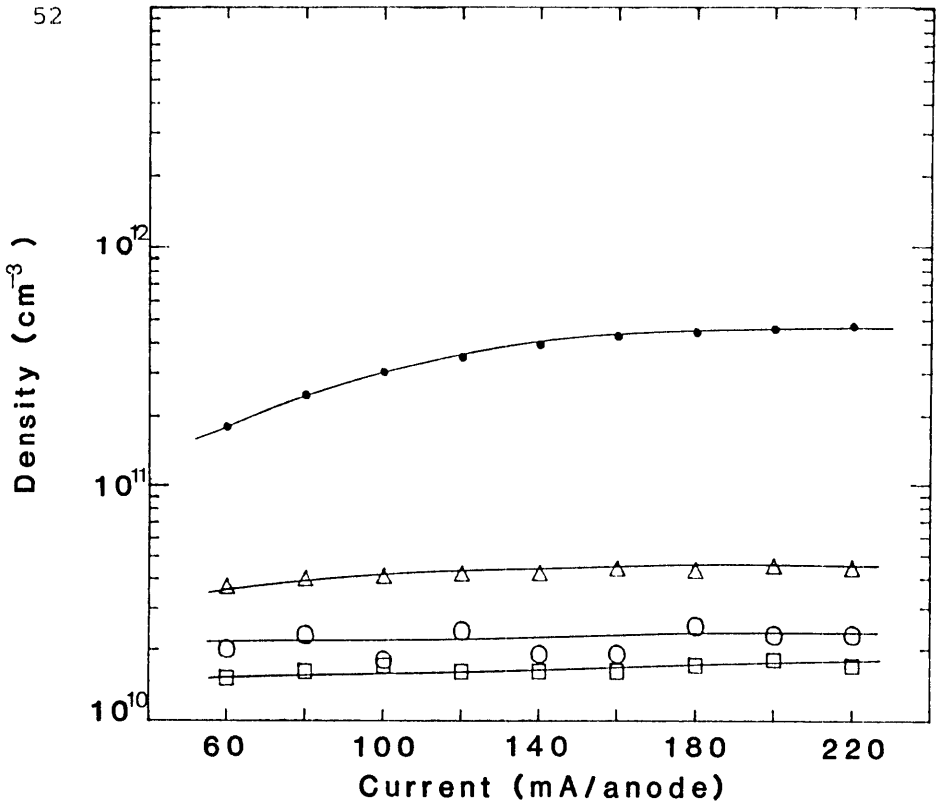

Figure 3.11 Current dependence of the 2^3S (•), 2^1S (Δ), 2^1P (0) and 2^3P (□) densities for an oven temperature of 320^0C and 20 Torr helium

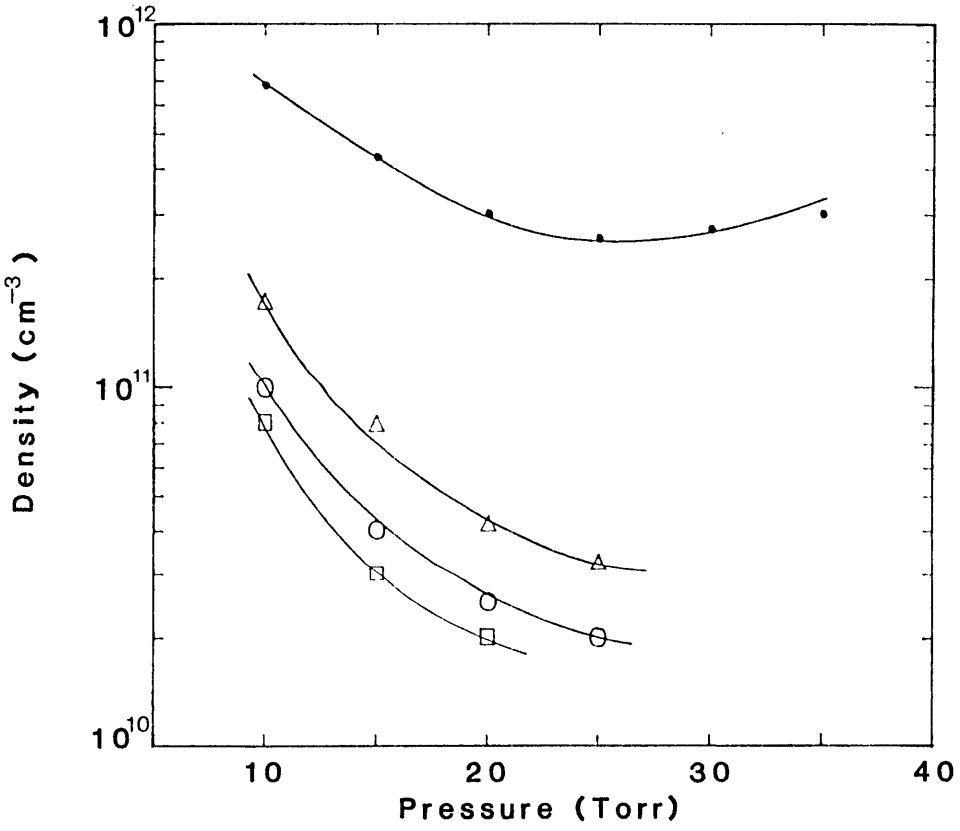

Figure 3.12 Pressure dependence of the 2^3S (•), 2^1S (Δ), 2^1P (0) and 2^3P (□) densities for an oven temperature of 320^0C and 120 mA/anode discharge current

results is difficult but all exhibit similar dependences on oven temperature, discharge current and helium pressure.

3.5.3 Check of Upper Level Effects with Cadmium Added to the Discharge

Because the 2^3S density decreases more significantly with cadmium concentration than the 2^1S, 2^1P and 2^3P levels it was felt that, although upper level effects appeared to be negligible in the studies in pure helium, this might not be true in the presence of cadmium. Again, for reasons already discussed, upper level effects could only be investigated for transitions terminating on the 2^1S metastable level and the results extrapolated to encompass the triplet metastable species. The measured ratio

$$\frac{k_0\ (3^1P - 2^1S)}{k_0\ (4^1P - 2^1S)} = 3.5 \pm 0.9$$

agreed with the expected value again suggesting that upper level effects are insignificant but the large experimental uncertainty associated with this measurement, due to the weak intensity at 3965 Å, means that this result should be treated with caution.

3.6 ERRORS ASSOCIATED WITH DETERMINATION OF THE METASTABLE DENSITY

Uncertainties associated with the results of the excited state density measurements arise through a number of factors. Firstly, there is the error associated with the measurement of the intensity ratios; secondly, there are errors associated with the evaluation of equation 2.5

(giving the theoretical value for $k_o l$); and thirdly, there are errors associated with the discharge length data of Grace (1978). As stated in section 2.3.5, errors in the evaluation of equation 2.5 are small, typically ~1%, and can be ignored when compared with the uncertainty in the discharge length which is the major contributor of uncertainty in the density measurement results.

The discharge length measurements of Grace used throughout this present study were obtained from measurements of the potential, with respect to the grounded cathode, of a small movable probe inserted along the discharge tube. The length of the discharge associated with each anode was arbitrarily taken as the distance between points where the probe voltage had fallen to one half of the value of the voltage when the probe was positioned under the anode. This assumption automatically results in errors of ± 20% in the quoted values for the discharge length. Further, day to day variations in the discharge tube operation would give rise to additional errors but no data can be found for this effect on the accuracy of the discharge length measurements.

In any case, the density measurements presented in the preceding sections are the average of ten individual experiments. While there was a large variation, of approximately ± 25%, in the calculated density between individual experiments, the current, pressure and oven temperature dependence of all experiments was identical. The errors described above refer to errors associated in the day to day measurement of the intensity ratios which, in turn, depend on the day to day performance of the hollow cathode discharge.

The combined effect of the uncertainties in discharge length and intensity ratios is to produce population densities whose absolute values

are accurate only to ± 25% but whose trends with changes in the discharge parameters are known with a high degree of reliability.

3.7 SIGNIFICANCE OF THE HELIUM METASTABLE DENSITY RESULTS

In the past, previous authors (for example Grace and McIntosh 1979; Browne and Dunn, 1973) have used results of a study of the parametric variation with current, pressure and cadmium concentration of the metastable density to establish the collision mechanisms leading to the formation of the $5s^2\ ^2D_{5/2}$ level of Cd II. If Penning ionization is the sole excitation mechanism then the parametric behaviour of the product of the cadmium ground state and metastable densities should follow that of the 4416 Å spontaneous emission.

The 4416 Å spontaneous emission was measured using the optical system described previously for the measurement of intensity ratios. The spontaneous emission from the discharge segment associated with only one anode was observed to enable a direct comparison, for identical discharge conditions, of the spontaneous emission and metastable densities. Although the use of a single glow segment differs from the overlapping multiple glows of the laser, Gill (1975) has shown that inferences made from the former can be applied directly to the latter.

Since the absorption experiment yielded the metastable density per unit volume of discharge, any comparison between this quantity and the 4416 Å spontaneous emission requires that we convert the latter to intensity per unit volume. Because absolute intensities of the 4416 Å signal were not required, the spontaneous emission per unit volume was determined simply by dividing the total signal by the discharge length

appropriate to the operating conditions.

3.7.1 Comparison of the 4416 Å Spontaneous Emission with the Penning Rate as a Function of Current

If it is assumed that the cadmium concentration is independent of the discharge current, then a direct comparison of the 4416 Å spontaneous emission with the current dependence of the 2^3S metastable density will give the required information. Figure 3.13 shows the current dependence of the metastable density and 4416 Å spontaneous emission. The 4416 Å spontaneous emission increases linearly up to a current of $\sim$90 mA/anode thereafter rising in a slightly less than linear rate to the limit of current investigated. On the other hand the metastable density rises to its maximum value at a current of 180 mA/anode and then saturates.

The differences between the 4416 Å spontaneous emission and the He (2^3S) metastable and the observation that the 4416 Å spontaneous emission has a near linear increase for currents greater than 70 mA has been used by Grace and McIntosh (1979) and Takasu et al. (1982) as evidence to suggest that electron excitation mechanisms are at least partly responsible for populating the $5s^2\ ^2D_{5/2}$ level of Cd II.

However, in the absence of any evidence to the contrary these workers have assumed that T_g is constant and that the Penning rate which was compared with I_{4416} was proportional to $N(2^3S).N(Cd)$. In fact, the results in Appendix A2 show that T_g is not constant and hence the comparison of I_{4416} and Penning rate must take into account the explicit dependence on T_g.

The Penning collision rate is given by

$$N_{Cd} < \sigma_p v > = N_{Cd} \int_0^\infty \sigma_p (v)\ v^2\ f(v)\ dv$$

where vf(v)dv is defined as the fraction of He (2^3S) metastable species with velocities in the range v to v+dv and $\sigma_p(v)$ the total Penning collision cross section. This expression can be reduced to

$$N_{Cd} < \sigma_p v > = N_{Cd}\ \sigma_p \bar{v}$$

provided that, over the thermal velocity ranges considered, $\sigma_p(v)$ is independent of velocity (temperature).

No theoretical calculations are available to validate this assumption but various experimental results suggest that it is not unreasonable. For example Baltayan et al. (1985) found the thermally averaged cross section for Penning collisions between cadmium neutral and the helium metastable atoms to be

$$\sigma_p = (6.4 \pm 1.3) \times 10^{-15}\ cm^2$$

which is in excellent agreement with the value obtained by Collins (1973) and Bochkova and Tolmachev (1979). In view of the fact that the results of Baltayan et al. were obtained at room temperatures whereas experiments reported by Collins and Bochkova and Tolmachev were performed at temperatures between 300K and 500K, these results can be interpreted to indicate that the energy (velocity) dependence of the Penning collision cross section is quite weak.

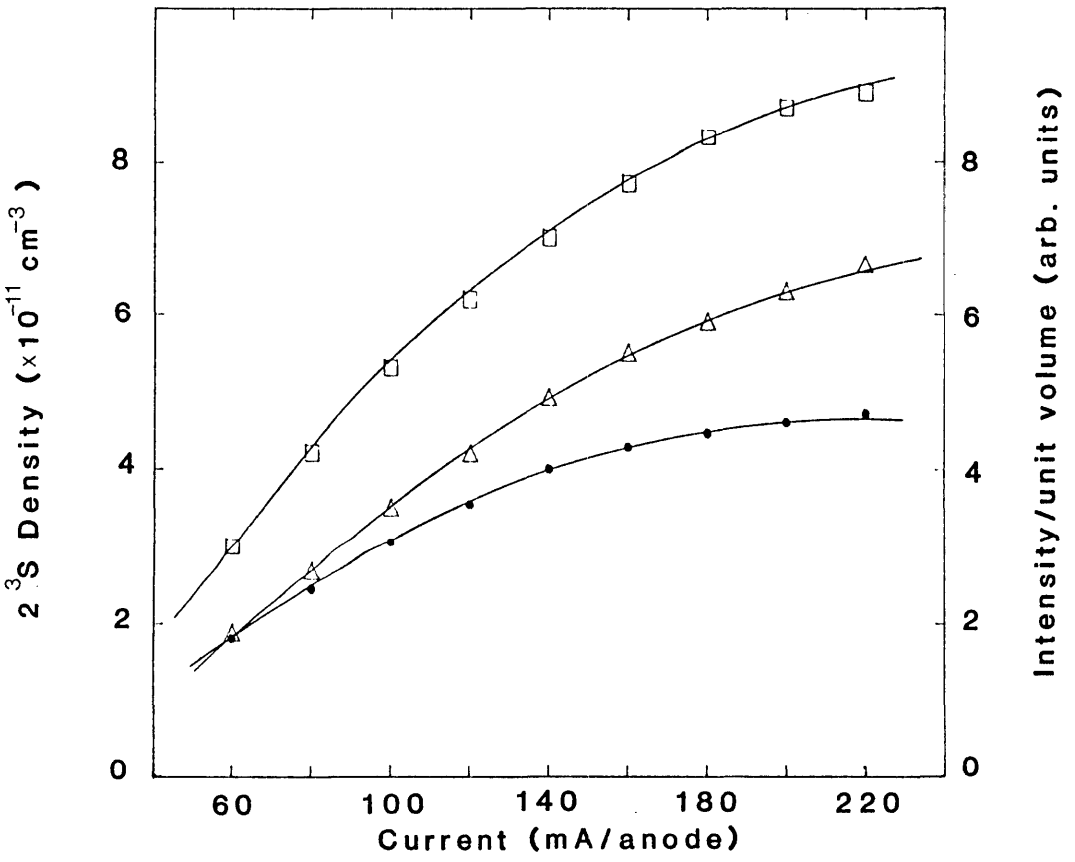

Figure 3.13 Comparison of the 4416 Å spontaneous emission/unit volume (□) with the 2^3S metastable density (•) and the product $N(2^3S)xT_g^{\frac{1}{2}}$ (Δ) for an oven temperature of 320^{0}C and 20 Torr helium

For a Maxwellian distribution of velocities (McDaniel, Chapter 2)

$$v = \sqrt{\frac{8\pi}{k}}\, T_g^{\frac{1}{2}} \left[\frac{1}{M_{He}} + \frac{1}{M_{Cd}}\right]^{\frac{1}{2}}$$

and the Penning rate is seen to be directly proportional to $T_g^{1/2}$.

The comparison between I_{4416} and the Penning rate at a constant

oven temperature is then made by comparing I_{4416} not with $N(2^3S)$ but with $N(2^3S) \times T_g^{1/2}$. The results, obtained using the data of Appendix A2, are shown in Figure 3.13.

The two curves now appear in quite reasonable agreement and the conclusion that I_{4416} is not solely due to Penning collisions can no longer be justified. The small discrepancies between these two curves can be explained in terms of an increase in the upper level effect and a possible variation in the cadmium ground state density with current, both resulting in an underestimate of the Penning rate at high currents.

3.7.2 Comparison of the 4416 Å Spontaneous Emission with the Product $N(2^3S).N(Cd)$ as a Function of Cadmium Concentration

Since the metastable density rapidly decreases and the cadmium concentration (partial pressure) rapidly increases as the oven temperature increases, the product $N(2^3S).N(Cd)$ must reach a maximum and thereafter decrease. This trend is shown in Figure 3.14. Also shown is the oven temperature dependence of the 4416 Å spontaneous emission/unit volume. As can be seen from this figure there is general agreement between these two curves except at high oven temperatures (cadmium concentrations).

The discrepancies evident at high oven temperatures could be due to a number of factors. Firstly, the upper level effects could lead to an underestimate of the true metastable density. Secondly, as discussed in Appendix A2 no results are available for the variation of gas temperature with cadmium concentration but T_g is expected to increase because of an increase in the electrical power input. Thus the gas temperature effects associated with the Doppler width and Penning collision rate coefficient

have not been included in calculating the Penning rate at high oven temperatures.

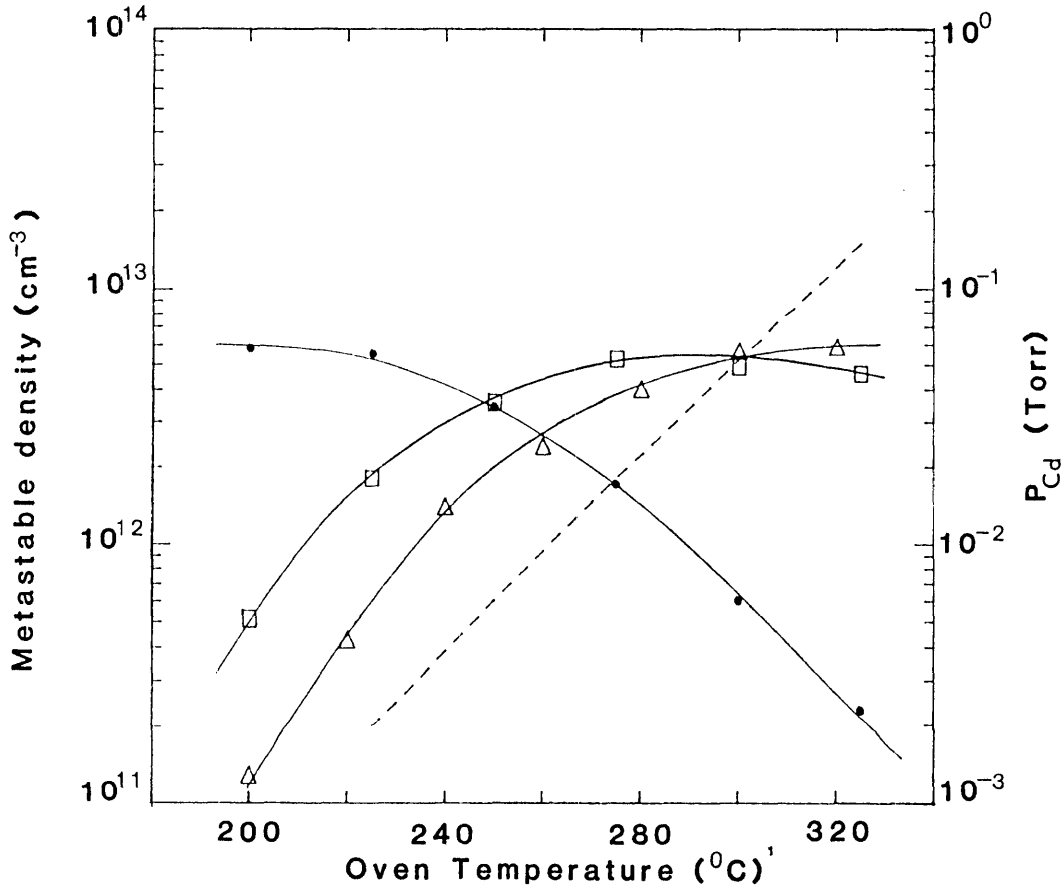

Figure 3.14 Variation of the 2^3S density (•) and saturated cadmium partial pressure (---) with oven temperature. Also shown are the variations of the product $N(2^3S).N(Cd)$ (□) and the 4416 Å spontaneous emission (Δ). Conditions: 20 Torr helium, 120 mA/anode

Finally, the use of the saturated vapour pressure equation for a flowing system could lead to an overestimate of the true cadmium density. Also, the experimental results of section 5.4 suggest that the oven temperature does not acquire the value as measured by the thermocouple placed externally on the oven sidearm. The discrepancy between the oven

temperature and sidearm temperature becomes more significant at the higher temperature values. As the sidearm temperature was used to calculate the cadmium partial pressure this suggests that the cadmium density (Figure 3.14) has been overestimated especially at high oven temperature values. An attempt was made to measure directly the cadmium neutral density (see Appendix A3) but, for reasons not fully understood, inconsistent results were obtained.

3.7.3 Comparison of the 4416 Å Spontaneous Emission with the Product $N(2^3S).N(Cd)$ as a Function of Helium Pressure

Figure 3.15 shows the comparison of the 4416 Å spontaneous emission and the He (2^3S) metastable density as a function of helium pressure. In this case it is assumed that the cadmium concentration and gas temperature are independent of pressure. While there is some qualitative agreement between the two curves, suggesting that the Penning collision mechanism is responsible for populating the upper level of the 4416 Å transition, there is a factor of 2-3 between the I_{4416}/He (2^3S) ratio at both high and low helium pressures.

Although it might be argued that this suggests the importance of some second excitation mechanism, the complexity of the discharge is such that it would be rash to base this conclusion on the basis of a single piece of evidence. It is for this reason, intro alia, that the present investigation proceeded to the afterglow experiments (Chapters 4-6) in an attempt to gain greater clarification of the excitation mechanisms.

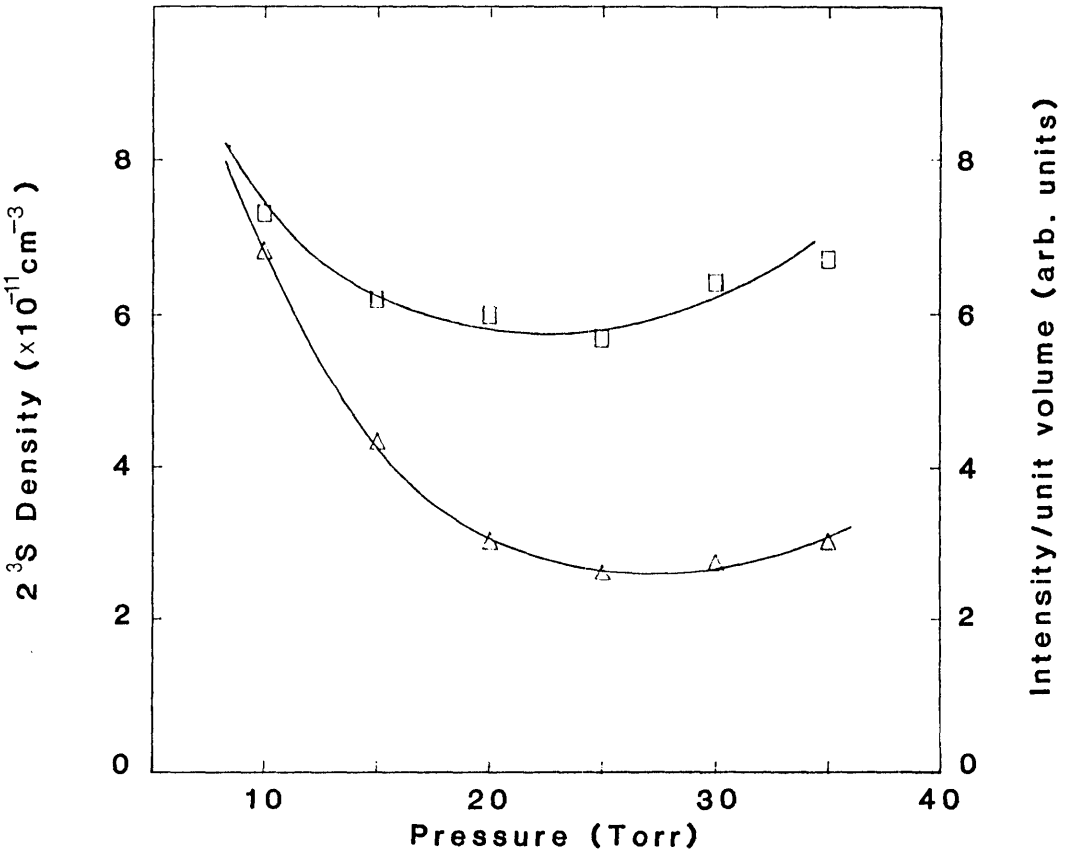

Figure 3.15 Comparison of the pressure dependence of the 2^3S density (Δ) and 4416 Å spontaneous emission/unit volume (□) at an oven temperature of 320^{0}C and discharge current of 120 mA/anode

3.8 CADMIUM ION GROUND STATE DENSITY

The results of the previous section suggest that Penning ionization is the dominant mechanism populating the $5s^2\ ^2D_{5/2}$ level of the cadmium ion and the contribution to the population of this level from direct electron excitation is negligible. However, as the cross section for stepwise excitation of the $5s^2\ ^2D_{5/2}$ level from the Cd^+ ground state is

large (Hane et al. 1983a, 1983b) the importance or otherwise of this mechanism should also be alluded to. Quantitative investigation of the significance of the stepwise excitation mechanism can be obtained from measurement of the cadmium ion ground state density and, as such measurements rely upon the same optical techniques used for the helium density measurements, it is opportune to present and discuss the results of this experiment at this stage.

The cadmium ion ground state density was measured using fractional absorption at 2145 Å ($5p^2P_{3/2} - 5s^2S_{1/2}$). In the calculation of the intensity ratio the isotope shift and hyperfine structure have been taken into consideration. Results showing the reduced ion density as a function of cadmium concentration and discharge current are shown in Figures 3.16 and 3.17.

The results presented in Figures 3.16 and 3.17 are the average of eight separate measurements. The variation amongst individual measurements was up to 25%, but each separate run through cadmium concentration and discharge current produced the same parametric variation.

As a function of increasing cadmium concentration, the reduced ion density increases monotonically over the range investigated. Unfortunately for oven temperatures greater than 300°C the absorption was too great to allow an accurate measurement of the ion density. Over the temperature range studied the ion density varied from $2 \times 10^{10} - 1 \times 10^{11} cm^{-3}$.

With increasing discharge current the reduced ion density at first increases, saturates and thereafter decreases. This apparent decrease in ion density is most probably due to an increase in the upper level

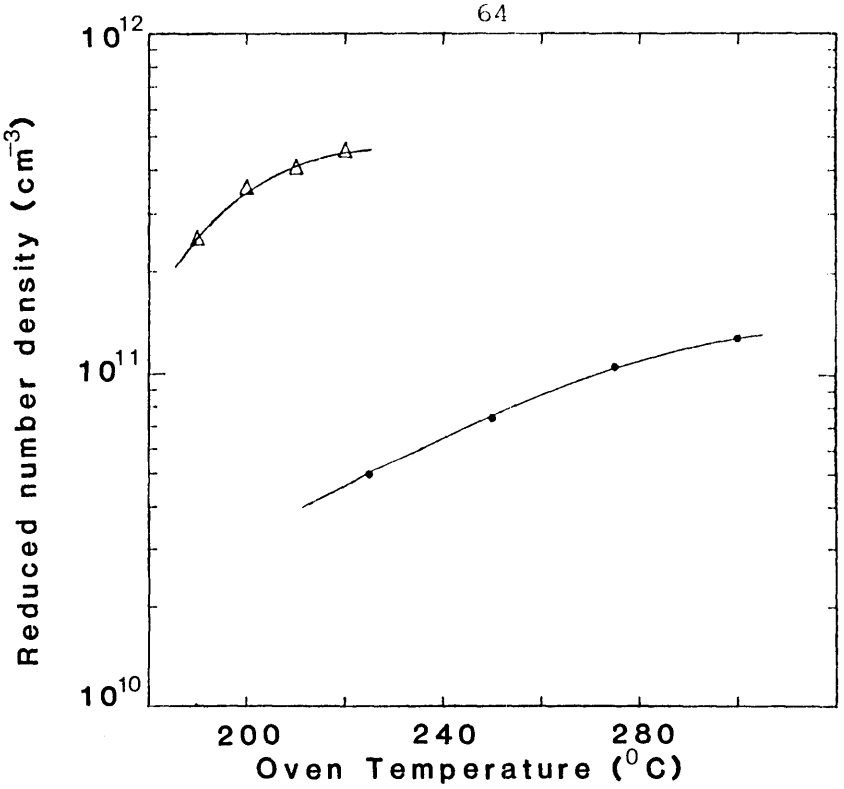

Figure 3.16 *Variation of the reduced cadmium ion density with oven temperature (•) at a helium pressure of 20 Torr and 120 mA/anode discharge current. Also shown are the results of Takasu* et al. *1982 (Δ)*

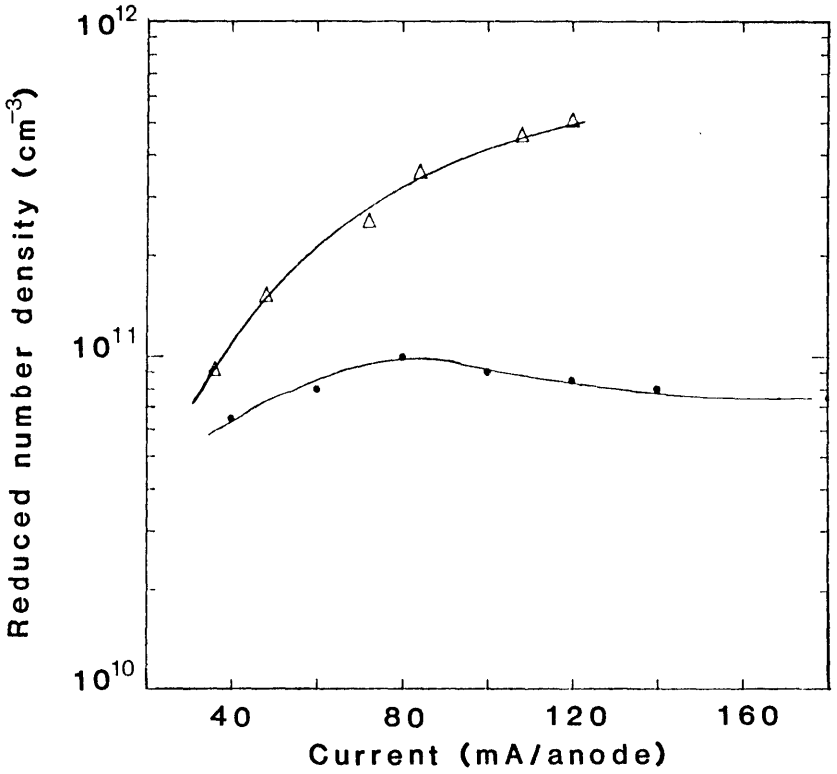

Figure 3.17 *Variation of the reduced cadmium ion density with discharge current (•) at an oven temperature of 250^{0}C and pressure of 20 Torr. Also shown are the results of Takasu* et al. *(1982) (Δ)*

density (the $5p^2P_{3/2}$ level) with increasing current either due to direct electron impact excitation or indirectly through decay into this level from levels populated by thermal charge transfer collisions with the helium ions. Apart from a direct measurement of the population density of the $5p^2P_{3/2}$ level no check can be made of the upper level effects on the Cd^+ ground state density measurements. This measurement was not made in the present study.

The results of Takasu et al. (1982) for a hollow cathode He-Cd device are also shown in Figures 3.16 and 3.17. Although these results exhibit the same parametric behaviour, the ion densities are substantially higher than those of the present study.

The low ion densities, being approximately two orders of magnitude smaller than that of the corresponding 2^3S metastable densities, would suggest that the contribution of this two step excitation mechanism in populating the $5s^2\ ^2D_{5/2}$ level would be negligible even given the large values for the collision cross section for this process.

3.9 RESULTS IN AN Ar-Cd HOLLOW CATHODE DISCHARGE

The comparisons of the parametric behaviour of the 4416 Å spontaneous emission with the Penning rate and/or the product $N(Cd).N(2^3S)$ suggest that Penning collisions alone are responsible for populating the $5s^2\ ^2D_{5/2}$ level of Cd II. A further means of investigating whether or not this is true is to remove the helium metastable atoms from the discharge while maintaining the other discharge parameters constant. To do this, the helium buffer gas was replaced by argon, for which the energies of the two metastable levels (at 11.55 and

11.72 eV) are much less than that required to excite the cadmium into the $5s^2\ ^2D_{5/2}$ level.

In replacing the helium by argon we have not guaranteed that other discharge parameters such as the electron density and electron energy distribution function remain the same. However, running the discharge so that the spectral intensities of transitions in Cd I were the same in Ar-Cd as in He-Cd ensures an identical electron impact excitation rate. Figure 3.18 shows a comparison of the Ar-Cd and He-Cd spectra. The intensity of all the Cd I lines are the same in He-Cd and Ar-Cd, but the intensities of the Cd II lines are greatly different, being essentially zero in many instances for Ar-Cd. This result supports the view that Penning collisions alone are responsible for populating the $5s^2\ ^2D_{5/2}$ level of Cd II.

3.10 SUMMARY

In the study of the d.c. discharge reported in this chapter, the hypothesis that the Penning collision mechanism is solely responsible for populating the upper level of the 4416 Å Cd II laser transition was tested. This was attempted by comparing the parametric variation of the Penning collision rate, calculated from the measured $He(2^3S)$ density, with the corresponding variation of the 4416 Å spontaneous emission. In this study careful consideration of the effects of gas temperature variations on the calculation of the Penning collision rate was made; the effects were shown to be significant especially when considering the current dependence of the collision rate.

The results of this study did not, however, provide conclusive evidence to support the hypothesis, nor was clear evidence obtained

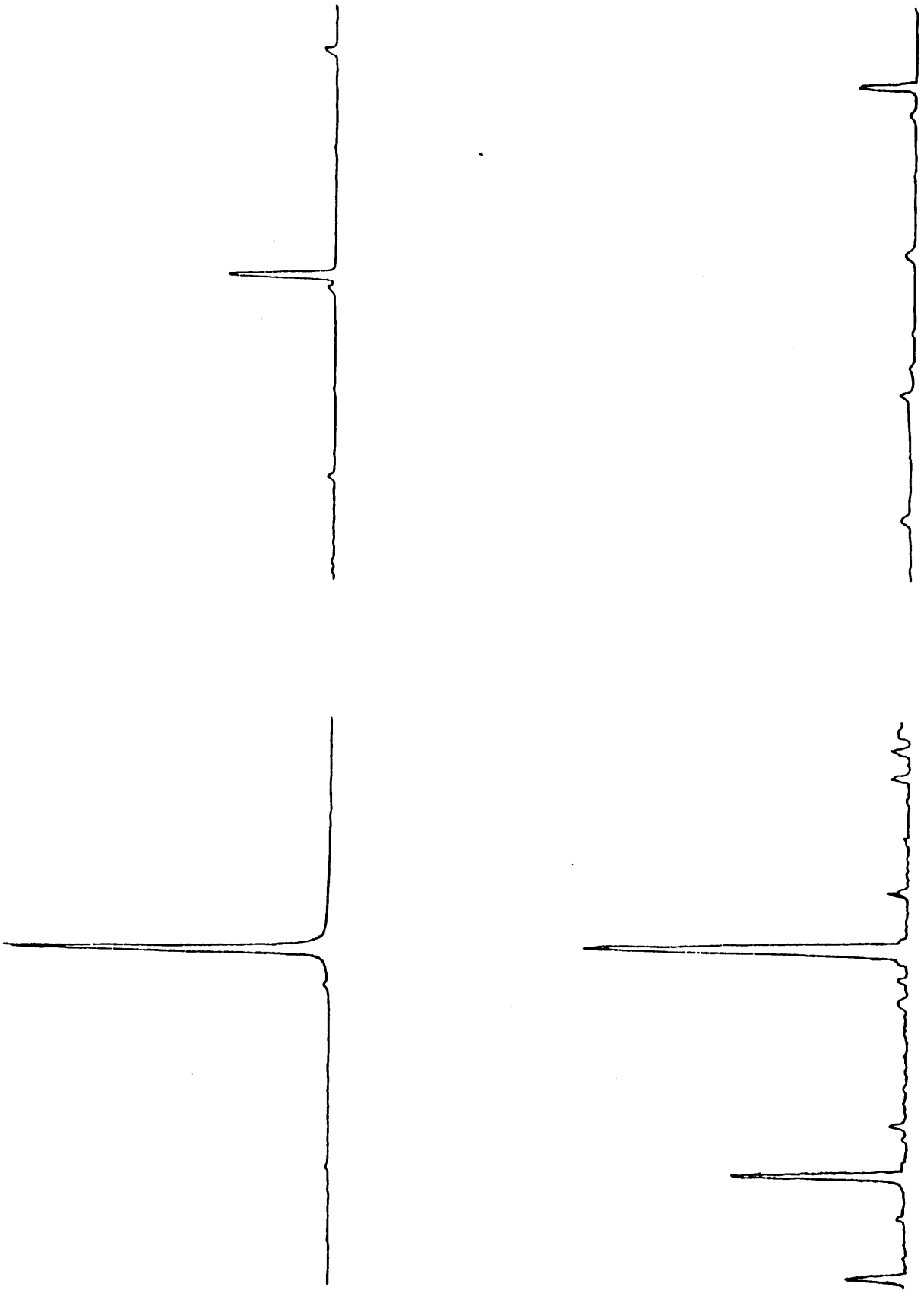

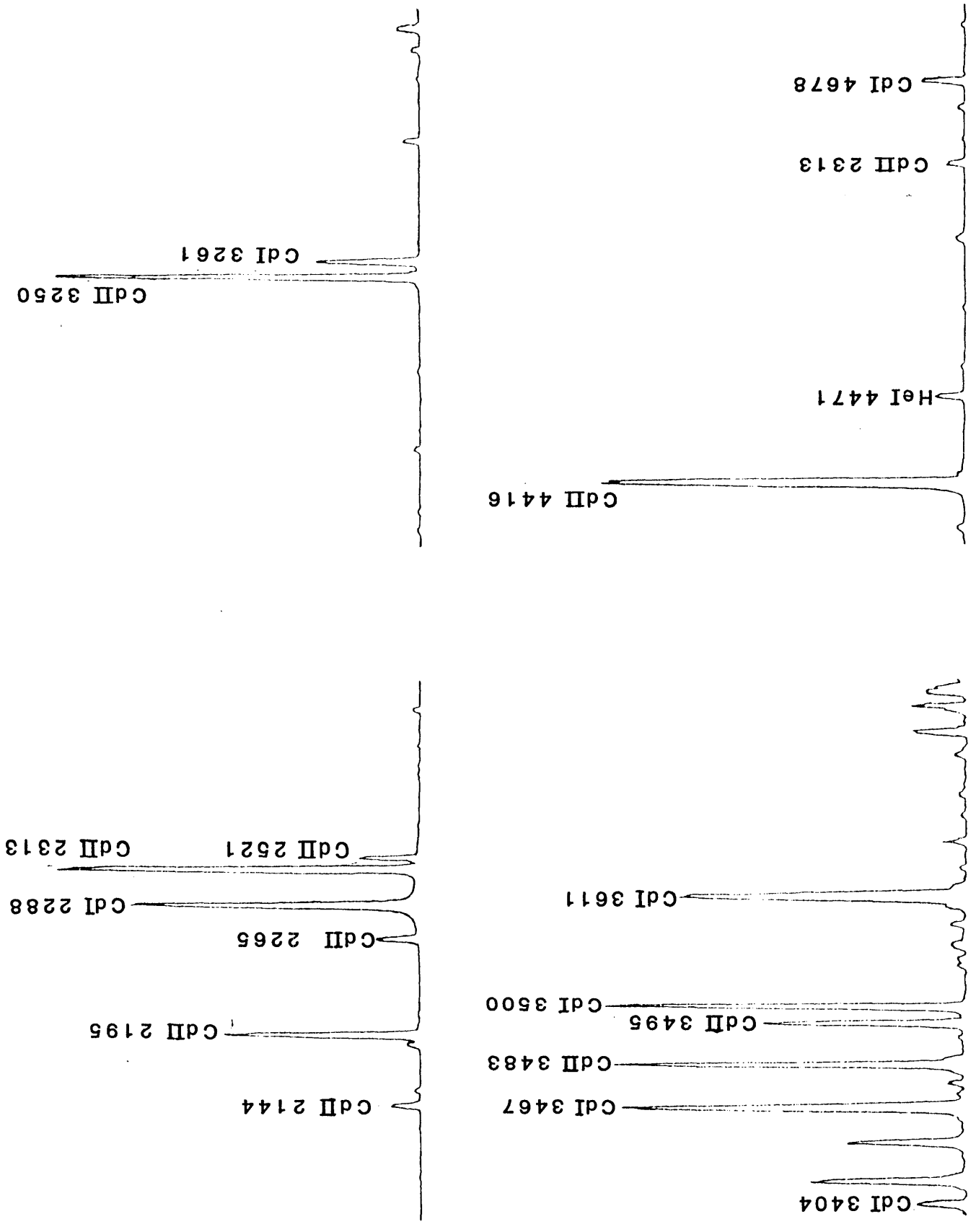

Figure 3.18 Comparison of the He-Cd and He-Ar spectra for an oven temperature of 320^{0}C and a buffer gas pressure of 20 Torr

supporting the view that electronic excitation of the $5s^2\ ^2D_{5/2}$ level accounted for a significant fraction of the excitation of this level.

For a constant cadmium concentration and helium pressure, the current dependence of I_{4416} and the calculated Penning collision rate were found to be in close agreement. The inclusion of the gas temperature variations in the calculation of the Penning rate removed the large ambiguity between these two curves that had been reported by previous investigators. However, there was still a 30-40% variation in the ratio $[I_{4416}/(\text{Penning rate})]$, a feature which could not be readily explained by the associated experimental uncertainties. Similarly, while there appeared to be qualitative agreement between the curves showing the pressure dependence of I_{4416} and the Penning rate, as discussed in section 3.7.3, the ratio $[I_{4416}/(\text{Penning Rate})]$ showed a more significant (2-3) variation with pressure. This latter result suggesting that some second collision mechanism, such as electronic excitation might, in fact, contribute to the excitation of the $5s^2\ ^2D_{5/2}$ level.

On the other hand, these inconsistencies could be due to either errors associated with the measurement of the He (2^3S) densities or the gas temperature (errors which are difficult to assess accurately because of the complex nature of the discharge) or, the error associated with the application of saturated vapour pressure data (used to calculate the cadmium neutral density) to a flowing system.

Further qualitative evidence supporting our hypothesis was obtained from spectroscopic observations of an Ar-Cd hollow cathode discharge. In this discharge no Cd^+ spectral lines were observed, a feature attributed to the fact that the argon metastable species have insufficient energy to ionize neutral cadmium. This result is again not

necessarily conclusive but rather, it can also be interpreted as to show that the electron eneregy distribution function of the Ar-Cd hollow cathode discharge has a depleted high energy tail thus reducing the efficiency of electronic processes in this discharge.

Also, measurements of the Cd^+ ground state density suggested that the proposed excitation pathway proceeding via this level may not be significant as the measured population densities of ion ground state were found to be small, nearly two orders of magnitude less than those of the He (2^3S) level.

Thus, although a variety of evidence in favour of Penning collisions being the dominant mechanism for populating the Cd^+ $5s^2\ ^2D_{5/2}$ level was gained from these studies of the d.c. discharge, there were still some uncertainties associated with some of the evidence and a number of unanswered questions were raised. For these reasons it was decided to investigate some related measurements in the He-Cd afterglow produced in the same hollow cathode discharge tube.

A description of the technique used, the results obtained and an analysis of the data produced is given in the following chapters (4-6) of this thesis.

CHAPTER 4

MEASUREMENT OF THE DECAY OF 4416 Å SPONTANEOUS EMISSION

4.1 INTRODUCTION

Although the essential conclusion for Chapter 3 was that Penning ionization was the dominant excitation mechanism of the $5s^2\ ^2D_{5/2}$ level of Cd II there were a number of inconsistencies between the comparison of the parametric variation of the 4416 Å spontaneous emission and the Penning collision rate. These may be interpreted to imply the existence of a second collision mechanism in populating this level, such as direct or stepwise electronic excitation. Thus, in order to remove this ambiguity, a further, more detailed investigation of the hollow cathode He-Cd discharge is warranted.

A convenient and potentially simple method for investigating the importance or otherwise of collision mechanisms occurring within a discharge is to examine the temporal evolution of selected transitions i the stationary afterglow created by rapidly terminating the current (and voltage) to the discharge. The nature of the decay of these spectral lines containing all the necessary information on excitation mechanisms in the afterglow which, by extrapolation, can be used to infer the significance or otherwise of the particular processes in the d.c. discharge.

In the afterglow the decay of the He (2^3S) atoms can be written as

$$\frac{dN(2^3S)}{dt} = -N(2^3S)\, N_{Cd} \langle \sigma_p v \rangle - \frac{D_m N(2^3S)}{\Lambda^2 p} \tag{4.1}$$

with solution

$$N(2^3S) = N^0_{2^3S} \exp(-\gamma t) \tag{4.2}$$

where

$$\gamma = N_{Cd} \langle \sigma_p v \rangle + \frac{D_m}{\Lambda^2 p} \tag{4.3}$$

Thus, if Penning collisions are solely responsible for the formation of the Cd II $5s^2\ ^2D_{5/2}$ level then the 4416 Å intensity should decay exponentially in the afterglow with a time constant equal to that given by equation (4.3).

In equation (4.1) the first term represents metastable destruction upon collision with cadmium neutral atoms and, the second term is the loss through diffusion of the metastables out of the discharge volume and subsequent destruction at the walls. $N(2^3S)$ and N_{Cd} represent the 2^3S metastable and cadmium neutral densities respectively, $\langle \sigma_p v \rangle$ is the Penning collision cross section (σ_p) averaged over the thermal velocities of the colliding atoms, D_m the diffusion coefficient, Λ the diffusion length for cylindrical geometry and p the helium pressure. $N(2^3S)$ and $N^0_{2^3S}$, in equation (4.2), represent the metastable density as a function of time and the initial metastable density respectively.

On the other hand if electronic excitation mechanisms, such as the single step excitation process directly into the $5s^2\ ^2D_{5/2}$ level from

the cadmium neutral state as proposed by Gill and Webb (1978) or the more complex two step mechanism proposed by Mori, Murayama, Goto and Hattori (1978) of

$$Cd + e \rightarrow Cd^{+} + e + e$$

followed by

$$Cd^{+} + e \rightarrow Cd^{+}(5s^{2}\ {}^{2}D_{5/2}) + e$$

are important then the 4416 Å decay would have a more complex structure. Early in the afterglow the number of energetic electrons capable of exciting the cadmium from either the neutral or ion ground states would be small. Removing this component of the excitation would result in a rapid decrease in the 4416 Å intensity leaving, at later times, a slow decay due to the contribution by Penning collisions. Comparison of these two decay schemes forms the main thrust of the present chapter.

Before proceeding with a discussion of the results of experiments showing the 4416 Å decay in the afterglow, section 4.2 contains a detailed discussion of the experimental procedure adopted for measuring the spontaneous emission decay and the method utilized to repetitively pulse the current to the hollow cathode tube. The important time response limitations of the detection and data recording instruments and their choice so as to minimize the convolution of the decay waveform with the instrument response function are discussed in section 4.3. Section 4.4 presents results showing the decay of a transition excited predominantly by electronic processes and highlights not only the limitations of the proposed technique (response time and current switching times) but also the rapid nature of cessation of electronic excitation processes in the He-Cd afterglow.

Sections 4.5.1, 4.5.2 and 4.5.3 present the results of the

measurements of the 4416 Å decay in the afterglow as a function of cadmium concentration, discharge current and helium pressure respectively. In all cases the observed decay is more complicated, showing greater structure, than has been reported previously (Goto, 1982; Grey-Morgan and Wong, 1983). This is a direct consequence of applying sophisticated waveform digitizing and signal averaging techniques to the study of the afterglow and hence improving the signal to noise ratio characteristics of the data has revealed structure obscured in previous studies of the He-Cd afterglow.

Under all experimental conditions, the nature of the late afterglow decay is found to be consistent with the view that Penning collisions dominate the production of the $5s^2\ ^2D_{5/2}$ level at these times. However, the early afterglow characteristics, in particular, the intensity increase and subsequent rapid decay, are not easily explained by the Penning collision model nor existing theories involving electronic excitation of this level.

The good signal to noise characteristics achieved were sufficient to show the small effects of diffusion of He (2^3S) on the slope of the late afterglow decay of the 4416 Å spontaneous emission. Indeed, as shown in section 4.5.3, it was possible to use the data to deduce values for the diffusion coefficient of the 2^3S metastable species which were in good agreement with the values quoted by Schearer and Padovani (1970).

Further, from the current and pressure dependence of the point of intersection of the extrapolated exponential late afterglow decay with the afterglow initiation axis it is clear that electronic processes, either directly or indirectly, play an important role in the early afterglow. However, the exact nature of these processes are not obvious from this data alone and thus a more comprehensive investigation of the

afterglow is justified if this technique is to be used to infer collision processes occurring within the d.c. discharge.

4.2 EXPERIMENTAL DETAILS

4.2.1 Experimental Method

The decay of the 4416 Å intensity was measured using the experimental arrangement shown in Figure 4.1 whereby the endlight intensity, from a discharge segment associated with one anode, was observed as the current to that anode was rapidly terminated.

After passing through a spectrometer (0.5 m Ebert scanning spectrometer) and an optical system designed to limit the viewing region to that of a narrow cone lying on the discharge axis the signal was detected by a photomultiplier (EMI 9750 QB). The design of the optical system was similar to that described in section 2.2 but some relaxation on the constraints regarding size and placement of the apertures was necessary in order to allow sufficient signal for data acquisition. The diameter of the principal stop (A) was set at 3 mm and that of stop B at 0.4 mm whilst the distance Z between stops A and B was reduced from its value of 1 m, used in the steady state absorption experiments, to 0.5 m. The effective viewing volume was then independent of distance for half the length of the tube.

After amplification by the differential input amplifier (AM 502) the output of the photomultiplier was fed into a waveform digitizer (LeCroy 2265A). To assist with data acquisition the digitizer output was connected to a CAMAC controller and signal averaging achieved using an

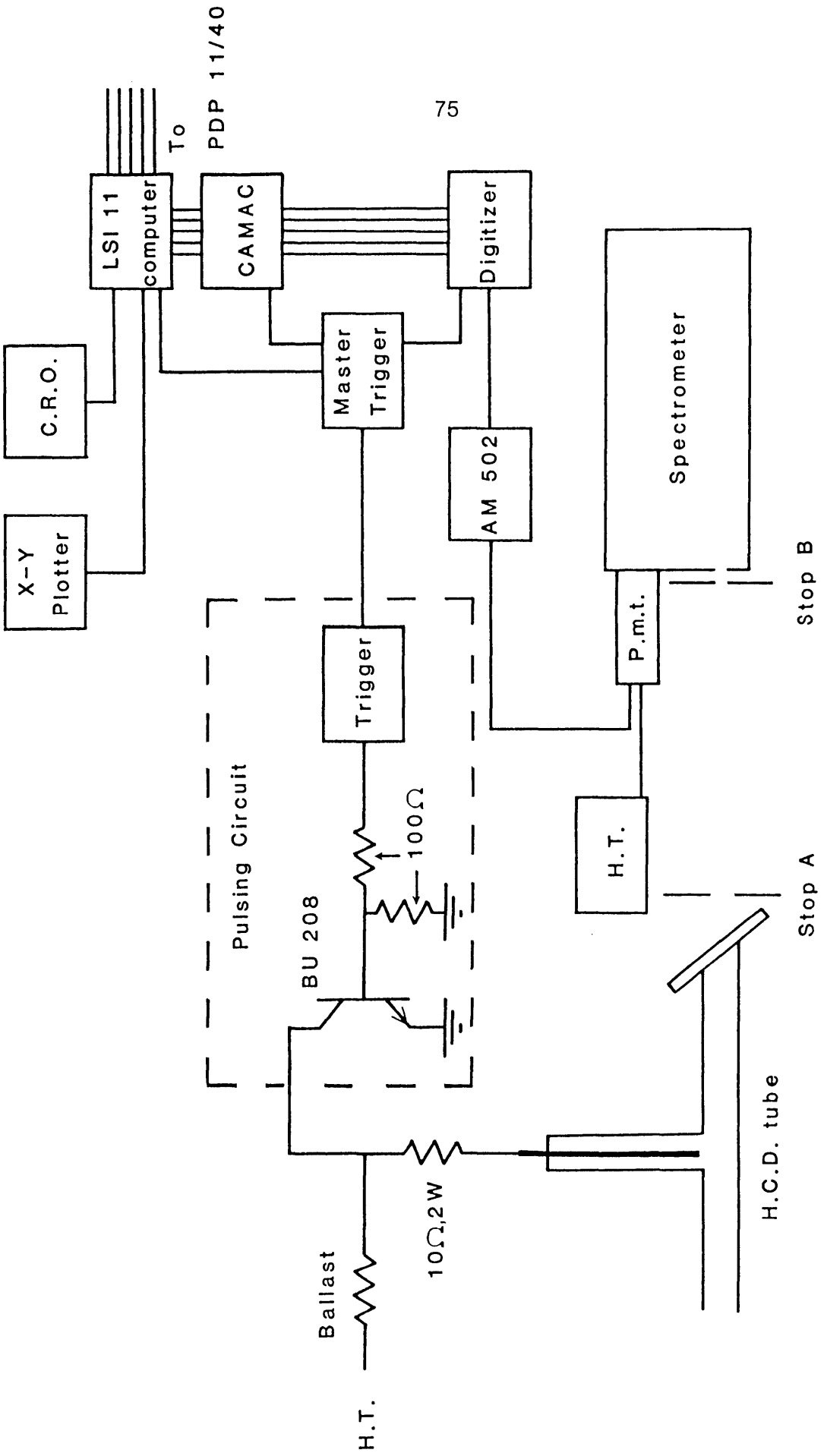

Figure 4.1 Schematic diagram of the experimental arrangement used to create the afterglow and record the subsequent decay of spectral lines

LSI II computer and associated software. The resulting signal could be displayed on a storage oscilloscope (HP 181A) or plotted out directly on an X-Y chart recorder (HP 7004B). The resolution of the digitizer could be varied from 50 nsec to 5 μsec per channel with the window of the digitizer fixed to a width of 1024 channels.

The overall timing of the data acquisition system and current pulsing circuit was done with the master trigger unit which provided two trigger pulses, one undelayed pulse initiating the data acquisition sequence and a second pulse, of variable time delay, activating the current switch. Variable delay on the second pulse was necessary to ensure that the resulting afterglow occurred within the viewing window of the digitizer.

The repetition rate of the signal averaging system was limited to 1 Hz and thus data acquisition times of up to 5-10 minutes were necessary for the weakest of the spectral lines investigated. External heating of the cathode was used to maintain a uniform temperature and keep the cadmium density constant over this period of time.

4.2.2 The Pulse System

As shown in Figure 4.1, the pulse circuit consisted of a power transistor (BU 208) connected in parallel with the discharge tube, the transistor collector being attached directly to the anode pin and the emitter to the cathode. When the transistor was switched on, by applying a square trigger pulse (5V, 50 nsec risetime) to the base-emitter junction, the potential difference between the anode and cathode was reduced from the operating value of approximately 250 V to 0 V and held at this value for periods of up to 1 second depending on the width of the

square pulse applied. No current flowed in the discharge during the transistor 'on' cycle. The width of the pulse was determined so that the discharge would reliably restrike following de-activation of the transistor.

Typical voltage and current waveforms of this pulse system are shown in Figures 4.2a and 4.2b. The voltage waveform was obtained using a compensated high voltage probe (Tektronix Model 015-039) and the corresponding current waveform from the potential difference across a small resistance (10Ω ,2W) connected in series with the anode pin. Decay times of the voltage and current were 0.5 μsec, independent of helium pressure, cadmium concentration and discharge current.

At the end of the transistor conduction mode the discharge current remains zero whilst the voltage rises to the full power supply potential, typically 600-1000 Volts. Under these overvoltage conditions the discharge breaks down resulting in a renewal of current flow and a return of the voltage to its steady state value. As shown in Figure 4.2a the current waveform closely follows that of the voltage.

4.3 RESPONSE TIME CONSIDERATIONS

In order to eliminate distortion of the signal careful consideration must be given to response time limitations of the detection and data acquisition systems, the major sources of RC limitation being the AM 502 amplifier and the photomultiplier. The frequency response of the amplifier was checked by observing the response of the amplifier to a square wave of 50 nsec risetime. Over all values of amplifier gain, the risetime of the output was measured to be 200 nsec. This will ultimately

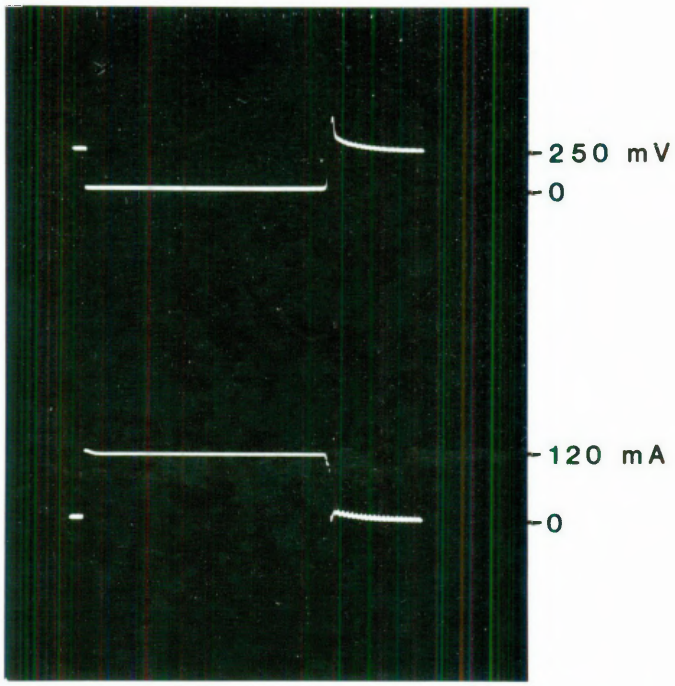

Figure 4.2a Voltage and Current waveforms of the pulsing system for discharge conditions of 120 mA/anode and 20 Torr helium. 20 μsec/division

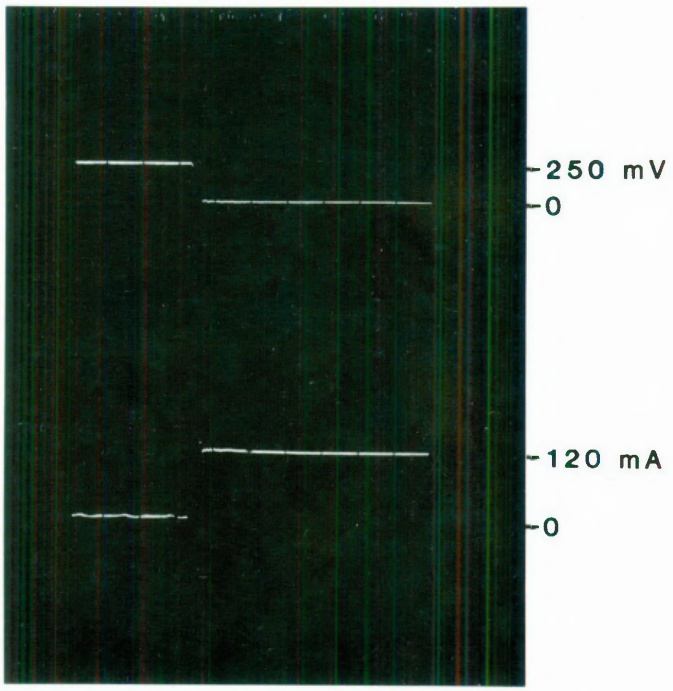

Figure 4.2b Decay times of the Voltage and Current waveforms for discharge conditions of 120 mA/anode and 20 Torr helium. 2 μsec/division

limit the temporal resolution of the present detection system.

In practice a more serious limitation arises from the choice of the photomultiplier output resistance. The resistance value must be small enough to eliminate RC effects due to the photomultiplier amplifier chain, while being of sufficient size to provide adequate signal levels for averaging. The effects of the output resistance value on the photomultiplier response were determined by observing the decay times of transitions populated by electron collisions. Results, showing decay times of the He I λ = 3889 Å transition as a function of resistance value are shown in Figure 4.3.

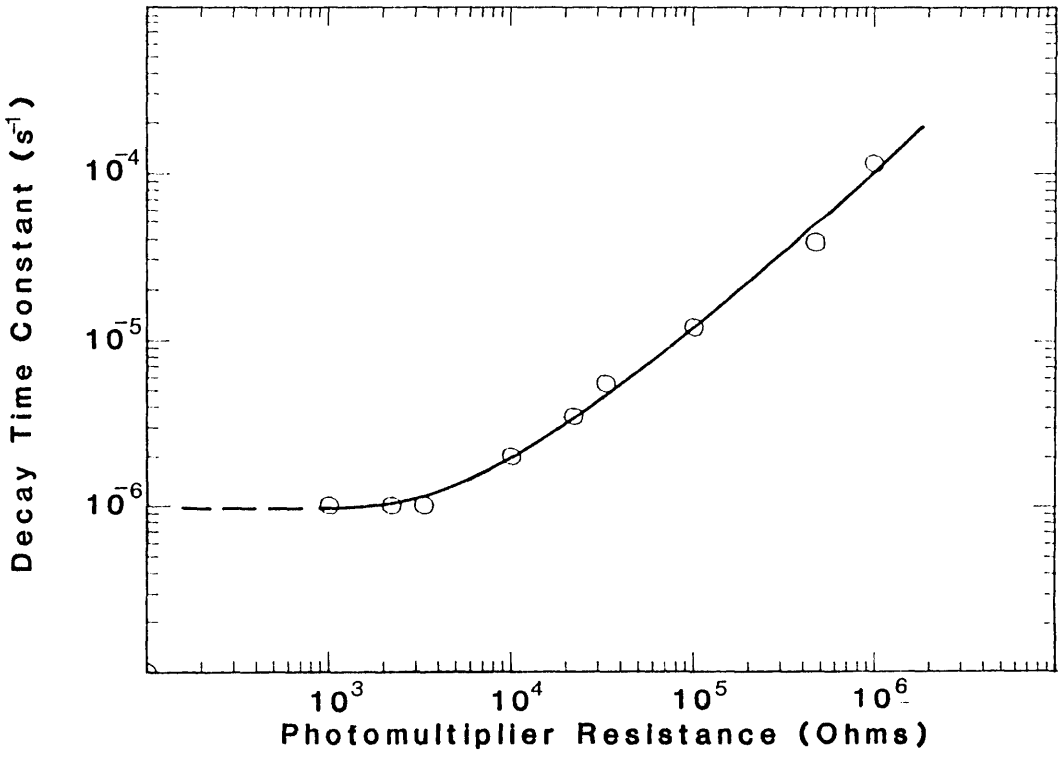

Figure 4.3 Decay times of the He I 3889 Å intensity as a function of photomultiplier output resistance

It is clear that for output resistances less than 3.3 kΩ the decay time is independent of resistance and all spontaneous emission data were obtained using this value.

With this value of resistance the minimum observable decay times are limited by the 0.5 μsec voltage fall time of the pulse circuit rather than by the detection system.

4.4 DECAY OF ELECTRONICALLY EXCITED TRANSITIONS

Figure 4.4 shows a typical output of the system for a transition populated by electron impact excitation processes. The curve is of the He I λ = 4471 Å (4^3D-2^3P) transition and shows light intensity as a function of time. The observed waveform is the result of signal averaging over 300 repetitions of the afterglow; each data point represents 1 μsec.

The signal to the left of the point T=0 gives the intensity under normal d.c. operation. At T=0 the afterglow is created and the intensity decays to zero in a time of 1 μsec. The afterglow lasts for a period of ~150 μsec after which the discharge reverts to normal d.c. operation. At tube switch on, the 4471 Å intensity follows closely the time dependence of the current with a sharp peak in intensity followed by a dip and then a return to the steady state intensity.

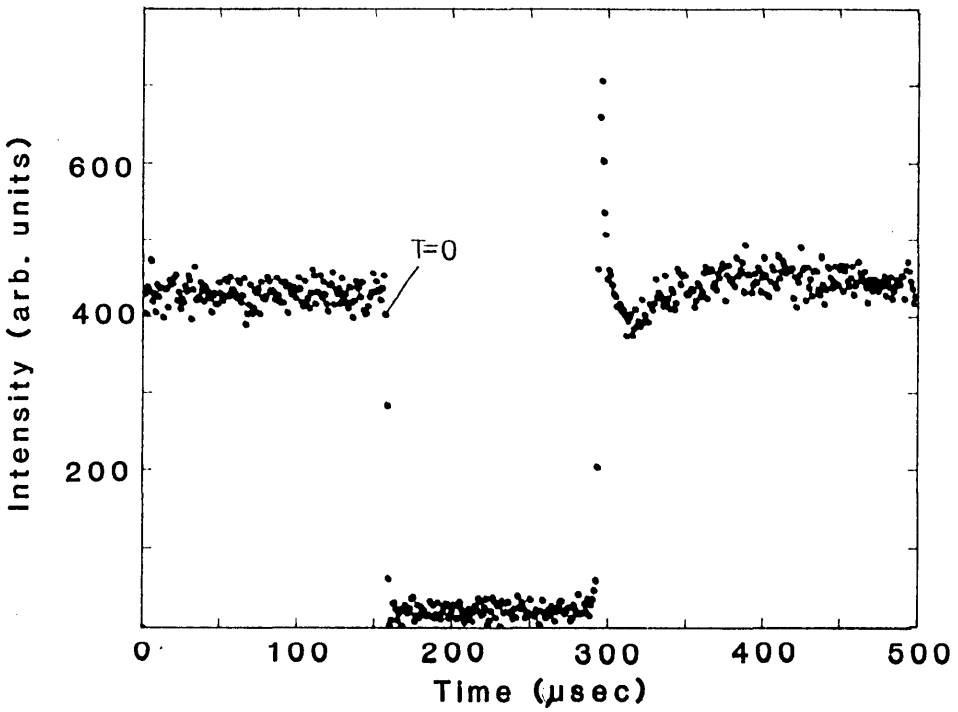

Figure 4.4 Decay of the He I λ = 4471 Å transition at an oven temperature of 225°C, 20 Torr helium and a current of 120 mA/anode. T=0 represents the channel at which the afterglow is created

4.5 DECAY OF 4416 Å SPONTANEOUS EMISSION IN THE AFTERGLOW

The decay of the Cd II transition at 4416 Å was measured for various values of helium pressure, cadmium concentration and discharge current. In each case the data were averaged over 300 separate afterglow events with a 500 nsec/channel time resolution, except at an oven temperature of 225°C where the data were recorded with a resolution of 1 μsec/channel.

4.5.1 4416 Å Decay as a Function of Cadmium Concentration

The decay of the 4416 Å intensity as a function of increasing oven temperature, at a constant helium pressure of 20 Torr and discharge current of 120 mA/anode, is shown in Figures 4.5a - 4.8a for oven temperatures up to and including 300°C. For oven temperatures beyond this value the observed decay was limited by the fall time of the voltage. A lower limit of 225°C was set because below this value the cadmium concentration was not determined by the oven temperature but rather by the vapour pressure of the cadmium condensed along the cathode bore.

The channel number at which the afterglow begins is identified on each diagram by a line drawn perpendicular to the time axis through the point labelled T=0, the signal to the left of the T=0 point giving the steady state intensity.

For the analysis of the decay it is essential that the T=0 point be accurately known. As it is extremely difficult to identify this point on the 4416 Å intensity curves the following method was adopted: immediately following measurement of the 4416 Å decay, the response of a transition excited by electron impact was recorded (this eliminated the possibility of the viewing window of the digitizer drifting significantly between measurements). The T=0 point is easily recognized for such a decay (c.f. diagram 4.4) and thus counting the number of data channels occurring before this point enabled an accurate determination of the corresponding point of the 4416 Å decay.

From Figures 4.5a - 4.8a it is seen that the decay is clearly more complex than the simple Penning collision or the electron impact plus

Penning collision model would at first suggest. This is highlighted by an increase in intensity immediately following the formation of the afterglow. This increase becomes less significant as the cadmium concentration rises. Following this initial increase the intensity decays in a manner which may or may not be exponential.

The nature of the decay can be determined from a plot of the logarithm of the intensity as a function of time. The semi-logarithmic plots corresponding to Figures 4.5a - 4.8a are given in Figures 4.5b - 4.8b and show that in every case the decay becomes linear late in the afterglow. With increasing oven temperature the slope of this linear region increases. The times to onset of the linear decay and the slope of the decays as a function of oven temperature are shown in Table 4.1.

TABLE 4.1

Time to Onset of Linear Decay and Slope of the Decay as a Function of Oven Temperature

OVEN TEMPERATURE ^{o}C	TIME TO ONSET OF LINEAR DECAY (μsec)	SLOPE $(sec)^{-1}$
225	12	3.7×10^4
250	8	7.69×10^4
275	5	1.67×10^5
300	3.5	3.45×10^5

The existence on a semi-logarithmic plot of a linear decrease in intensity late in the afterglow and the observation that the slope of this decay increases with increasing cadmium concentration are both consistent with the view that the Cd II $5s^2\ ^2D_{5/2}$ level is populated by Penning

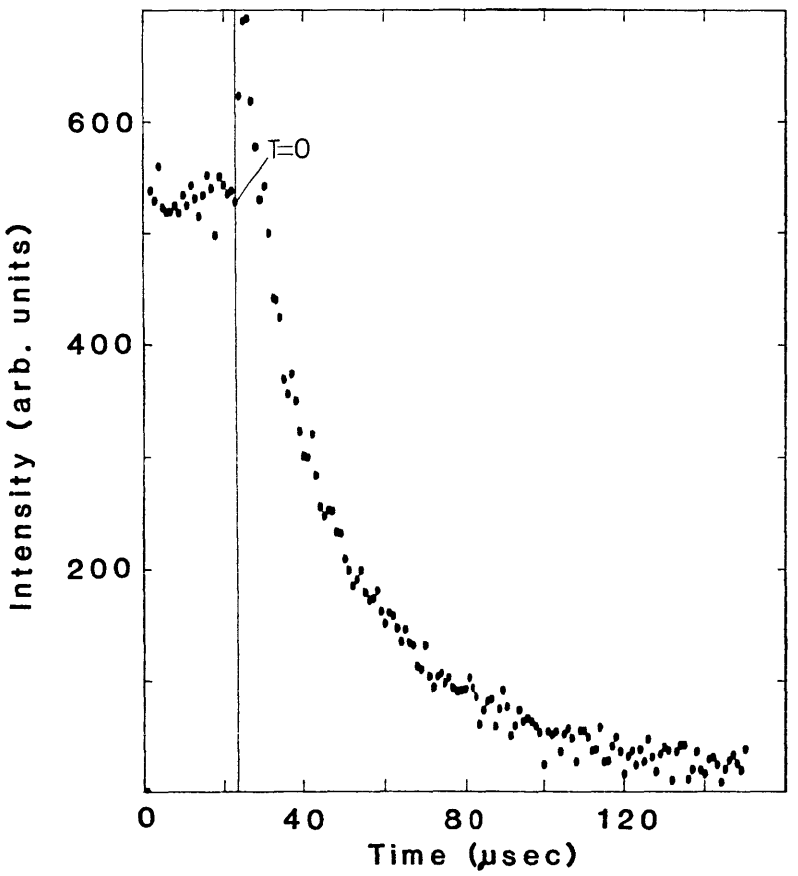

Figure 4.5a 4416 Å decay at an oven temperature of 225°C, 20 Torr helium pressure and a current of 120 mA/anode

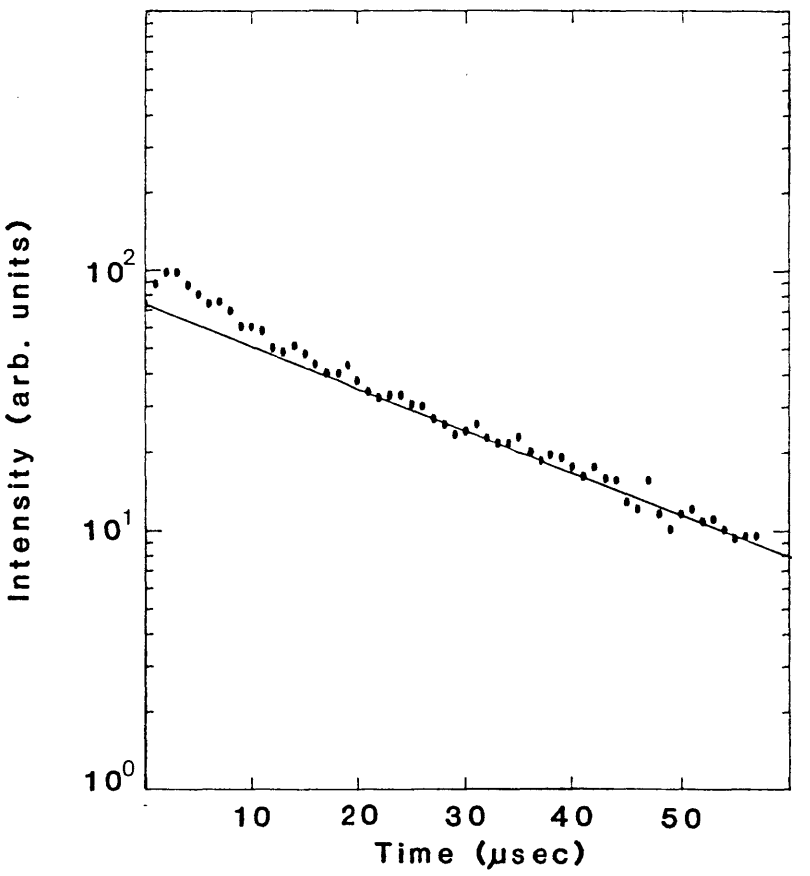

Figure 4.5b Corresponding semi-logarithmic plot of the 4416 Å decay

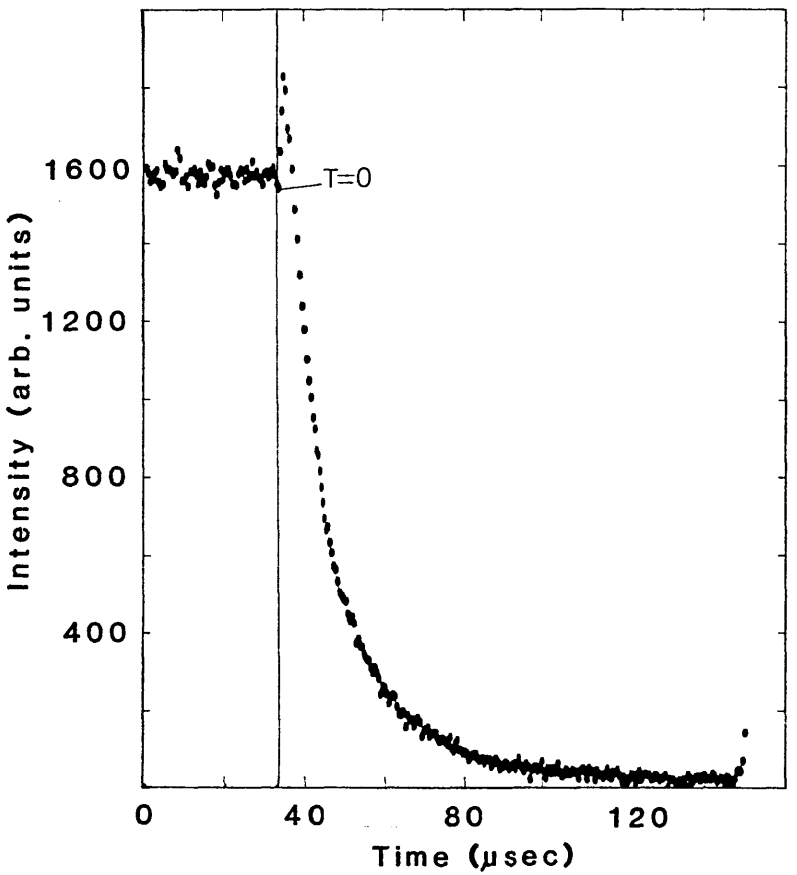

Figure 4.6a 4416 Å decay at an oven temperature of 250°C, 20 Torr helium pressure and a current of 120 mA/anode

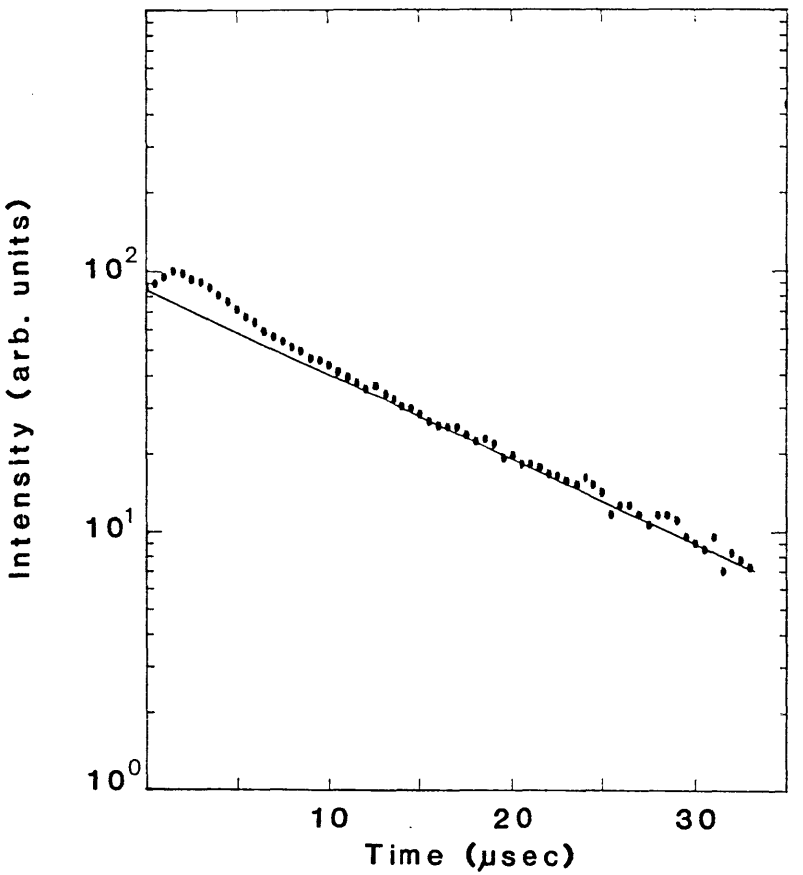

Figure 4.6b Corresponding semi-logarithmic plot of the 4416 Å decay

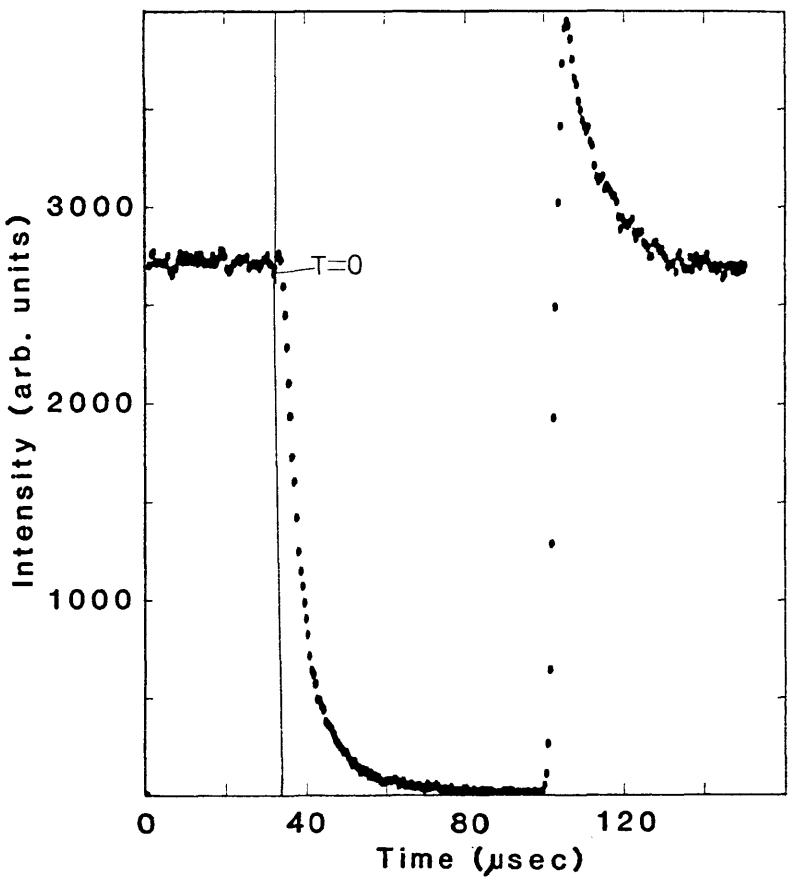

Figure 4.7a 4416 Å decay at an oven temperature of 275°C, 20 Torr helium pressure and a current of 120 mA/anode

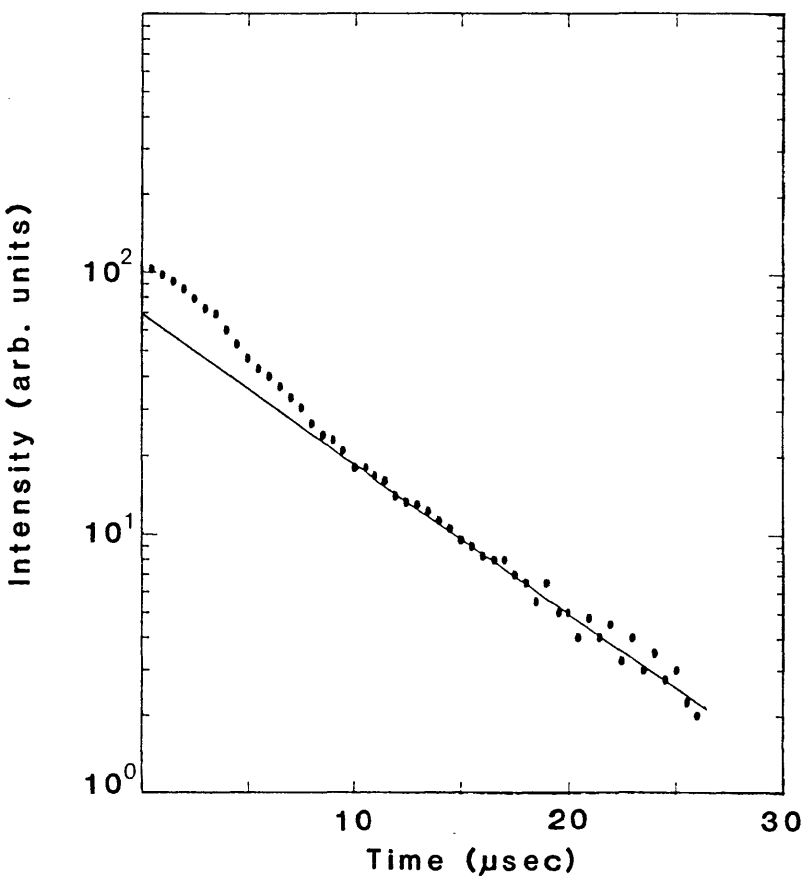

Figure 4.7b Corresponding semi-logarithmic plot of the 4416 Å decay

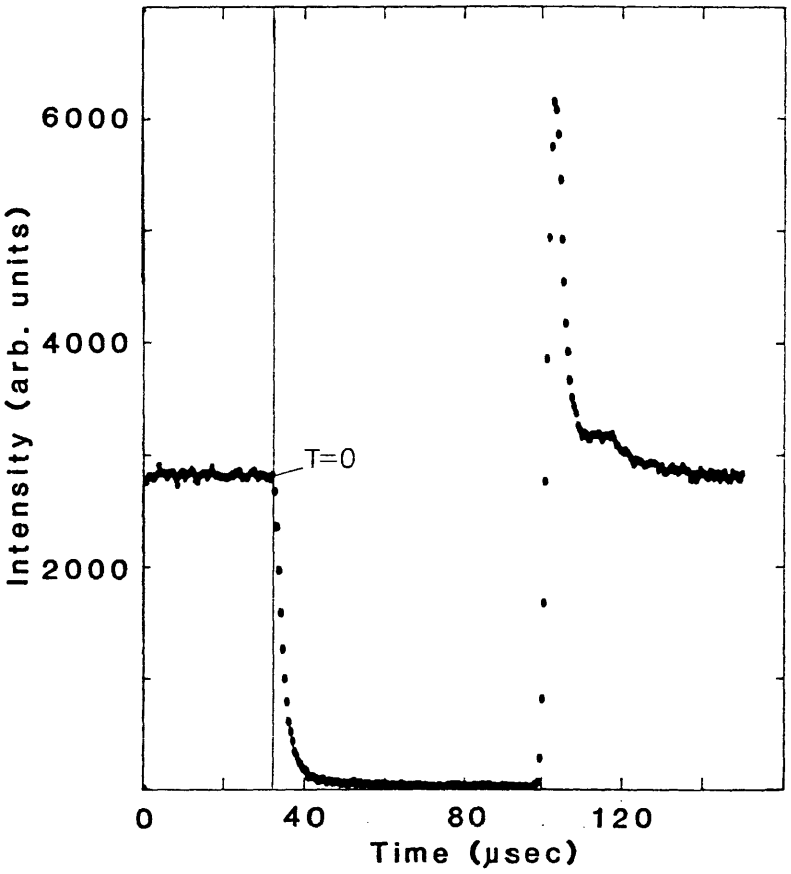

Figure 4.8a 4416 Å decay at an oven temperature of 300°C, 20 Torr helium pressure and a current of 120 mA/anode

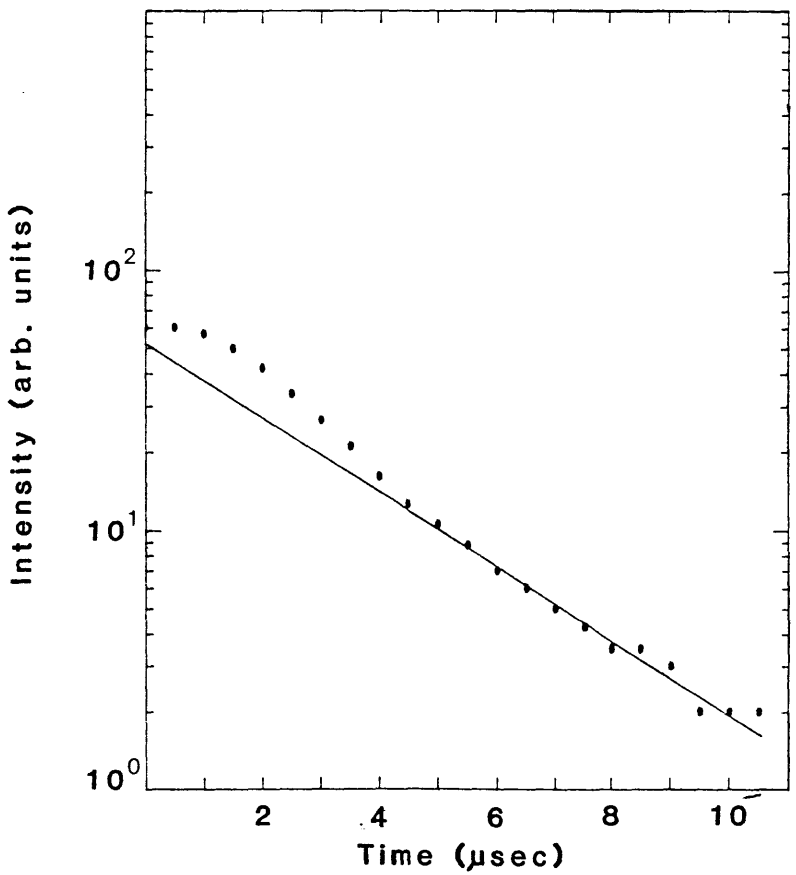

Figure 4.8b Corresponding semi-logarithmic plot of the 4416 Å decay

collisions at these times. On the other hand, it is not clear how this mechanism can explain the changes in intensity which occur early in the afterglow and further investigation of this region is clearly required. One means available for investigating this region (and in particular the collision processes leading to the formation of the intensity peak) is to examine the current and pressure dependence of the decay.

4.5.2 Decay as a Function of Discharge Current

The decay of the 4416 Å intensity as a function of current at a constant helium pressure of 20 Torr is shown in Figures 4.9a - 4.12a for oven temperatures between 225°C and 300°C. The discharge current was varied from 60 mA/anode, the minimum current for which the discharge would reliably restrike following the afterglow, to a maximum of 200 mA/anode limited by the onset of arcing. Corresponding semi-logarithmic plots are shown in Figures 4.9b - 4.12b.

Figures 4.9b - 4.12b show that, for a constant oven temperature, increasing the discharge current did not change the overall shape of the observed decay with all curves having an initial intensity increase followed by a period of non-linear decay eventually giving way to a linear decay late in the afterglow.

As the gas temperature is expected to increase with current (Appendix A2) some change in the slope of the linear decay might be expected. For the current range studied the maximum variation expected would be 25% and although some increase in slope was evident the effects of gas temperature variation were largely obscured by the uncertainty in the experimental points late in the afterglow.

The current dependence of the relative peak height (peak intensity/steady state intensity) is of special interest as any scaling of this quantity with the discharge current would indicate that electron collisions are responsible for producing the peak. At low oven temperatures, where the intensity increase is most significant, increasing the current resulted in a decrease of the relative peak height. This trend is also present at higher oven temperatures although the effect is less pronounced. This behaviour shows that the existence of the peak cannot be explained by direct electron collisional excitation of the $5s^2\ ^2D_{5/2}$ level.

The point of intersection of the extrapolation of the linear decay with the T=0 axis also shows a marked dependence on current. At an oven temperature of 225°C and low discharge currents, the point of intersection lies above the steady state intensity but decreases towards this intensity as the current rises. At an oven temperature of 250°C the point of intersection initially lies above that of the steady state intensity but decreases to a value below this intensity with increasing current. A similar trend is observed at an oven temperature of 275°C and with greater uncertainty at 300°C.

The observation that the point of intersection of the linear decay with the T=0 axis is dependent upon discharge current suggests that electron collision processes must play an important role in determining the nature of the 4416 Å decay early in the afterglow. On the other hand the behaviour of the intensity peak with increasing current shows that this role is not one involving direct electron excitation of the $5s^2\ ^2D_{5/2}$ level.

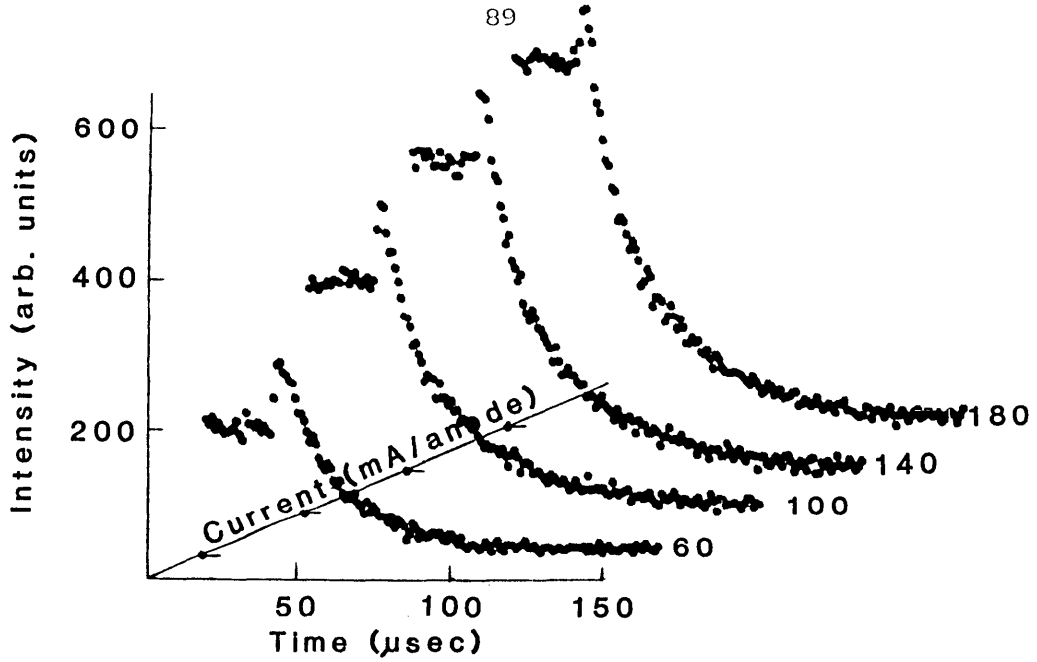

Figure 4.9a *4416 Å decay as a function of discharge current at an oven temperature of 225^{0}C and a pressure of 20 Torr helium*

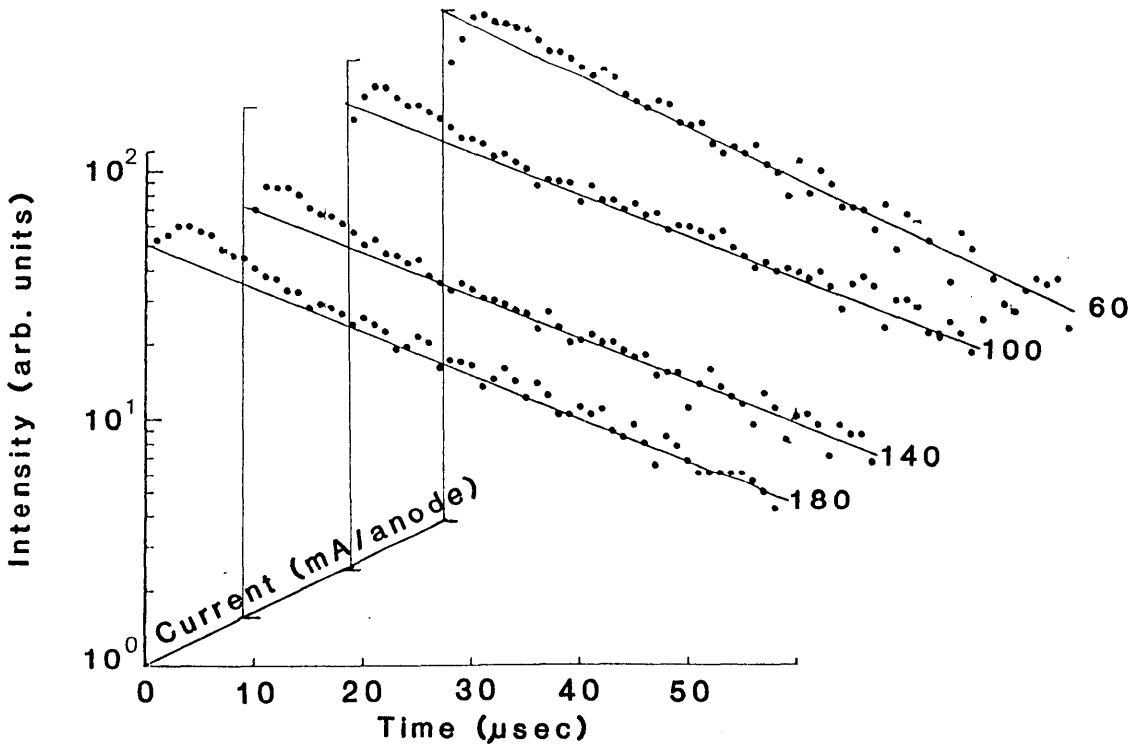

Figure 4.9b *Corresponding semi-logarithmic plots showing the current dependence of the decay*

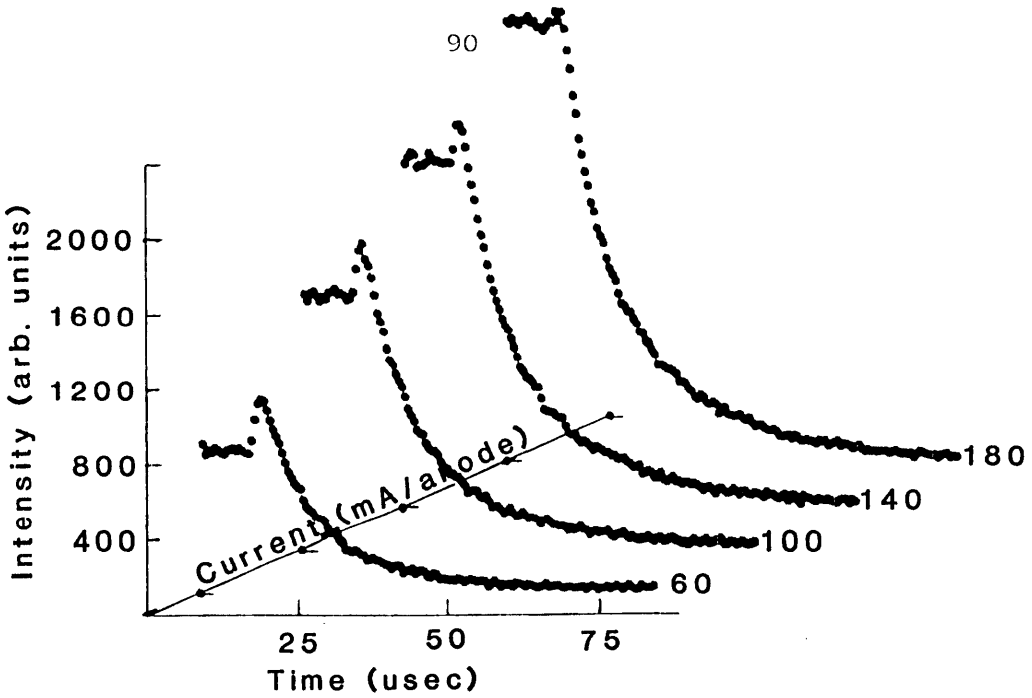

Figure 4.10a 4416 Å decay as a function of discharge current at an oven temperature of 250°C and a helium pressure of 20 Torr

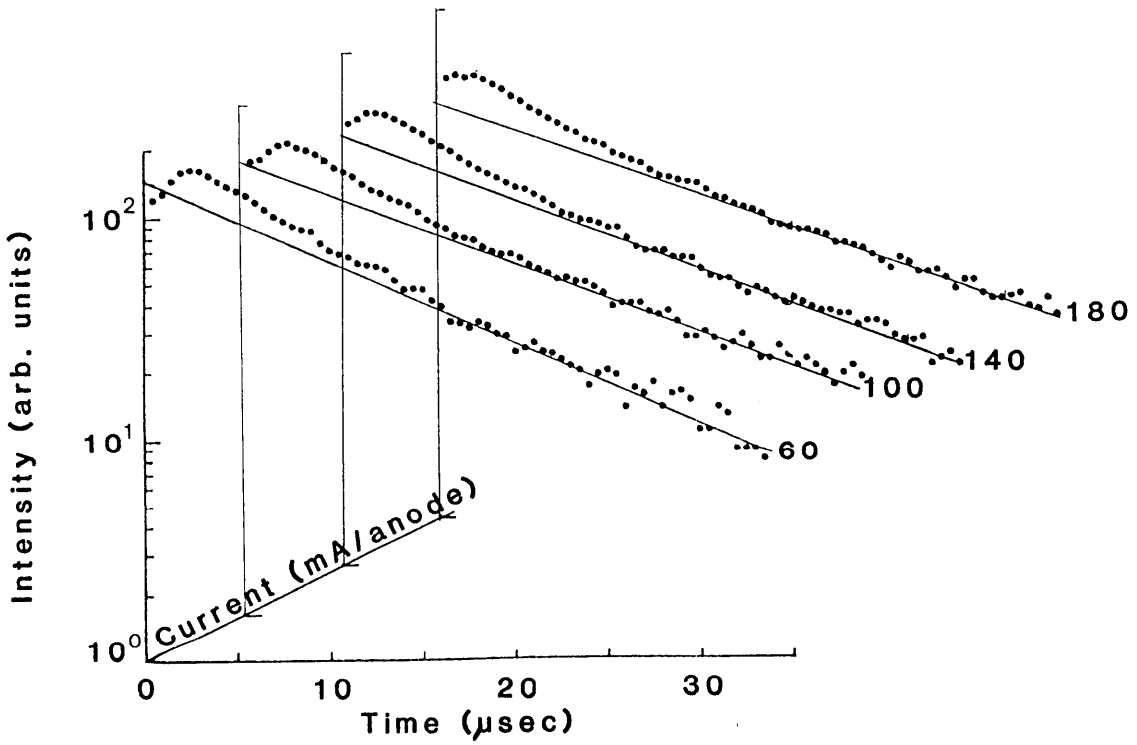

Figure 4.10b Corresponding semi-logarithmic plots showing the current dependence of the decay

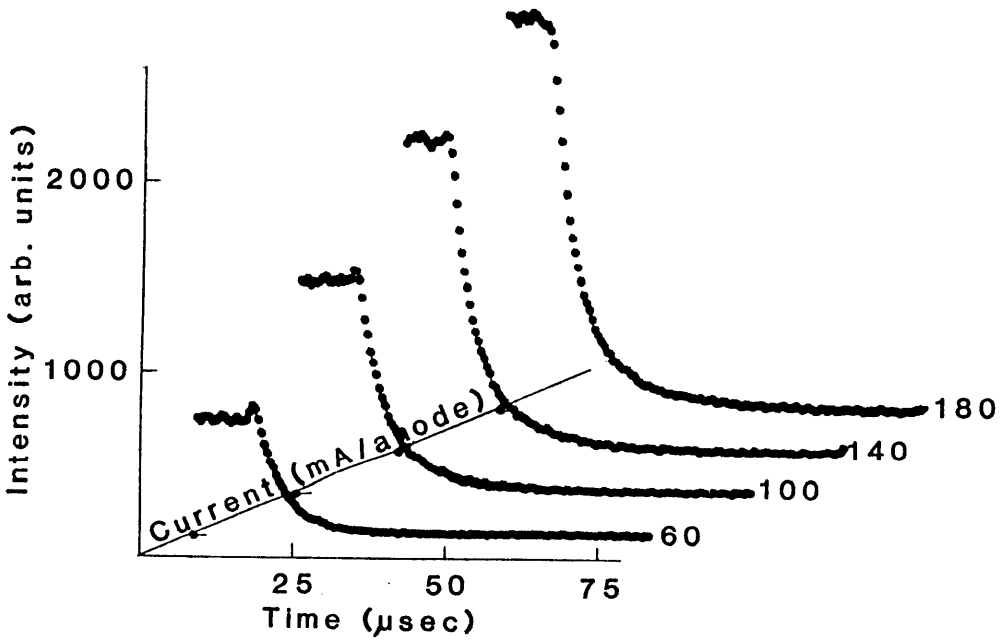

Figure 4.11a *4416 Å decay as a function of discharge current at an oven temperature of 275°C and a helium pressure of 20 Torr*

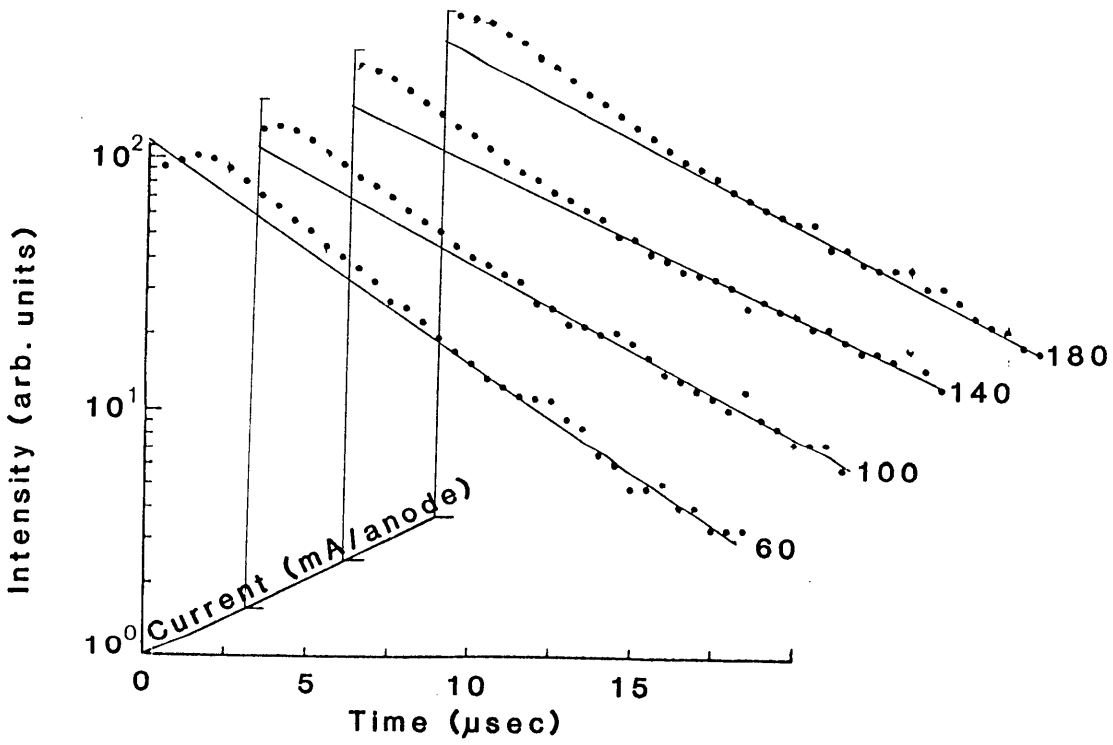

Figure 4.11b *Corresponding semi-logarithmic plots showing the current dependence of the decay*

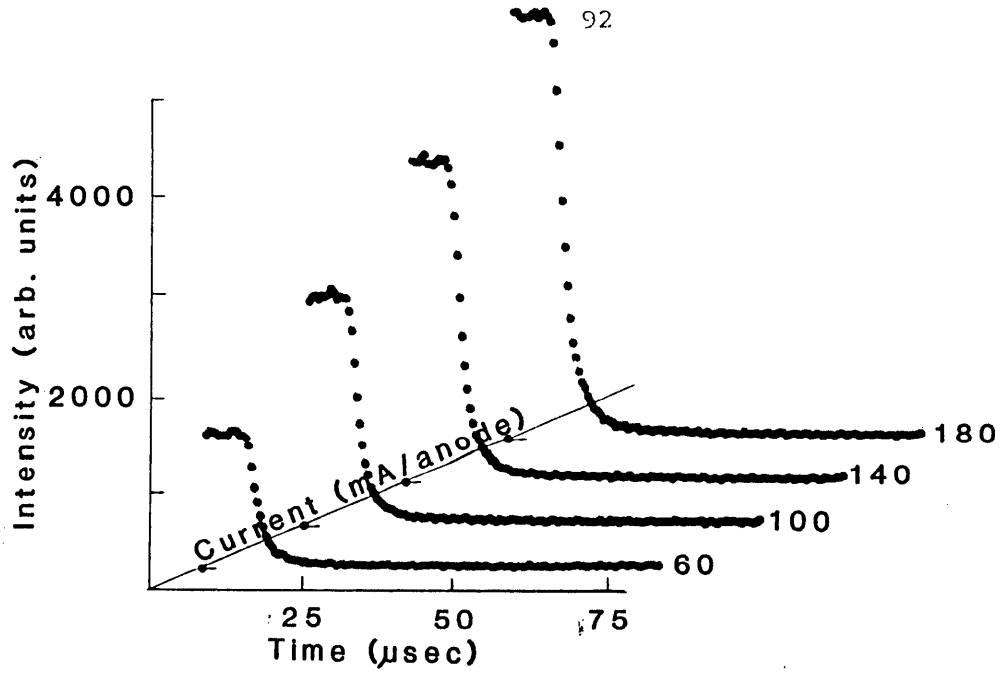

Figure 4.12a *4416 Å decay as a function of discharge current at an oven temperature of 300^{0}C and a helium pressure of 20 Torr*

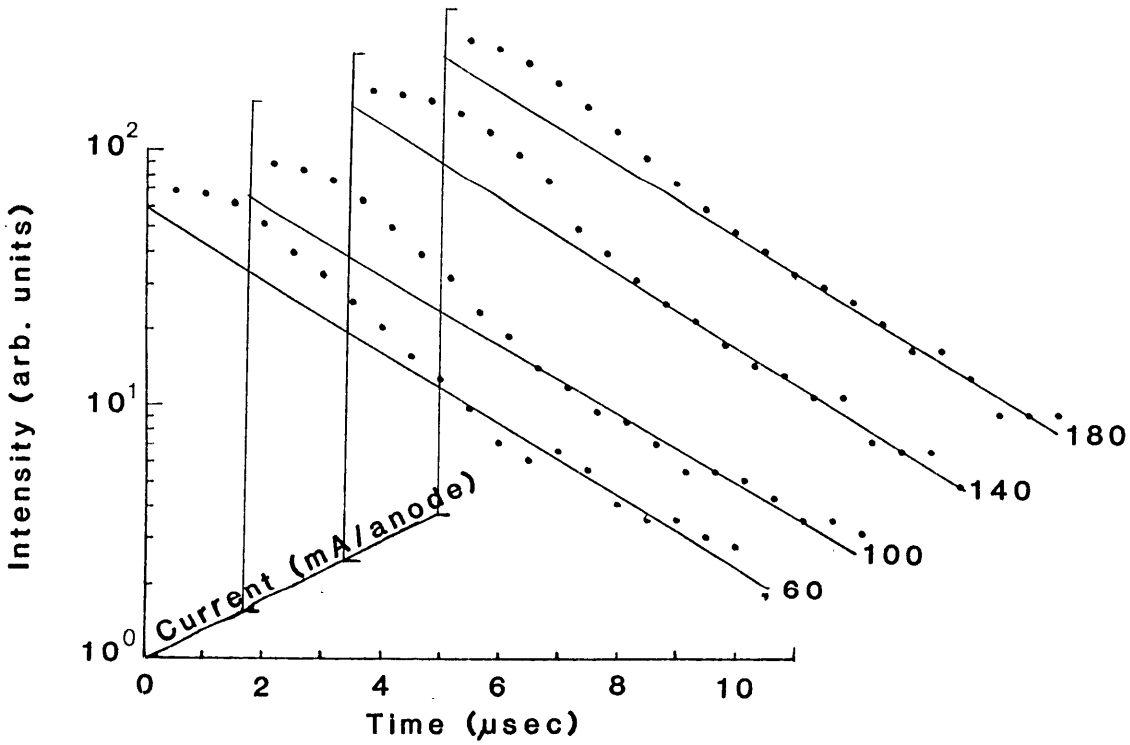

Figure 4.12b *Corresponding semi-logarithmic plots showing the current dependence of the decay*

4.5.3 4416 Å Decay as a Function of Helium Pressure

Results of experiments showing the decay of the 4416 Å intensity as a function of helium pressure, at a constant current of 120 mA/anode and oven temperatures ranging from 225°C to 300°C, are presented in Figures 4.13a - 4.16a with the corresponding semi-logarithmic plots being shown in Figures 4.13b - 4.16b. The helium pressure was varied from a minimum of 15 Torr to a maximum of 40 Torr. Decay curves for pressures less than 15 Torr could not be obtained because the discharge would not reliably restrike at these low pressures. This problem could be overcome by reducing the width of the pulse applied to the transistor but the pulse width required was then such that most, if not all, of the information about the exponential decay in the late afterglow was lost. An upper limit of 40 Torr was set because, for helium pressures greater than this, the glow region was confined to the cathode wall, forming the annular discharge characteristic of hollow cathode devices at high pressure.

At low cadmium concentrations (for oven temperatures less than 250°C), increasing the helium pressure resulted in a small but noticeable decrease in the slope of the late afterglow linear decay. This observation is consistent with the view that Penning collisions are responsible for populating the upper level of the 4416 Å transition because the slope of the decay, as given by

$$\gamma = N_{Cd} \langle \sigma_p v \rangle + \frac{D_m}{\Lambda^2 p}$$

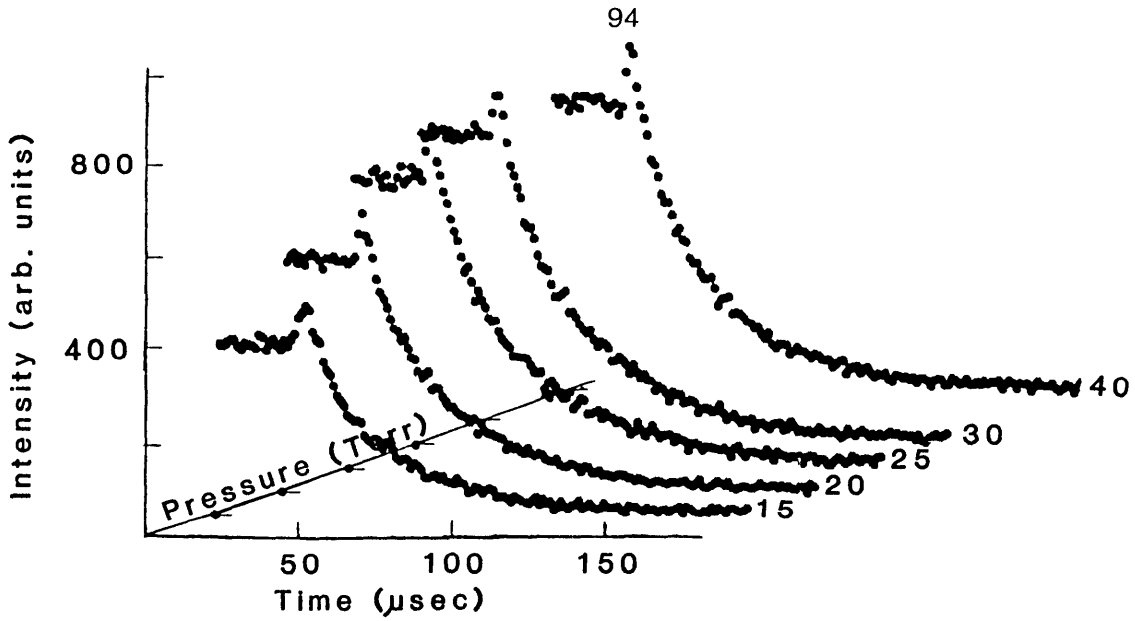

Figure 4.13a *4416 Å decay as a function of helium pressure at an oven temperature of 225^{0}C and a discharge current of 120 mA/ anode*

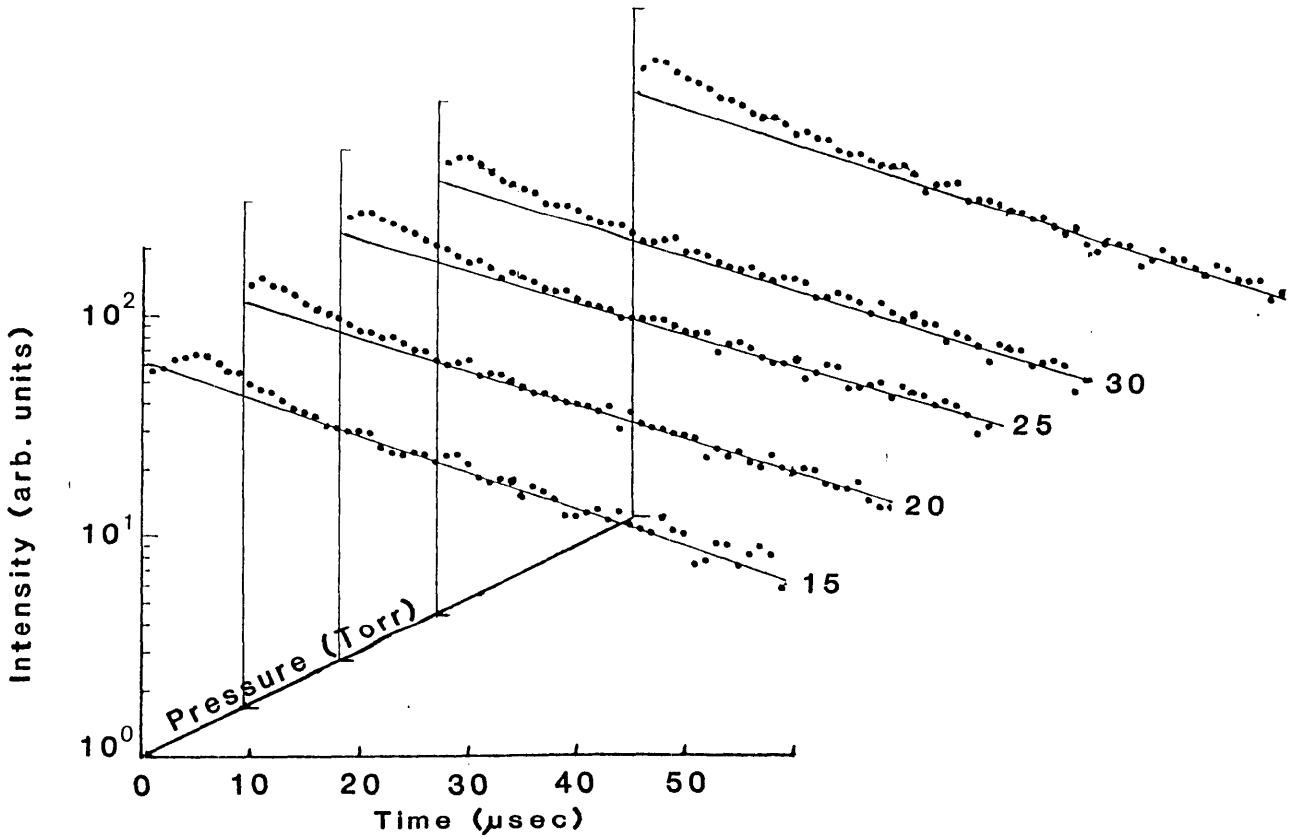

Figure 4.13b *Corresponding semi-logarithmic plots showing the pressure dependence of the decay*

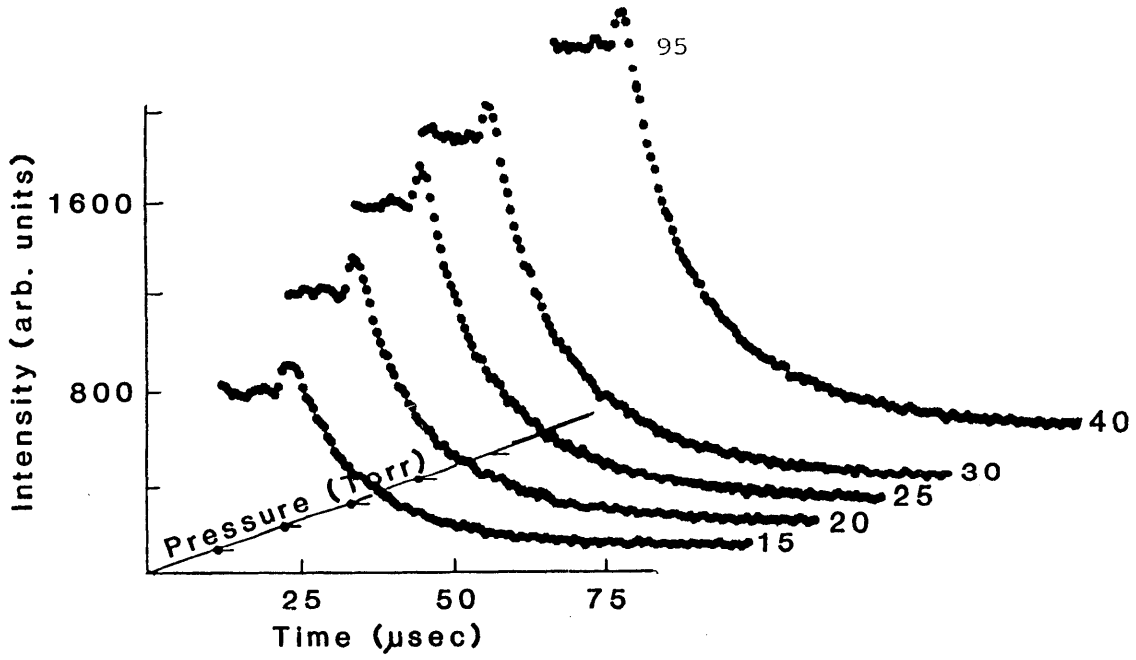

Figure 4.14a *4416 Å decay as a function of helium pressure at an oven temperature of 250°C and a discharge current of 120 mA/ anode*

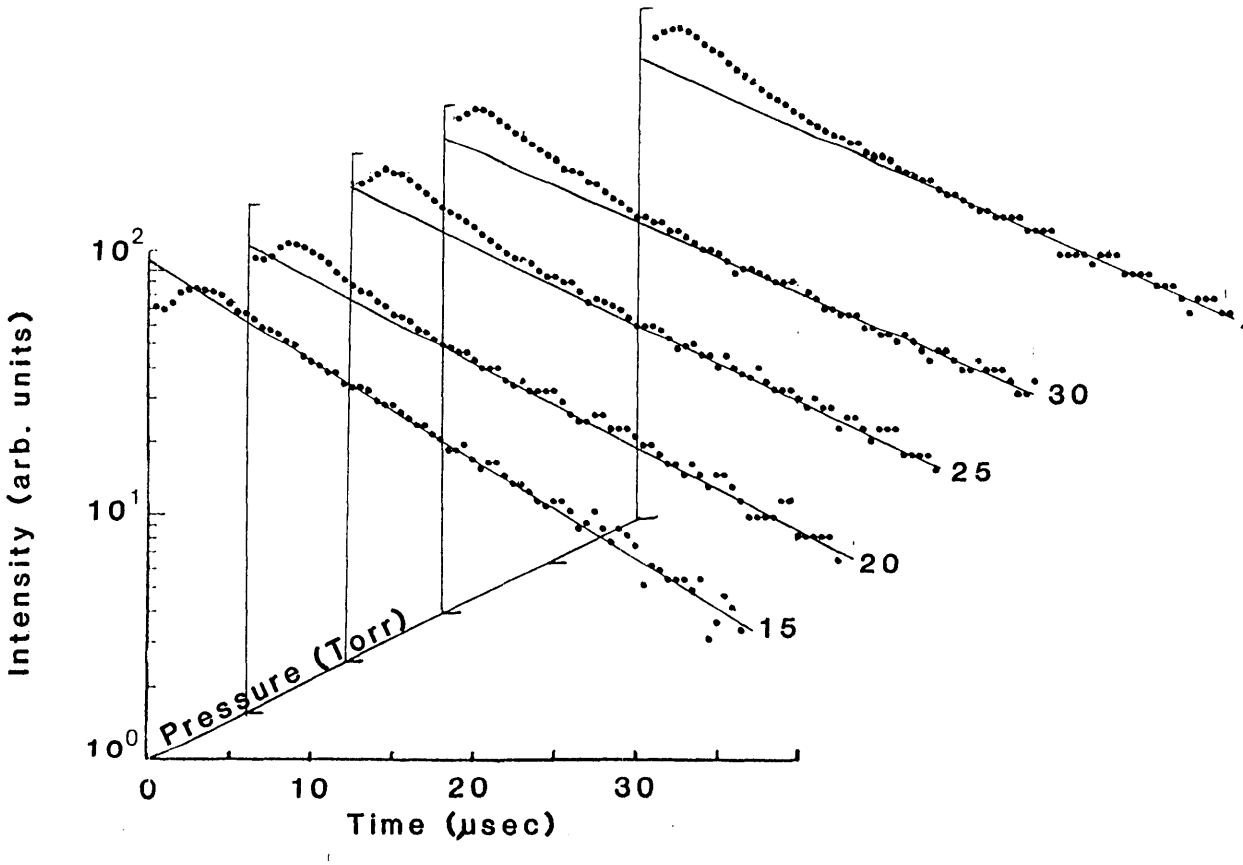

Figure 4.14b *Corresponding semi-logarithmic plots showing the pressure dependence of the decay*

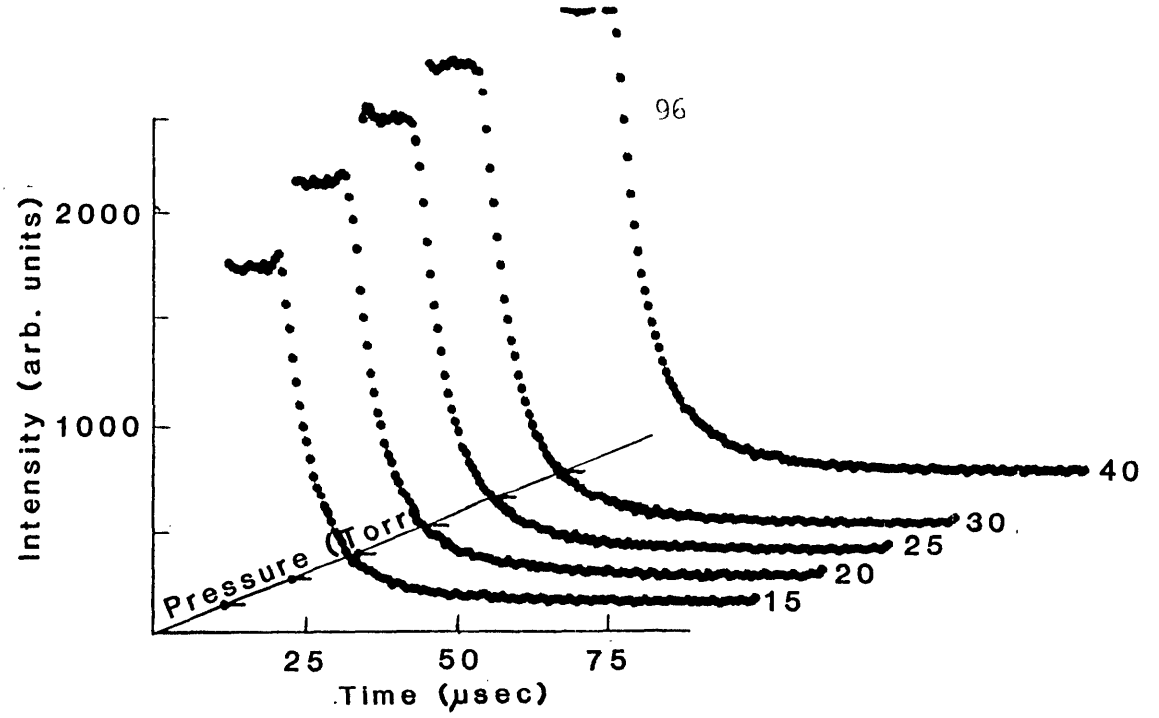

Figure 4.15a *4416 Å decay as a function of helium pressure at an oven temperature of 275°C and a discharge current of 120 mA/ anode*

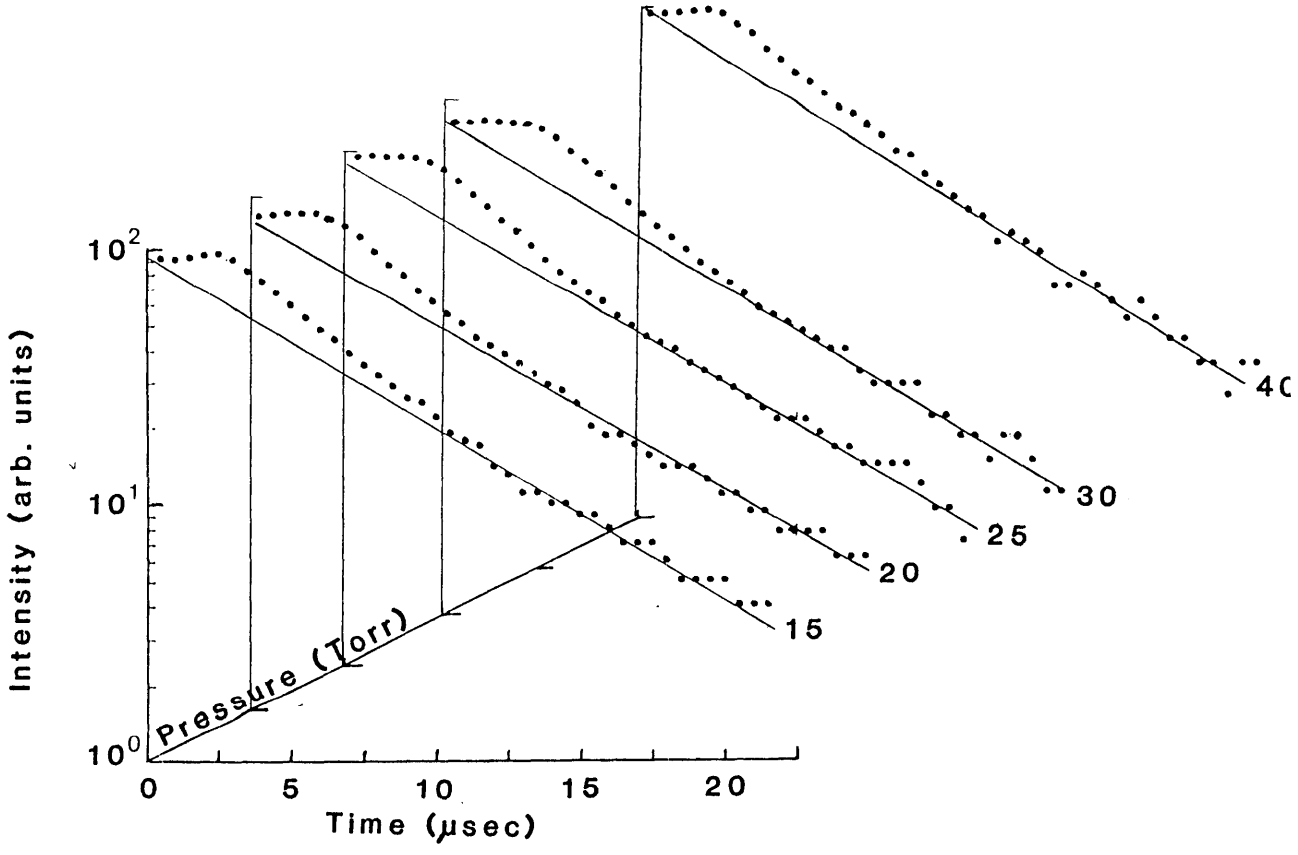

Figure 4.15b *Corresponding semi-logarithmic plots showing the pressure dependence of the decay*

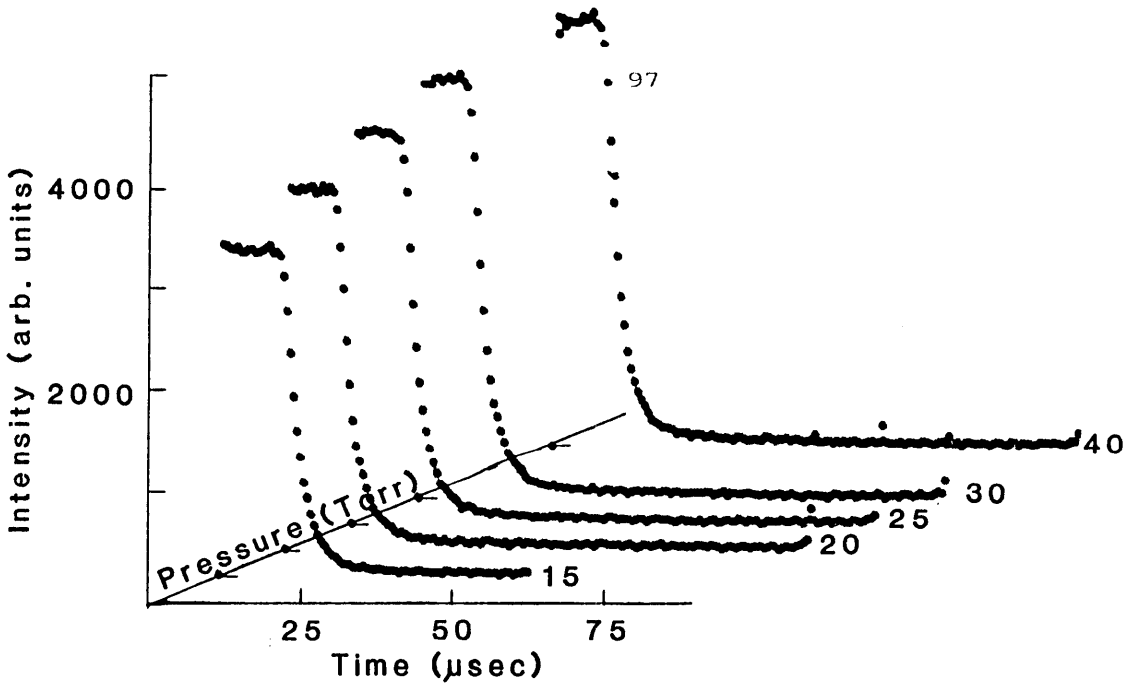

Figure 4.16a *4416 Å decay as a function of helium pressure at an oven temperature of 300^{0}C and a discharge current of 120 mA/ anode*

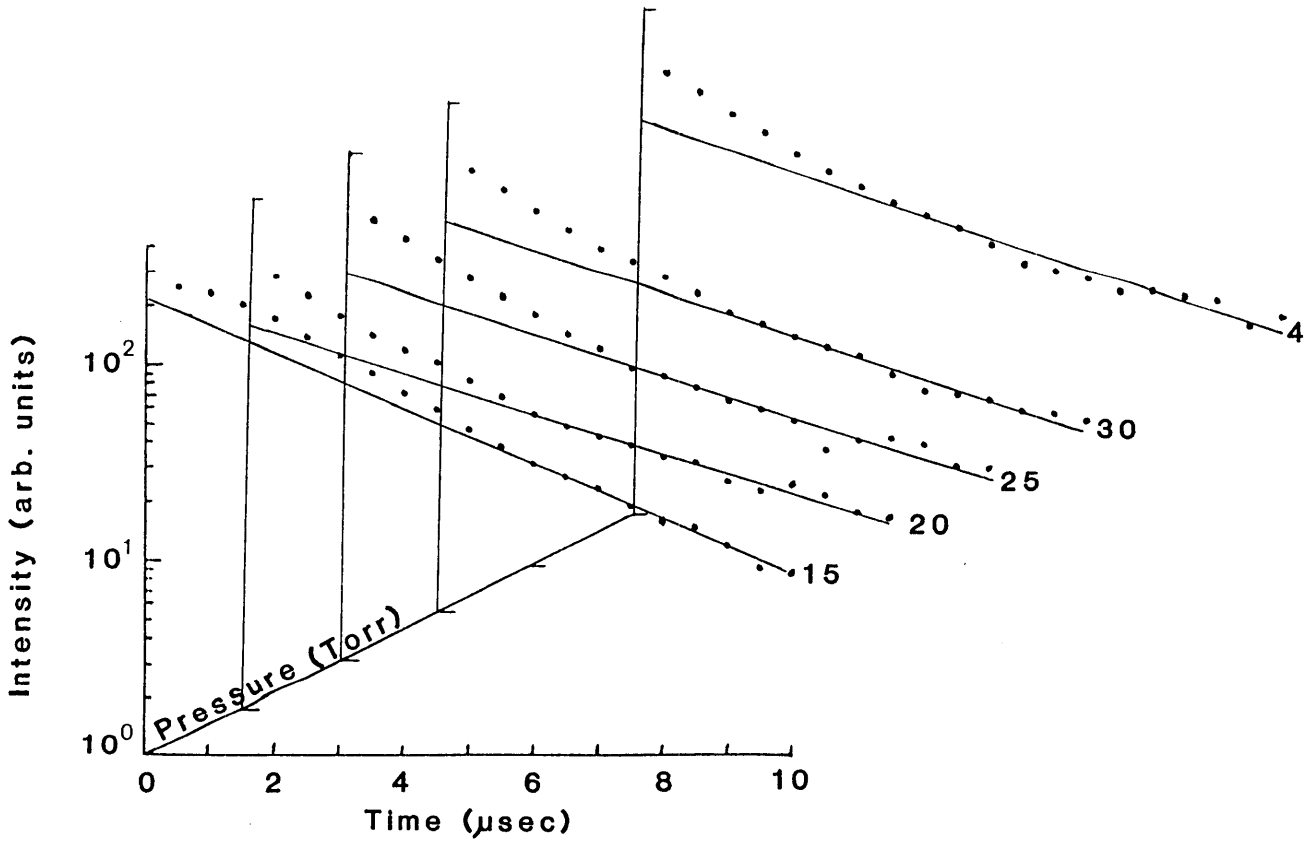

Figure 4.16b *Corresponding semi-logarithmic plots showing the pressure dependence of the decay*

should decrease with increasing pressure. This effect is only noticeable at low oven temperatures because at high temperatures the slope is dominated by the Penning collision term.

If the observed decrease in slope of the linear decay is in fact due to the pressure dependence of the diffusive losses, then a graph of the slope as a function of 1/p should result in a straight line of slope D_m/Λ^2. Figure 4.17 shows that this is observed at oven temperatures of 225^oC and 250^oC.

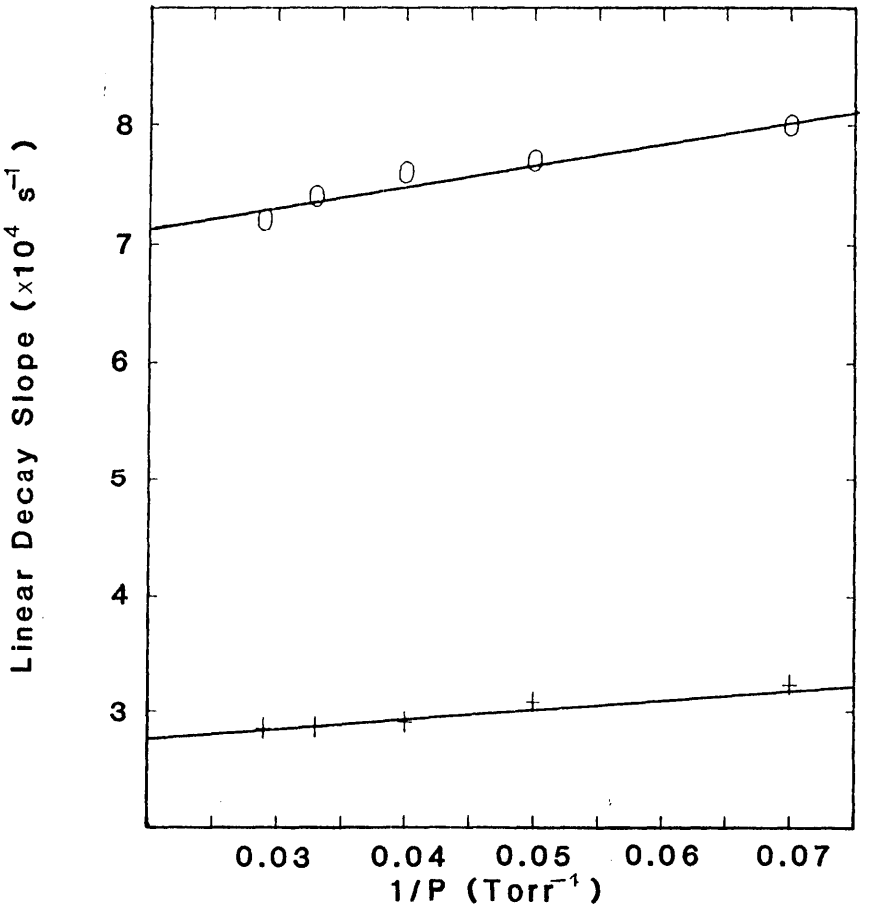

Figure 4.17 Graph of linear decay slope versus (I/P) for determination of the diffusion coefficient of the 2^3S metastable atoms in He-Cd
+-result at an oven temperature of 225^0C
0-result at an oven temperature of 250^0C

From Figure 4.17 and the diffusion length (Λ), calculated for a cylindrical discharge geometry from

$$\frac{1}{\Lambda^2} = \left(\frac{2.405}{r_0} \right)^2 + \left(\frac{\pi}{H} \right)^2$$

where r_o is the tube radius and H the discharge length, the diffusion coefficient for the He (2^3S) metastable atoms in a He-Cd hollow cathode discharge was found to be

$$D_m = 740 \pm 200 \text{ cm}^2 \text{ Torr}^{-1}\text{sec}^{-1} \text{ at } 225^oC$$

and

$$D_m = 1185 \pm 400 \text{ cm}^2 \text{ Torr}^{-1}\text{sec}^{-1} \text{ at } 250^oC$$

These values are in reasonable agreement with the value obtained by Schearer and Padovani (1970) of

$$D_m = 840 \pm 180 \text{ cm}^2 \text{ Torr}^{-1}\text{sec}^{-1}$$

A study of the 4416 Å decay reveals other pressure dependent trends. With increasing pressure the point of intersection of the extrapolated linear tail with the T=0 axis is observed to decrease, relative to the steady state intensity. This behaviour is observed for pressures up to 35 Torr but for pressures above this value the trend reverses. It has been shown by Lorinzcz et al. (1979) that the variation of the cathode fall potential with pressure correlates with that of the electron

density. For the discharge tube used in the present study, experiment reveals that the cathode fall potential reaches a maximum at 35 Torr and thereafter decreases, and it is therefore expected that the electron density will behave in the same manner. This is supported by studies of the pressure dependence of electron density in hollow cathode discharges by Gill and Webb (1978) and Belal and Dunn (1978). Thus the pressure dependence of the point of intersection is consistent with the view that electron processes are somehow involved in the early afterglow decay mechanism.

With increased cadmium concentration the time to peak intensity decreases. This is consistent with a decrease in electron temperature with increasing oven temperature. Also, for a constant oven temperature the time to peak intensity decreases with increasing pressure again consistent with a decrease in the electron cooling time with increasing pressure. For a constant oven temperature the value of the relative peak height, which showed a marked dependence on discharge current, remains essentially constant only falling slightly at high pressures.

4.6 SUMMARY

Afterglow studies were undertaken in order to clarify the excitation mechanisms resulting in the population of the $5s^2\ ^2D_{5/2}$ level of Cd II. This initial study consisted of the observation and measurement of the decay of the 4416 Å spontaneous emission as a function of cadmium concentration, discharge current and helium pressure. Sophisticated digitizing and data recording/processing equipment was utilized to record the decay. As a result of the excellent signal to noise characteristics of the experimental data, the observed decay showed greater structure

than either anticipated or reported by other researchers.

In view of the fact that the late afterglow decay was exponential and, coupled with the observation that the time constant of this exponential decay decreased with cadmium concentration, it was concluded that at these times in the afterglow Penning ionization was the dominant excitation mechanism of the $5s^2\ ^2D_{5/2}$ level. Further evidence supporting this conclusion was found when the pressure dependence of the decay was investigated. With increasing pressure the time constant of the exponential decay was observed to decrease. This feature was attributed to the effect of pressure on the diffusion of the $He(2^3S)$ species. From the experimental data, values for the diffusion coefficient were derived and these were found to be in favourable agreement with those published by Schearer and Padovani (1970).

While the interpretation of the collision processes in the late afterglow was relatively straightforward, no simple explanation satisfactorily explaining the 4416 Å decay characteristics in the early afterglow was obvious. This difficulty is highlighted by the observed increase in intensity of the 4416 Å emission at these times.

Careful and systematic investigation of the current and pressure dependence also revealed some interesting features. The inverse current dependence of the relative peak height of the decay suggested that direct electronic processes were not involved in the production of the $5s^2\ ^2D_{5/2}$ level early in the afterglow. On the other hand, the observation that the point of intersection of the extrapolated exponential tail with the afterglow initiation axis showed a marked dependence on current and pressure indicated that electronic processes must, either directly or indirectly, affect the nature of the decay in the early afterglow.

In view of the complex nature of the 4416 Å decay, the results obtained from this investigation cannot easily be extrapolated back to the conditions prevailing in the d.c. discharge. Such a procedure can only be attempted when all processes in the afterglow have been identified and thus further investigation of the afterglow is warranted.